Microbial metabolomics in polar oceans: responses to temperature and salinity changes associated with sea ice.

Hannah Michelle Dawson

A dissertation

submitted in partial fulfillment of the

requirements for the degree of

Doctor of Philosophy

University of Washington

2022

Reading Committee:

Jodi N. Young, Chair

Jody W. Deming

Anitra E. Ingalls

Program Authorized to Offer Degree:

Oceanography

University of Washington

Abstract

Microbial metabolomics in polar oceans: responses to temperature and salinity changes associated with sea ice.

Hannah Michelle Dawson

Chair of the Supervisory Committee:
Jodi N. Young
School of Oceanography

Polar oceans and sea ice are among Earth's major biomes, but are experiencing rapid environmental changes associated with climate change that may shift polar marine ecosystems into new, potentially unstable, states. Warming temperatures, alterations in sea-ice dynamics, and enhanced glacial freshwater input into coastal regions at the poles all stand to alter the temperature and salinity seascapes of an environment already marked by pronounced seasonal fluctuations. This dissertation examines the role of temperature and salinity change associated with sea-ice formation and melt in structuring the chemical inventory of organic matter in microbially dominated polar systems, with a focus on sea-ice algae. Much of this work utilizes liquid chromatography-mass spectrometry (LC-MS) to observe pools of small biomolecules (metabolites) that can serve as currencies of microbial metabolism and provide a snapshot of

cellular activity. Specifically, I focus on gaps in our knowledge regarding protective compounds that are temperature- and salinity-sensitive (compatible solutes), many of which are highly labile metabolites with the capacity to fuel the microbial loop upon their release from cells.

Chapter 1 introduces sea-ice microbial communities and the cellular strategies they use to grapple with the temperature and salinity fluctuations that characterize polar marine habitats. In Chapters 2 and 3, I examine the covarying impact of temperature and salinity on compatible solutes in the sea-ice diatom *Nitzschia lecointei* (Chapter 2) and analyze organic metabolite pools across cultured diatom species (Chapter 3). These chapters reveal that sea-ice algae can contain diverse and species-specific suites of labile compatible solutes at high concentrations (up to ~1 M; Chapter 3) with complex and varying cellular sensitivities to temperature and salinity change (Chapter 2), whereby the solutes are strongly accumulated under cold and salty conditions compared to warmer and fresher conditions. In Chapter 2 I also offer some of the first observations of multiple metabolites in natural Arctic sea ice and hypothesize on their impacts on the cycling of nutrients through this environment. In Chapter 4, I explore whole community metabolomes paired with environmental sequencing of 18S and 16S rRNA genes in distinct but interconnected Antarctic marine habitats (sea-ice meltwater, seawater, and sea ice) with unique physicochemical settings, including temperature and salinity. This chapter reveals unique communities in each habitat, all distinguishable by metabolomics. Chapter 4 also presents short-term experiments on natural microbial communities in polar seawater incubated under different temperature and salinity conditions mimicking sea-ice formation and melt, which demonstrated strong, community-wide metabolome reorganization, including alterations to the pools of numerous compatible solutes, but in the absence of corresponding community composition change. In full, this dissertation provides some of the first metabolite measurements in polar

marine environments, identifies and explores the roles of key metabolites in microbial adaptation to environmental change, and provides a unique, metabolite-centered perspective on the potential impacts of continued environmental change on the production and use of organic matter in polar food webs and on the detection of life in icy environments beyond the Earth.

TABLE OF CONTENTS

LIST OF FIGURES

LIST OF TABLES

ACKNOWLEDGEMENTS

Thank you to my advisor, Jodi Young, for taking a chance and choosing me as her first graduate student. Jodi always pushed me to make strong connections and learn by doing, and I will be forever for grateful for the opportunities she brought into existence. I have had the privilege of working in both the Arctic and Antarctic as her graduate student, and I would have never discovered my passion for polar environments or my love of field work without these life-altering experiences. My committee members, Jody Deming, Anitra Ingalls, Drew Gorman-Lewis, and Gordon Holtgrieve have all supported me throughout my graduate career, and I thank them for always asking the hard, but important, questions.

I have had the honor of working with a wonderful group of people in the Young lab. Anders Torstensson, Meng Li, Katrin Schmidt, Susan Rundell, Rachel Liu, Kaitlin Harrison, Gio Kanaan, Veronica Mierzejewski, and Hanis Zulaikha have been fantastic lab mates and I have learned so much from each of them. Anders Torstensson was an amazingly kind mentor and friend who happily took me by the hand and taught me all there is to know about culturing sea-ice diatoms. Anders also carried the *Nitzschia lecointei* cultures that formed a large portion of my research all the way from Sweden to their new home in Seattle, for which I am so thankful. Susan Rundell was the best lab mate, officemate, and field mate I could have ever asked for. Her joie de vivre is infectious and I hope we always get in trouble for laughing too loud. Meng Li is an extremely thoughtful, kind, and bright scientist and working with him has been a pleasure. Your warm smile and kind words will always stick with me. Veronica Mierzejewski, who integrates metabolomics

data faster than I ever could, is such a devoted and curious learner and will make any future mentor so proud. Working with her was a treat during her short time with us. Rachel Liu, a lab mate and dear friend, is a force to be reckoned with. I have learned so much from Rachel in the past year and have been constantly inspired by her fierce devotion to friendship, community, silliness, and pastries. I have loved working alongside talented undergraduates in the lab, including Viviana Castillo, Rebecca Schmidt, Ashlee Somol, Finn Mander, Dominic Eastburn, and Bailee Porter.

I am fortunate to have had three lab families in oceanography that kept me afloat throughout graduate school. The second, the Deming Ecosystem, welcomed me in with open arms and introduced me to life in ice. Jody Deming is truly an inspiration and trailblazer, and I hope to attain even a fraction of her passion, boldness, and wisdom in my lifetime. Jody is a steadfast supporter that has always pushed me to think deeply and creatively, for which I am so thankful. Max Showalter, Zac Cooper, and Josephine Rapp have all been fantastic collaborators and friends from the weird and wonderful Deming circle. Shelly Carpenter, arguably the weirdest, has been the best teacher and supporter I could have asked for. Shelly has shown me the ropes in the lab and in the field more times than I can count, all with a huge smile and hearty laugh.

The Ingalls lab has also been a safe haven and support group that I could not have survived without. Anitra Ingalls has always given it to me straight, with a touch of humor, and I so much appreciate her influence on my science and writing. Laura Carlson is a mass spectrometry wizard who taught me so much about lab work and made every set of extractions more fun than the last with her talented hands and kind spirit. I can confidently say that without Laura, the data that underpins this dissertation would not exist. Katherine Heal and Angie Boysen have been strong mentors, allies, and friends that made my foray into metabolomics possible. Katherine and Angie taught me most everything I know about metabolites, and definitely everything I know about

coding in R. It has been an honor to work with and learn from such strong, inspiring, women scientists. It has also been a pleasure to work with the entire Ingalls crew, including Josh Sacks, Will Kumler, Natalie Kellogg, Regina Lionheart, Rachel Lundeen, Alec Meyers, Leland Wood, and Everetta Rasyid. You all have never hesitated to share your knowledge and time with me, and I so much appreciate it.

I have been extremely fortunate to learn from so many scientists at UW and beyond. Bryn Durham made many of my organosulfur metabolite measurements possible and has shaped how I think sulfur cycling in the ocean. She is a generous person and scientist and has been a kind and supportive voice throughout my journey. Aaron Morello and Kathy Krogslund in the Marine Chemistry Lab at UW have been instrumental in gathering ancillary data to support my findings. Aaron is such a patient and detailed teacher, and I so much appreciate all that I learned from him. The Bowman lab at Scripps includes amazing scientists that have bolstered my understanding of microbial ecosystems. Jeff Bowman is a strong collaborator and supporter that welcomed me into his lab without a second thought and quickly jumps in whenever help is needed. Natalia Erazo and Beth Connors are bright and optimistic scientists and it has been such a joy to work with them. Thank you to the Thamatrakoln lab at Rutgers for being my home away from home during my astrobiology rotation, granting me a return to lab work during the pandemic, and introducing me to viromics. Kim Thamatrakoln, Chana Kranzler, Udi Zelzion, Kay Bidle, Liti Haramaty, Chris Johns, Austin Grubb, and Ben Diaz all taught me so much about the weird world of viruses.

I will be forever grateful to the UW community that made this graduate journey more rich, fun, and supportive by being the wonderful people they are. Thanks to my friends: Karina, Robert, Claire, Sasha, Ann, Andrew, Zach, David, Hannah, Erik, Tess, Brendan, Jiwoon, Ryan, Megan,

Ashley, Susanna, Rosalind, Christina, Theresa, Amy, Haila, Anna, Sarah, Isaiah, Katy, and too many others to thank, including my entire 2016 cohort, the OSB fifth floor crew, the astrobiology community, and the entire Oceanography graduate student community.

My dissertation research would not have been possible without the logistical support that made my field work possible. Thank you to the Ukpeaġvik Iñupiat Corporation for providing the facilities and support to collect sea ice in the Chukchi Sea off Ukpeaġvik, AK. Thank you to the United States Antarctic Program for gearing me up and getting me to Antarctica twice. I would also like to thank the crew of the *Lawrence M. Gould* and *Nathaniel B. Palmer* for safely guiding our teams safely through the Drake passage and along the Western Antarctic Peninsula. I also could not have completed my field work without all of the wonderful people I worked with at Palmer Station and aboard the NBP. Antarcticans are a special breed and have changed my outlook on life. Thank you to my friends: Rebecca Trinh, Shawnee Traylor-Biglio, Leigh West, Jack Conroy, Anna Bashkirova, Megan and Daren Roberts, Keri Nelson, Diane Hutt, Wade Jeffrey, Bob Sanders, Chris Carnivale, Leila Harris, Nicolle Millette, and Jean-David Grattepanche.

The friendships I found in Seattle (and Antarctica) have been a source of joy and inspiration. Thank you to Marie Zahn and Sam May for being strong friends and supporters who never fail to teach me something new each time we are together. You all have made Seattle feel like home and I will always cherish your love and laughter. Thanks to the Angells, the best neighbors and Seattle family Chris and I could have asked for. Steve, Sarah, Greg, and Kelsey have pulled us into their home and made us feel like part of the family. Thank you to the City Fruit family and the 2022 Fruit Tree Stewards for giving me a deeply fulfilling reason to get outside and learn about fruit trees while I was in the thick of my dissertation writing.

My family has always been my biggest source of support and love and I would not be where I am without them. My parents have always pushed me to shoot for the stars and provided me with a safe place to land if things did not go as planned. My parents also fostered my love of the ocean from the ripe age of four months old on the beaches of Delaware. My lovely, talented, and loving sisters have been built-in best friends and supporters my whole life. They have constantly reminded me that they believe in me even when I do not, and I have made it through the highs and lows of this journey with their love and support. Charlotte and Frank have been the pest pep squad and party starters that I have ever known. They reminded me throughout this process (and my whole life) to take breaks and make time for adventures. My aunt Brenda has been a guiding light in my life and graduate journey, and I cannot thank her enough for always reminding me what is really important in this life. Finally, thank you to my partner Chris LaComb. You took a leap of faith and moved to Seattle with me so I could finish my PhD, and I am so glad that you did. You are my best friend, biggest supporter, and the funniest person I have met or ever will meet. I can confidently say that you have made me laugh every single day for the last six years.

DEDICATION

To my aunt Brenda, for teaching me how to stay strong in the face of hard work and always leave room for laughter.

Chapter 1. INTRODUCTION

1.1 CLIMATE IMPACTS ON POLAR ENVIRONMENTS

Earth's climate is currently undergoing rapid changes in response to anthropogenic greenhouse gas emissions (IPCC, 2022), with global air temperatures expected to rise at least 1–3°C over the next century (Bronselaer et al., 2018). Dramatic ecological responses to both rising atmospheric CO_2 and global warming have been documented in diverse environments (Walther et al., 2002; Sheridan and Bickford, 2011; Jansson and Hofmockel, 2020; Woolway et al., 2020), but the nature of these responses can be highly complex, nonlinear, and sometimes abrupt (Burkett et al., 2005; Walther, 2010). Polar environments in particular are experiencing rapid, dramatic change, including changes in marine carbonate chemistry (Hoegh-guldberg and Bruno, 2010) and increases in air and ocean temperatures, particularly in the Arctic (Overland et al., 2019; Jansen et al., 2020) and along the Western Antarctic Peninsula (WAP), where surface ocean temperatures have increased by > 1°C since the 1950s (Meredith and King, 2005). Associated reductions in sea-ice extent, sea-ice thickness, and length of the sea-ice season as well as the increased occurrence of low-salinity features (freshwater melt ponds, under-ice melt lenses, enhanced glacial freshwater input), have already been observed in the Arctic and along the WAP and are expected to continue (Vaughan et al., 2003; Arrigo et al., 2008; Stammerjohn et al., 2008; Stammerjohn et al., 2012; Arrigo et al., 2014; Cape et al., 2019). As polar environments continue to change rapidly, accurately predicting the ecological responses of seawater and sea-ice communities to those changes will become increasingly important. This dissertation aims to improve foundational knowledge on organism- and community-level responses of polar marine microbes, which drive ecosystem productivity and nutrient recycling, to temperature and salinity change associated with

sea ice to both characterize modern communities and aid in predictions of future responses to continued climate change.

1.2 SEA ICE AS A MICROBIAL HABITAT

Sea ice is one of the most extensive habitats on Earth, with approximately 4–6% of the global ocean area covered by sea ice throughout the year (Arrigo, 2014). In addition to climate-related environmental change, existing seasonal cycles of sea-ice formation and melt from and into the surrounding seawater make sea ice-associated microbial habitats both extreme and variable, with fluctuations in temperature, salinity, light, pH, and nutrients on temporal scales ranging from < 1 day to months (Dieckmann and Thomas, 2002; Ewert and Deming, 2013; Ewert and Deming, 2014). Temperature and salinity are tightly coupled in sea ice (Cox and Weeks, 1983) and govern the extent of liquid brine space available for microbial life. Diverse microbial assemblages can inhabit these interconnected brine pores, with bacteria, viruses, and unicellular microalgae at times reaching densities much higher than those observed in seawater (Arrigo 2016; Deming and Collins 2017). These communities are exposed to temperatures and salinities colder and saltier than seawater during ice formation and maturation, with temperatures reaching below –20˚C and salinities above 200 ppt in upper Arctic sea ice during winter (Ewert and Deming, 2014), and can be exposed to near-freshwater salinities during sea-ice melt (Boetius et al., 2015). Sea-ice algae in particular are generally found within bottom layers of sea ice near the ice/water interface, where temperatures are warmer (−1.5˚C) and salinity remains closer to underlying seawater (approximately 35) (Eicken, 1992; Arrigo, 2014), but can be found throughout the ice, particularly in melt layers common in Antarctic sea ice (Lizotte and Sullivan, 1991; Arrigo, 2016).

1.3 SEA-ICE COMMUNITIES

Despite pronounced seasonal variability in environmental conditions, sea ice maintains microbial activity throughout the year. Spring algal blooms within sea ice can contribute to a large proportion of primary production in polar oceans, with 10–28% of annual primary production in the ice-covered waters of the Southern Ocean (Arrigo and Thomas, 2004) and 55–65% of coastal Antarctic primary production attributed to sea-ice algae (Andrew McMinn et al., 2010). These blooms are often dominated by diatoms and can reach densities up to 10 g Chl *a* m^{-3} or > 10^9 cells L^{-1} (Arrigo, 2016). This abundant source of primary production is a critical source of fixed carbon fueling microbial food webs and higher trophic levels in polar ecosystems, especially during the winter and early spring when primary production in the water column is often near zero (O'Brien, 1987; A. McMinn et al., 2010; Kohlbach et al., 2017; Kohlbach et al., 2018). Prokaryotic community dynamics within sea ice are often tightly coupled to eukaryotic algae, with concentrations of bacteria reaching close to 3×10^7 mL^{-1} in bottom sea ice following algal blooms (Deming and Collins, 2016). This coupling is largely mediated by highly concentrated, labile dissolved organic matter (DOM) produced by algae, fueling heterotrophic production during the bloom season (Smith & Clement 1990; Grossmann & Dieckmann 1994) and recycling nutrients as a result (Garrison et al., 1986; Kottmeier et al., 1987). Deciphering the roles of this highly concentrated biological community in polar biogeochemical cycling, and the influence of environmental shifts on those roles, is an active area of research (Vancoppenolle et al., 2013; van Leeuwe et al., 2018), complicated by high spatial heterogeneity, difficulties in sampling, and a general lack of data compared to pelagic systems.

Sea-ice microbial dynamics are also tied to processes in the underlying water column and benthic environment. Sea ice forms from seawater which supplies, in conjunction with sediments

and multiyear ice, the starting community of microorganisms within the ice (Olsen et al., 2017). After sea-ice melt, polar seawater may act as a storage vessel for sea-ice microbes (e.g., *Nitzschia frigida*; Koch et al. 2020) when sea ice is not available. Others remain abundant in seawater, particularly small diatoms that resist sinking (e.g., *Fragilariopsis cylindrus*; Kang and Fryxell 1992) and may act as a seeding population for highly productive summertime phytoplankton blooms (Lizotte, 2001; Riaux-Gobin et al., 2011). The pulse of organic matter that enters the water column once ice melt has begun, which is often rich in essential fatty acids required in animal diets (Søreide et al., 2010), can also be an important food source for pelagic grazers (Brown and Belt, 2012) or benthic invertebrates upon settling on the seafloor (Boetius et al., 2013).

Transitions into and out of sea ice are associated with shifting environmental conditions (noted above). These shifts may alter microbial community composition and the composition of associated organic matter, impacting the nutritional quality of organic matter, the export of carbon, and production of climate-active organic aerosols in polar oceans. Physiological responses to polar conditions include changes in ice-binding protein and exopolymer production, fatty acid content and composition, ribosome and protein abundance, enzyme activity, and compatible solute concentrations, all potentially impacting organic matter composition (Deming and Young, 2017; Young and Schmidt, 2020).

1.4 COMPATIBLE SOLUTES IN POLAR MARINE SYSTEMS

Compatible solutes are small organic molecules that can be maintained at high concentrations in a cell's cytosol without compromising macromolecular function. Compatible solutes are used by all organisms in some fashion and often act as osmolytes and cryoprotectants (Yancey et al., 1982; Welsh, 2000; Lyon and Mock, 2014), though they also serve other metabolic roles (Yancey et al.,

1982; Welsh, 2000). This dissertation uses the term compatible solutes to refer to abundant small polar compounds that have been suggested to mitigate cold and osmotic stress.

Compatible solutes are of particular interest in polar contexts, where routine temperature and salinity change may impact the reservoirs and cycling of these abundant, labile compounds. Previous work has shown that sea-ice diatoms and bacteria can accumulate compatible solutes (via synthesis or exogenous uptake) during periods of low temperature and high salinity exposure (e.g., winter sea-ice brines) and lower their concentrations (via respiration, incorporation in macromolecules, or release) upon warming and freshening (e.g., melting sea ice) (Krell et al., 2007; Firth et al., 2016; Lyon et al., 2016; Torstensson et al., 2019). Those studies that have focused on sea-ice algae addressed individual compatible solutes or selected species in culture, with little attention given to the effects of realistic shifts on natural communities.

If released, compatible solutes can enter the labile DOM pool, where they can be taken up by other microorganisms for the purpose of osmoregulation (Kiene and Williams, 1998; Torstensson et al., 2019) or as a source of carbon, nitrogen, or energy in the microbial loop (Welsh, 2000; Durham et al., 2019; McParland et al., 2021; Moran et al., 2022). A change in temperature and salinity could thus influence the chemical composition of DOM in polar oceans on a seasonal basis, with compatible solute release adding to the pulse of DOM released from melting sea ice into seawater, where they are readily available for microbial processing. For example, the remineralization of nitrogen-rich compatible solutes by sea-ice bacteria during freshening liberates CO_2 but may also provide an avenue for regenerating inorganic nitrogen (e.g., ammonium) for reuse by sea-ice algae during photosynthesis and growth (Collins and Deming, 2013; Firth et al., 2016), making compatible solutes a potential mediator in algal-bacterial interactions in sea ice.

In addition to seasonal cycles, short-term temperature and salinity fluctuations that occur within the sea ice on the order of hours to days (Petrich and Eicken, 2010) could cause more frequent repartitioning between compatible solute pools (synthesis, uptake, release, respiration), making them highly labile and mobile compounds in this environment. Other than DMSP, a compatible solute and precursor to the primary natural sulfate aerosol dimethyl sulfide (Kirst et al., 1991; Malin et al., 1992; Welsh, 2000; Bobbie and Lyon, 2011; Vancoppenolle et al., 2013), the importance of compatible solutes in polar ecosystems has been based largely on estimated environmental concentrations (Firth et al., 2016; Torstensson et al., 2019). Direct measurements of the diversity and concentration of compatible solutes in polar environments, and marine systems more broadly, have been hindered until recently by analytical challenges in quantitatively measuring chemically diverse compounds in seawater.

1.5 CULTURE AND COMMUNITY METABOLOMICS

Advances in the field of metabolomics, the simultaneous measurement of all small organic molecules produced by cellular metabolism in a system, have extended capabilities for the measurement and quantification of metabolites beyond individual compounds or groups of compounds towards a more complete view of the chemical composition of marine organic matter (Fernie et al., 2012). This type of data is challenging to acquire and process, but recent analytical developments in liquid chromatography-mass spectrometry (LC-MS) and data processing (Boysen et al. 2018), allow for quantitative measurements of diverse metabolites, including compatible solutes, both in cultured organisms and those in the environment. Metabolomics studies have already shown that marine microbes grown in culture alter their metabolite pools in response to changes in nutrient availability, temperature, growth phase, sexual phase, and microbial interactions (Amin et al., 2015; Durham et al., 2015; Hano and Tomaru, 2019; Heal et al., 2019;

Fiorini et al., 2020). Metabolomic profiling of natural marine communities is still limited, but previous work has shown that intracellular metabolites change across spatial and temporal environmental gradients (Llewellyn et al., 2015; Kujawinski et al., 2017; Johnson et al., 2019; Boysen et al., 2021; Heal et al., 2021) and vary with changes in taxonomy (Heal et al. 2020). This methodology has not previously been applied to sea-ice algae in culture or to *in situ* polar seawater or sea-ice communities, but can provide unique insights into microbial adaptations to environmental change.

In this dissertation, I leverage LC-MS metabolomics to explore organism- and community-level responses to environmental change, specifically temperature and salinity change, as reflected in the small molecule pools within polar marine particulate organic matter. In Chapter 2, I present results from a laboratory study of the Antarctic sea-ice diatom *Nitzschia lecointei* to investigate how metabolite pools change with a moderate shift in temperature and salinity to understand how these important polar microbes mitigate temperature and salinity stress, with a particular interest in alterations to their compatible solute pools. Chapter 3 builds upon these analyses to evaluate how metabolome distinctions across individual diatom species compare to intraspecies distinctions in response to environmental perturbation. In Chapter 4, I analyze whole community metabolomes alongside DNA amplicon sequencing in three distinct polar marine habitats along the WAP (sea-ice meltwater, seawater, and sea ice) to interrogate the role of temperature and salinity in shaping microbial community composition and the composition of marine particulate organic matter. While each chapter represents a different ecological scale, from species to communities, together they demonstrate that the labile chemical inventory of polar marine communities is highly sensitive to temperature and salinity change, which informs our understanding of microbial adaptations to

the sea-ice environment and highlights important consequences for organic matter cycling as polar regions experience continued warming and freshening.

1.6 SEA-ICE METABOLOMICS AND ASTROBIOLOGY

The potential for life on icy worlds, such as Europa and Enceladus, is often discussed in the context of a subsurface ocean or at the interface between solid and liquid phases of water, where inhabitants would face multiple physicochemical stressors, including extreme and dynamic temperature and salinity conditions (Carr et al., 1998; Schmidt et al., 2011; Fischer et al., 2016; Rivera-Valentín et al., 2020). Terrestrial sea ice, with variable and extreme temperature, salinity, light, and nutrient conditions, provides an analog for subzero and briny environments beyond Earth (Marion et al., 2003; Dudeja et al., 2012; Martin and McMinn, 2017). How microbial communities, including both prokaryotes and single-celled eukaryotes, are metabolically adapted to thrive in frozen and salty environments at the poles, and the signatures these adaptations leave on the environment, has been a focus of this dissertation.

The tools of environmental metabolomics can be used to explore the interactions between microorganisms and their environment, but have not previously been applied to polar environments. Metabolomic profiling, using tandem LC-MS, can assist in understanding how microbial communities are metabolically adapted to extreme conditions and their responses to environmental change (Blachowicz et al., 2019), as well the preservation of metabolites in extreme environments. Because organic compound-based biochemistries are likely to involve the processing of low molecular weight compounds (Hoehler et al., 2018) and different organisms adapted to similar environmental conditions may have many shared metabolites (Poli et al., 2017), characterizing the diversity and abundance of small organic metabolites in modern microbial

communities associated with sea ice may aid the search for biomarkers in icy environments of the Solar System and beyond.

Compared to nucleic acids, metabolites may serve as longer lasting, process-agnostic biosignatures (Johnson et al., 2018; Chan et al., 2019) on other worlds, where noncanonical modes of information storage and metabolism may be present but an abundance of chemically labile compounds may suggest extant organisms (Seyler et al., 2020). Metabolome profiling may also reveal intermediates or products diagnostic of specific metabolic pathways (Zamboni et al., 2015), including those for which genome annotations are incomplete (Tang et al., 2009), or reveal novel metabolic pathways altogether (Fürch et al., 2009). Liquid chromatography coupled with electrospray ionization mass spectrometry, as employed in this dissertation, could be particularly powerful in the search for extraterrestrial biomarkers, as it allows for the detection of the large number of metabolites (Jonsson et al., 2005; Schrimpe-Rutledge et al., 2016) in complex mixtures of compounds that range over 10,000-fold differences in abundance (Aldridge and Rhee, 2014). Multiple high-resolution mass spectrometer prototypes are under development for use in a potential future lander mission to Europa's icy surface (NASA Instrument Concepts for Europa Exploration (ICEE) 2), making terrestrial observations of biosignatures in ice environments using similar methodologies of particular interest before these instruments fly.

This dissertation employs high resolution mass spectrometry to investigate the use of intracellular organic compounds (compatible solutes) as survival strategies to buffer environmental change in sea-ice microbial cultures (Chapters 2) and in mixed polar communities (Chapter 4). The high intracellular concentrations of certain solutes in sea-ice microbes presented in Chapter 3 demonstrate the potential use of metabolites, and specifically abundant compatible solutes, as unique signatures of the sea-ice environment and its associated adaptive metabolisms

(biosignatures). Chapter 4 demonstrates a unique community metabolome within sea ice as compared to seawater and melting sea ice, all distinguishable by LC-MS metabolomics. This work highlights the power of combining experimental and *in situ* observations of microbial physiology to better understand the formation of organism-specific metabolic fingerprints in analog environments (sea ice) and their inherent connection to parameters unique to that environment (low temperature, high salinity, low light, etc.), as called for in the 2015 NASA Astrobiology Strategy. Together, these data suggest that microbial metabolome remodeling, including active repartitioning of intracellular compatible solute pools, plays a role in the adaptation to sea-ice conditions.

References

Aldridge BB, Rhee KY. 2014. Microbial metabolomics: Innovation, application, insight. *Curr Opin Microbiol* 19(1): 90–96. doi: 10.1016/j.mib.2014.06.009

Amin SA, Hmelo LR, Van Tol HM, Durham BP, Carlson LT, Heal KR, Morales RL, Berthiaume CT, Parker MS, Djunaedi B, et al. 2015. Interaction and signalling between a cosmopolitan phytoplankton and associated bacteria. *Nature* 522(7554): 98–101. doi: 10.1038/nature14488

Arrigo KR. 2014. Sea Ice Ecosystems. *Ann Rev Mar Sci* 6(1): 439–467. doi: 10.1146/annurev-marine-010213-135103

Arrigo KR. 2016. Sea ice as a habitat for primary producers. *Sea Ice: Third Edition*, edited by Thomas DN, 352–369. West Sussex, UK: John Wiley and Sons, Ltd. doi: 10.1002/9781118778371.ch14

Arrigo KR, van Dijken G, Pabi S. 2008. Impact of a shrinking Arctic ice cover on marine primary production. *Geophys Res Lett* 35(19): 1–6. doi: 10.1029/2008GL035028

Arrigo KR, Perovich DK, Pickart RS, Brown ZW, van Dijken GL, Lowry KE, Mills MM, Palmer MA, Balch WM, Bates NR, et al. 2014. Phytoplankton blooms beneath the sea ice in the Chukchi sea. *Deep Res Part II Top Stud Oceanogr* 105: 1–16. doi: 10.1016/j.dsr2.2014.03.018

Arrigo KR, Thomas DN. 2004. Large scale importance of sea ice biology in the Southern Ocean. *Antarct Sci* 16(4): 471–486. doi: 10.1017/S0954102004002263

Blachowicz A, Chiang AJ, Elsaesser A, Kalkum M, Ehrenfreund P, Stajich JE, Torok T, Wang CCC, Venkateswaran K. 2019. Proteomic and metabolomic characteristics of extremophilic fungi under simulated Mars conditions. *Front Microbiol* 10 (MAY): 1–16. doi: 10.3389/fmicb.2019.01013

Boetius A, Albrecht S, Bakker K, Bienhold C, Felden J, Fernández-Méndez M, Hendricks S, Katlein C, Lalande C, Krumpen T, et al. 2013. Export of algal biomass from the melting arctic sea ice. *Science* 339(6126): 1430–1432. doi: 10.1126/science.1231346

Boetius A, Anesio AM, Deming JW, Mikucki JA, Rapp JZ. 2015. Microbial ecology of the cryosphere: Sea ice and glacial habitats. *Nature Reviews Microbiology* 13: 677–690. doi: 10.1038/nrmicro3522

Boysen AK, Carlson LT, Durham BP, Groussman RD, Aylward FO, Ribalet F, Heal KR, White AE, DeLong EF, Armbrust EV, et al. 2021. Particulate metabolites and transcripts reflect diel oscillations of microbial activity in the surface ocean. *mSystems* 6(3): 1–18. doi: 10.1128/msystems.00896-20

Boysen AK, Heal KR, Carlson LT, Ingalls AE. 2018. Best-matched internal standard normalization in liquid chromatography-mass spectrometry metabolomics applied to environmental samples. *Anal Chem* 90(2): 1363–1369. doi: 10.1021/acs.analchem.7b04400

Bronselaer B, Winton M, Griffies SM, Hurlin WJ, Rodgers KB, Sergienko O V, Stouffer RJ, Russell JL. 2018. Change in future climate due to Antarctic meltwater. *Nature* 564(7734): 53–58. doi: 10.1038/s41586-018-0712-z

Brown TA, Belt ST. 2012. Closely linked sea icepelagic coupling in the Amundsen Gulf revealed by the sea ice diatom biomarker IP25. *J Plankton Res* 34(8): 647–654. doi: 10.1093/plankt/fbs045

Burkett VR, Wilcox DA, Stottlemyer R, Barrow W, Fagre D, Baron J, Price J, Nielsen JL, Allen CD, Peterson DL, et al. 2005. Nonlinear dynamics in ecosystem response to climatic change: Case studies and policy implications. *Ecol Complex* 2(4): 357–394. doi: 10.1016/j.ecocom.2005.04.010

Cape MR, Vernet M, Pettit EC, Wellner J, Truffer M, Akie G, Domack E, Leventer A, Smith CR, Huber BA. 2019. Circumpolar deep water impacts glacial meltwater export and coastal biogeochemical cycling along the west Antarctic Peninsula. *Front Mar Sci* 6(MAR): 1–23. doi: 10.3389/fmars.2019.00144

Carr MH, Belton MJS, Chapman CR, Davies ME, Geisslerk P, Greenbergk R, Mcewenk AS, Tuftsk BR, Greeley R, Sullivan R, et al. 1998. Evidence for a subsurface ocean on Europa. *Lett to Nat* 391: 363–365. doi: 10.1038/34857

Chan MA, Hinman NW, Potter-Mcintyre SL, Schubert KE, Gillams RJ, Awramik SM, Boston PJ, Bower DM, Des Marais DJ, Farmer JD, et al. 2019. Deciphering biosignatures in planetary contexts. *Astrobiology* 19(9): 1075–1102. doi: 10.1089/ast.2018.1903

Collins RE, Deming JW. 2013. An inter-order horizontal gene transfer event enables the catabolism of compatible solutes by *Colwellia psychrerythraea* 34H. *Extremophiles* 17(4): 601–610. doi: 10.1007/s00792-013-0543-7

Cox GFN, Weeks WF. 1983. Equations for determining the gas and brine volumes in sea-ice sample. *J Glaciol* 29(102): 306–316. doi: 10.1017/s0022143000008364

Deming JW, Collins RE. 2016. Sea ice as a habitat for Bacteria, Archaea and viruses. In *Sea Ice: Third Edition*, edited by Thomas DN, 326–351. West Sussex, UK: John Wiley and Sons, Ltd. doi: 10.1002/9781118778371.ch13

Deming JW, Young JN. 2017. The role of exopolysaccharides in microbial adaptation to cold habitats. In *Psychrophiles: From Biodiversity to Biotechnology*, edited by Rosa Margesin, 1225–1228. New York City, USA: Springer Cham. doi: 10.1007/978-3-319-57057-012

Dieckmann GS, Thomas DN. 2002. Antarctic sea ice – a habitat for extremophiles. *Science*

295(5555): 641–644. doi: 10.1007/sl0869-007-9037-x

Dudeja S, Bhattacherjee AB, Chela-Flores J. 2012. Antarctica as a model for the possible emergence of life on Europa. In: *Life on Earth and Other Planetary Bodies*. Springer, Dordrecht. pp. 407-419. doi: 10.1007/978-94-007-4966-5

Durham BP, Boysen AK, Carlson LT, Groussman RD, Heal KR, Cain KR, Morales RL, Coesel SN, Morris RM, Ingalls AE, et al. 2019. Sulfonate-based networks between eukaryotic phytoplankton and heterotrophic bacteria in the surface ocean. *Nat Microbiol* 4(10): 1706–1715. doi: 10.1038/s41564-019-0507-5

Durham BP, Sharma S, Luo H, Smith CB, Amin SA, Bender SJ, Dearth SP, Van Mooy BAS, Campagna SR, Kujawinski EB, et al. 2015. Cryptic carbon and sulfur cycling between surface ocean plankton. *Proc Natl Acad Sci* 112(2): 453–457. doi: 10.1073/pnas.1413137112

Eicken H. 1992. Salinity profiles of Antarctic sea ice: Field data and model results. *J Geophys Res* 97(92): 15545–15557. doi: 10.1029/92JC01588

Ewert M, Deming J. 2013. Sea ice microorganisms: Environmental constraints and extracellular responses. *Biology (Basel)* 2(2): 603–628. doi: 10.3390/biology2020603

Ewert M, Deming JW. 2014. Bacterial responses to fluctuations and extremes in temperature and brine salinity at the surface of Arctic winter sea ice. *FEMS Microbiol Ecol* 89(2): 476–489. doi: 10.1111/1574-6941.12363

Fernie AR, Obata T, Allen AE, Araújo WL, Bowler C. 2012. Leveraging metabolomics for functional investigations in sequenced marine diatoms. *Trends Plant Sci* 17(7): 395–403. doi: 10.1016/j.tplants.2012.02.005

Fiorini F, Borgonuovo C, Ferrante MI, Brönstrup M. 2020. A metabolomics exploration of the sexual phase in the marine diatom *Pseudo-nitzschia multistriata*. *Mar Drugs* 18(6): 1–18. doi: 10.3390/md18060313

Firth E, Carpenter SD, Sørensen HL, Collins RE, Deming JW. 2016. Bacterial use of choline to tolerate salinity shifts in sea-ice brines. *Elem Sci Anthr* 4: 000120. doi: 10.12952/journal.elementa.000120

Fischer E, Martínez GM, Renn NO. 2016. Formation and persistence of brine on mars: Experimental simulations throughout the diurnal cycle at the phoenix landing site. *Astrobiology* 16(12): 937–948. doi: 10.1089/ast.2016.1525

Fürch T, Preusse M, Tomasch J, Zech H, Wagner-Döbler I, Rabus R, Wittmann C. 2009. Metabolic fluxes in the central carbon metabolism of *Dinoroseobacter shibae* and *Phaeobacter gallaeciensis*, two members of the marine Roseobacter clade. *BMC Microbiol* 9: 209. doi: 10.1186/1471-2180-9-209

IPCC, 2022: Climate Change 2022: Impacts, Adaptation and Vulnerability. Contribution of Working Group II to the Sixth Assessment Report of the Intergovernmental Panel on Climate Change [H.-O. Pörtner, D.C. Roberts, M. Tignor, E.S. Poloczanska, K. Mintenbeck, A. Alegría, M. Craig, S. Langsdorf, S. Löschke, V. Möller, A. Okem, B. Rama (eds.)]. Cambridge University Press. Cambridge University Press, Cambridge, UK and New York, NY, USA, 3056 pp., doi:10.1017/9781009325844.

Hano T, Tomaru Y. 2019. Metabolomics-based approach to explore growth phase-dependent markers in cultured diatom *Chaetoceros tenuissimus*. *J Chromatogr B Anal Technol Biomed Life Sci* 1128(August): 121779. doi: 10.1016/j.jchromb.2019.121779

Heal KR, Durham BP, Boysen AK, Carlson LT, Qin W, Ribalet F, White AE, Bundy RM, Armbrust EV, Ingalls AE. 2021. Marine community metabolomes carry fingerprints of phytoplankton community composition. *mSystems* 6(3). doi: 10.1128/msystems.01334-20

Heal KR, Kellogg NA, Carlson LT, Lionheart RM, Ingalls AE. 2019. Metabolic consequences of cobalamin scarcity in the diatom *Thalassiosira pseudonan*a as revealed through metabolomics. *Protist* 170(3): 328–348. doi: 10.1016/j.protis.2019.05.004

Hoegh-guldberg AO, Bruno JF. 2010. The Impact of Climate Change on the World ' s Marine Ecosystems. *Science* 328(5985): 1523–1528. doi: 10.1126/science.1189930

Hoehler TM, Som SM, Kiang NY. 2018. Life's Requirements. In: DeegJuan H, Belmonte A, editors. *Handbook of Exoplanets*. Cham, Switzerland: Springer International Publishing. p. 1–22. doi: 10.1007/978-3-319-30648-3_74-1

Jansen E, Christensen JH, Dokken T, Nisancioglu KH, Vinther BM, Capron E, Guo C, Jensen MF, Langen PL, Pedersen RA, et al. 2020. Past perspectives on the present era of abrupt Arctic climate change. *Nat Clim Chang* 10(8): 714–721. doi: 10.1038/s41558-020-0860-7

Jansson JK, Hofmockel KS. 2020. Soil microbiomes and climate change. *Nat Rev Microbiol* 18(1): 35–46. doi: 10.1038/s41579-019-0265-7

Johnson SS, Anslyn E V., Graham H V., Mahaffy PR, Ellington AD. 2018. Fingerprinting non-terran biosignatures. *Astrobiology* 18(7): 915–922. doi: 10.1089/ast.2017.1712

Johnson WM, Longnecker K, Kido Soule MC, Arnold WA, Bhatia MP, Hallam SJ, Van Mooy BAS, Kujawinski EB. 2019. Metabolite composition of sinking particles differs from surface suspended particles across a latitudinal transect in the South Atlantic. *Limnol Oceanogr*: 1–17. doi: 10.1002/lno.11255

Jonsson P, Bruce SJ, Moritz T, Trygg J, Sjöström M, Plumb R, Granger J, Maibaum E, Nicholson JK, Holmes E, et al. 2005. Extraction, interpretation and validation of information for comparing samples in metabolic LC/MS data sets. *Analyst* 130(5): 701–707. doi: 10.1039/b501890k

Kang SH, Fryxell GA. 1992. *Fragilariopsis cylindrus* (Grunow) Krieger: The most abundant diatom in water column assemblages of Antarctic marginal ice-edge zones. *Polar Biol* 12(6–7): 609–627. doi: 10.1007/BF00236984

Kiene RP, Williams LPH. 1998. Glycine betaine uptake, retention, and degradation by microorganisms in seawater. *Limnol Oceanogr* 43(7): 1592–1603. doi: 10.4319/lo.1998.43.7.1592

Kirst GO, Thiel C, Wolff H, Nothnagel J, Wanzek M, Ulmke R. 1991. Dimethylsulfoniopropionate (DMSP) in ice algae and its possible biological role. *Mar Chem* 35(1–4): 381–388. doi: 10.1016/S0304-4203(09)90030-5

Koch CW, Cooper LW, Lalande C, Brown TA, Frey KE, Grebmeier JM. 2020. Seasonal and Latitudinal Variations in Sea Ice Algae Deposition in the Northern Bering and Chukchi Seas Determined by Algal Biomarkers. PLoS ONE. 15(4): e0231178. doi: 10.1371/journal.pone.0231178

Kohlbach D, Graeve M, Lange BA, David C, Schaafsma FL, van Franeker JA, Vortkamp M, Brandt A, Flores H. 2018. Dependency of Antarctic zooplankton species on ice algae-produced carbon suggests a sea ice-driven pelagic ecosystem during winter. *Glob Chang Biol* 24(10): 4667–4681. doi: 10.1111/gcb.14392

Kohlbach D, Lange BA, Schaafsma FL, David C, Vortkamp M, Graeve M, van Franeker JA, Krumpen T, Flores H. 2017. Ice algae-produced carbon is critical for overwintering of Antarctic krill *Euphausia superba*. *Front Mar Sci* 4(September): 310. doi: 10.3389/fmars.2017.00310

Krell A, Funck D, Plettner I, John U, Dieckmann G. 2007. Regulation of proline metabolism under salt stress in the psychrophilic diatom *Fragilariopsis cylindrus* (Bacillariophyceae). *J Phycol* 43(4): 753–762. doi: 10.1111/j.1529-8817.2007.00366.x

Kujawinski EB, Longnecker K, Alexander H, Dyhrman ST, Fiore CL, Haley ST, Johnson WM. 2017. Phosphorus availability regulates intracellular nucleotides in marine eukaryotic phytoplankton. *Limnol Oceanogr Lett* 2(4): 119–129. doi: 10.1002/lol2.10043

van Leeuwe MA, Tedesco L, Arrigo KR, Assmy P, Campbell K, Meiners KM, Rintala J-M, Selz V, Thomas DN, Stefels J, et al. 2018. Microalgal community structure and primary production in Arctic and Antarctic sea ice: A synthesis. *Elem Sci Anth* 6(4). doi: 10.1525/elementa.267

Lizotte MP. 2001. The contributions of sea ice algae to Antarctic marine primary production. *Am Zool* 41(1): 57–73. doi: 10.1093/icb/41.1.57

Lizotte MP, Sullivan CW. 1991. Photosynthesis-irradiance relationships in microalgae associated with Antarctic pack ice: evidence for in situ activity. *Mar Ecol Prog Ser* 71(2): 175–184.

doi: 10.3354/meps071175

Llewellyn CA, Sommer U, Dupont CL, Allen AE, Viant MR. 2015. Using community metabolomics as a new approach to discriminate marine microbial particulate organic matter in the western English Channel. *Prog Oceanogr* 137: 421–433. doi: 10.1016/j.pocean.2015.04.022

Lyon B, Mock T. 2014. Polar microalgae: New approaches towards understanding adaptations to an extreme and changing environment. *Biology (Basel)* 3(1): 56–80. doi: 10.3390/biology3010056

Lyon BR. 2011. A proteomics approach to investigate the physiology of dimethylsulfoniopropionate production in the sea-ice diatom, *Fragilariopsis cylindrus* [dissertation]. Charleston, SC: Medical University of South Carolina, Department of Molecular and Cellular Biology and Pathobiology.

Lyon BR, Bennett-Mintz JM, Lee PA, Janech MG, Ditullio GR. 2016. Role of dimethylsulfoniopropionate as an osmoprotectant following gradual salinity shifts in the sea-ice diatom Fragilariopsis cylindrus. *Environ Chem* 13(2): 181–194. doi: 10.1071/EN14269

Malin G, Turner SM, Liss PS. 1992. Sulfur : The plankton/climate connection. *J Phycol* 28(5): 590–597. doi: 10.1111/j.0022-3646.1992.00590.x

Marion GM, Fritsen CH, Eicken H, Payne MC. 2003. The search for life on Europa: Limiting environmental factors, potential habitats, and Earth analogues. *Astrobiology* 3(4): 785–811. doi: 10.1089/153110703322736105

Martin A, McMinn A. 2017. Sea ice, extremophiles and life on extra-terrestrial ocean worlds. *Int J Astrobiol* 17(1): 1–16. doi: 10.1017/S1473550416000483

McMinn A., Martin A, Ryan K. 2010. Phytoplankton and sea ice algal biomass and physiology during the transition between winter and spring (McMurdo Sound, Antarctica). *Polar Biol* 33(11): 1547–1556. doi: 10.1007/s00300-010-0844-6

McMinn Andrew, Pankowskii A, Ashworth C, Bhagooli R, Ralph P, Ryan K. 2010. In situ net primary productivity and photosynthesis of Antarctic sea ice algal, phytoplankton and benthic algal communities. *Mar Biol* 157(6): 1345–1356. doi: 10.1007/s00227-010-1414-8

McParland EL, Alexander H, Johnson WM. 2021. The osmolyte ties that bind: genomic insights into synthesis and breakdown of organic osmolytes in marine microbes. *Front Mar Sci* 8(July). doi: 10.3389/fmars.2021.689306

Meredith MP, King JC. 2005. Rapid climate change in the ocean west of the Antarctic Peninsula during the second half of the 20th century. *Geophys Res Lett* 32(19): 1–5. doi: 10.1029/2005GL024042

Moran MA, Kujawinski EB, Schroer WF, Amin SA, Bates NR, Bertrand EM, Braakman R, Brown CT, Covert MW, Doney SC, et al. 2022. Microbial metabolites in the marine carbon cycle. *Nat Microbiol* 7(4): 508–523. doi: 10.1038/s41564-022-01090-3

O'Brien DP. 1987. Direct observations of the behavior of *Euphausia superba* and *Euphausia crystallorophias* (Crustacea: Euphausiacea) under pack ice during the Antarctic spring of 1985. *Journal of Crustacean Biology* 7(3): 437–448. doi: 10.2307/1548293

Olsen LM, Laney SR, Duarte P, Kauko HM, Fernández-Méndez M, Mundy CJ, Rösel A, Meyer A, Itkin P, Cohen L, et al. 2017. The seeding of ice algal blooms in Arctic pack ice: The multiyear ice seed repository hypothesis. *J Geophys Res Biogeosciences* 122(7): 1529–1548. doi: 10.1002/2016JG003668

Overland J, Dunlea E, Box JE, Corell R, Forsius M, Kattsov V, Olsen MS, Pawlak J, Reiersen LO, Wang M. 2019. The urgency of Arctic change. *Polar Sci* 21(July 2018): 6–13. doi: 10.1016/j.polar.2018.11.008

Petrich C, Eicken H. 2010. Growth, Structure and Properties of Sea Ice. In *Sea Ice: Second Edition*, edited by Thomas DN and Dieckmann GS, Oxford, UK: Wiley-Blackwell. p. 23–77. doi: 10.1002/9781444317145.ch2

Poli A, Finore I, Romano I, Gioiello A, Lama L, Nicolaus B. 2017. Microbial diversity in extreme marine habitats and their biomolecules. *Microorganisms* 5(2): 1–30. doi: 10.3390/microorganisms5020025

Riaux-Gobin C, Poulin M, Dieckmann G, Labrune C, Vétion G. 2011. Spring phytoplankton onset after the ice break-up and sea-ice signature (Adélie Land, East Antarctica). *Polar Res* 30(1). doi: 10.3402/polar.v30i0.5910

Rivera-Valentín EG, Chevrier VF, Soto A, Martínez G. 2020. Distribution and habitability of (meta)stable brines on present-day Mars. *Nat Astron* 4(8): 756–761. doi: 10.1038/s41550-020-1080-9

Schmidt BE, Blankenship DD, Patterson GW, Schenk PM. 2011. Active formation of "chaos terrain" over shallow subsurface water on Europa. *Nature* 479(7374): 502–505. doi: 10.1038/nature10608

Schrimpe-Rutledge AC, Codreanu SG, Sherrod SD, McLean JA. 2016. Untargeted metabolomics strategies—Challenges and emerging directions. *J Am Soc Mass Spectrom* 27(12): 1897–1905. doi: 10.1007/s13361-016-1469-y

Seyler L, Kujawinski EB, Azua-Bustos A, Lee MD, Marlow J, Perl SM, Cleaves HJ. 2020. Metabolomics as an emerging tool in the search for astrobiologically relevant biomarkers. *Astrobiology* 20(10): 1251–1261. doi: 10.1089/ast.2019.2135

Sheridan JA, Bickford D. 2011. Shrinking body size as an ecological response to climate change. *Nat Clim Chang* 1(8): 401–406. doi: 10.1038/nclimate1259

Søreide JE, Leu EVA, Berge Jør, Graeve M, Falk-Petersen S. 2010. Timing of blooms, algal food quality and *Calanus glacialis* reproduction and growth in a changing Arctic. *Glob Chang Biol* 16(11): 3154–3163. doi: 10.1111/j.1365-2486.2010.02175.x

Stammerjohn S, Massom R, Rind D, Martinson D. 2012. Regions of rapid sea ice change: An inter-hemispheric seasonal comparison. *Geophys Res Lett* 39(6): 1–8. doi: 10.1029/2012GL050874

Stammerjohn SE, Martinson DG, Smith RC, Iannuzzi RA. 2008. Sea ice in the western Antarctic Peninsula region: Spatio-temporal variability from ecological and climate change perspectives. *Deep Res Part II Top Stud Oceanogr* 55(18–19): 2041–2058. doi: 10.1016/j.dsr2.2008.04.026

Tang YJ, Yi S, Zhuang WQ, Zinder SH, Keasling JD, Alvarez-Cohen L. 2009. Investigation of carbon metabolism in "*Dehalococcoides ethenogenes*" strain 195 by use of isotopomer and transcriptomic analyses. *J Bacteriol* 191(16): 5224–5231. doi: 10.1128/JB.00085-09

Torstensson A, Young JN, Carlson LT, Ingalls AE, Deming JW. 2019. Use of exogenous glycine betaine and its precursor choline as osmoprotectants in Antarctic sea-ice diatoms. *J Phycol* 70: 1–13. doi: 10.1111/jpy.12839

Vancoppenolle M, Meiners KM, Michel C, Bopp L, Brabant F, Carnat G, Delille B, Lannuzel D, Madec G, Moreau S, et al. 2013. Role of sea ice in global biogeochemical cycles: Emerging views and challenges. *Quat Sci Rev* 79: 207–230. doi: 10.1016/j.quascirev.2013.04.011

Vaughan DG, Marshall GJ, Connolley WM, Parkinson C, Mulvaney R, Hodgson DA, King OC, J. PC, Turner J. 2003. Recent rapid regional climate warming on the Antarctic Peninsula. *Clim Change* 60: 243–274. doi: 10.1023/A

Walther G, Post E, Convey P, Menzel A, Parmesank C, Beebee TJC, Fromentin J, I OH, Bairlein F. 2002. Ecological response to recent climate cnahge. *Nature* 416: 389–395. doi: 10.1038/416389a

Walther GR. 2010. Community and ecosystem responses to recent climate change. *Philos Trans R Soc B Biol Sci* 365(1549): 2019–2024. doi: 10.1098/rstb.2010.0021

Welsh DT. 2000. Ecological significance of compatible solute accumulation by micro-organisms: from single cells to global climate. *FEMS Microbiol Rev* 24(3): 263–290. doi: 10.1111/j.1574-6976.2000.tb00542.x

Woolway RI, Kraemer BM, Lenters JD, Merchant CJ, O'Reilly CM, Sharma S. 2020. Global lake responses to climate change. *Nat Rev Earth Environ* 1(8): 388–403. doi: 10.1038/s43017-020-0067-5

Yancey PH, Clark ME, Hand SC, Bowlus RD, Somero GN. 1982. Living with water stress: Evolution of osmolyte systems. *Science* 217(4566): 1214–1222. doi: 10.1126/science.7112124

Young JN, Schmidt K. 2020. It's what's inside that matters: physiological adaptations of high-latitude marine microalgae to environmental change. *New Phytol* 227: 1307–1318. doi: 10.1111/nph.16648

Zamboni N, Saghatelian A, Patti GJ. 2015. Defining the metabolome: Size, flux, and regulation. *Mol Cell* 58(4): 699–706. doi: 10.1016/j.molcel.2015.04.021

Chapter 2. POTENTIAL OF TEMPERATURE- AND SALINITY-DRIVEN SHIFTS IN DIATOM COMPATIBLE SOLUTE CONCENTRATIONS TO IMPACT BIOGEOCHEMICAL CYCLING WITHIN SEA ICE

A version of this chapter has been previously published as:

Dawson, H.M., Heal K.R., Boysen A.K., Carlson L.T., Ingalls A.E., Young J.N. (2020). Potential of temperature- and salinity-driven shifts in diatom compatible solute concentrations to impact biogeochemical cycling within sea ice. *Elem Sci Anth*. 8(25). https://doi.org/10.1525/elementa.421

2.1 ABSTRACT

Sea-ice algae are an important source of primary production in polar regions, yet we have limited understanding of their responses to the seasonal cycling of temperature and salinity. Using a targeted liquid chromatography mass spectrometry based metabolomics approach, we found that axenic cultures of the Antarctic sea-ice diatom, *Nitzschia lecointei*, displayed large differences in their metabolomes when grown in a matrix of conditions that included temperatures of –1 and 4°C, and salinities of 32 and 41, despite relatively small changes in growth rate. Temperature exerted a greater effect than salinity on cellular metabolite pool sizes, though the N- or S-containing compatible solutes, 2, 3-dihydroxypropane-1-sulfonate (DHPS), glycine betaine (GBT), dimethylsulfoniopropionate (DMSP), and proline responded strongly to both temperature and salinity, suggesting complexity in their control. We saw the largest (> 4-fold) response to salinity for proline. DHPS, a rarely studied but potential compatible solute, had the highest intracellular

concentrations among all compatible solutes of ~85 mM. When comparing the culture findings to natural Arctic sea-ice diatom communities, we found extensive overlap in metabolite profiles, highlighting the relevance of culture-based studies to probe environmental questions. Large changes in sea-ice diatom metabolomes and compatible solutes over a seasonal cycle could be significant components of biogeochemical cycling within sea ice.

2.2 INTRODUCTION

Sea ice is one of the most extensive habitats on Earth, accounting for 15–22 million km^2, or 4.1–6.1%, of global ocean area throughout the year (Arrigo et al., 2014). This unique biome is host to diverse microbial assemblages, including unicellular microalgae that are able to exploit microhabitats produced during sea-ice formation and aging (Arrigo, 2016). Sea-ice algae contribute to carbon fixation via photosynthesis in polar ecosystems, fixing an estimated 10–36 Tg C $year^{-1}$ in the Arctic and 24–36 Tg C $year^{-1}$ in the Antarctic, 2–10% and 1–3% of total annual production (ice + water column) in those regions, respectively (Arrigo, 2016). Though a relatively low fraction of annual production, sea-ice algae are a major source of fixed carbon for higher trophic levels in ice-covered waters, particularly through winter months (Horner and Schrader, 1982; Kottmeier and Sullivan, 1987; Arrigo, 2016; Kohlbach et al., 2017; O'Brien, 1987), and may act as a seeding population for highly productive summertime phytoplankton blooms (Lizotte, 2001; Riaux-Gobin et al., 2011; Tedesco et al., 2012; Arrigo, 2016). Sea-ice algae play an important role in polar biogeochemical cycling of carbon and other nutrients as well as climate-active gas production, namely dimethyl sulfide (DMS) and methane production mediated by bacterial transformations (Welsh, 2000; Vancoppenolle et al., 2013).

Sea-ice algae inhabit the underside of sea ice and its interior, within liquid brine inclusions formed by the exclusion and concentration of salt ions during ice formation (Hsiao, 1980; Horner and Schrader, 1982; Eicken, 1992). Seasonal cycles of ice formation and loss make this habitat both extreme and variable with respect to temperature, salinity, light and nutrients (Dieckmann and Thomas, 2002; Ewert and Deming, 2014). Diatoms dominate sea ice (Horner, 1985; Arrigo, 2014), with pennate diatoms (e.g., *Nitzschia*, *Fragilariopsis*, *Navicula*) being the most common (Günther and Dieckmann, 2001; Fiala et al., 2006).

One strategy diatoms use to mitigate thermal and osmotic stress is accumulating compatible solutes to high intracellular concentrations. Compatible solutes are used by cells of numerous organisms including animals, plants and microorganisms (Welsh, 2000; Chen and Murata, 2002; Yancey, 2005). Most compatible solutes are neutral at physiological pH, either zwitterionic or uncharged (Yancey, 2005), and generally fall into four major classes: free amino acids and derivatives, quaternary ammonium compounds, tertiary sulfonium compounds, and sugars or sugar alcohols (Slama et al., 2015). Compatible solutes can be accumulated to high concentrations without interfering with biochemical processes and can confer osmoprotection by maintaining turgor pressure and stabilizing enzymes (Yancey et al., 1982). Compatible solutes can also aid in cryoprotection by reducing the intracellular freezing point and helping maintain the protein hydration sphere, effectively a layer of free water around the protein, thus stabilizing the tertiary structure of cytosolic enzymes (Welsh, 2000; Lyon and Mock, 2014).

Polar marine diatoms produce a number of compatible solutes, including the sulfur-containing dimethylsulfoniopropionate (DMSP) and isethionic acid (Kirst et al., 1991; Boroujerdi et al., 2012; Lyon et al., 2016) and nitrogen-containing glycine betaine (GBT), proline, and homarine (Krell et al., 2007; Boroujerdi et al., 2012). Many compatible solutes also have other functions (e.g., proline is an amino acid), such that discerning the particular intracellular role(s) they are serving at any time may be difficult. For the purpose of this study on temperature and salinity, we use the term compatible solute broadly to refer to all metabolites that have been reported previously to display osmo- and/or cryoprotective capacity.

The production of high concentrations of compatible solutes, which requires considerable resources and energy, may influence cellular metabolism and resource allocation (Dickson and Kirst, 1987; Welsh, 2000; Spielmeyer and Pohnert, 2012). For example, the polar marine diatom

Fragilariopsis cylindrus accumulates proline in excess of 15 fmol cell^{-1}, approximately 150 mM, when grown at salinity 70 (Krell et al., 2007), and GBT can exceed 100 mM concentrations in mesopelagic phytoplankton (Spielmeyer and Pohnert, 2012). Highly abundant compatible solutes can also be released rapidly from marine algal and bacterial cells into the environment in response to relatively large salinity downshifts (>14) (Fulda et al., 1990; Firth et al., 2016; Torstensson et al., 2019). Once in the surrounding environment, microalgal-produced compatible solutes can be taken up by other members of the microbial community, such as heterotrophic bacteria, for the purpose of osmoregulation (Kiene and Hoffmann Williams, 1998; Spielmeyer et al., 2011) or as a source of carbon, nitrogen or energy (Welsh, 2000; Durham et al., 2019). This catabolism of compatible solutes by bacteria can lead to the production of climate-active gases such as DMS from DMSP (Kirst et al., 1991; Lyon et al., 2011). Additionally, the production and release of sulfur-containing compatible solutes may strongly impact the cryptic cycling of sulfur in sea ice and polar surface oceans through preferential exchange with bacterial partners, as suggested for cosmopolitan pelagic diatoms and bacteria (Durham et al. 2015; Durham et al. 2017; Durham et al. 2019). Thus the release and subsequent transformation of abundant compatible solutes may significantly contribute to the well-documented coupling between primary production and microbial heterotrophy in global oceans (Azam and Malfatti, 2007) and alter the flux of organic matter and the resultant balance between remineralization and storage of key elements (C, N, S, etc.) in polar oceans on a seasonal basis.

This study compares the metabolomes of the sea-ice diatom, *Nitzschia lecointei*, when grown in a matrix of conditions that include temperatures of –1 and 4°C, and salinities of 32 and 41. Most studies of compatible solute use in sea-ice diatoms have focused on more extreme shifts in temperature and salinity and/or single compatible solutes; here we focus on a more modest range

of conditions that have comparatively little effect on growth, which allows us to better isolate the impacts of temperature and salinity. Although we are focused on compatible solutes, our metabolomics approach detects other metabolites, some of which are also affected by growth conditions. We compare cultures with diatom-dominated Arctic sea-ice communities so that we can infer how the abundance of small, labile organic molecules impacts sea-ice communities and biogeochemical cycling.

2.3 METHODS

2.3.1 *Culture setup and experimental manipulation*

The obligately psychrophilic diatom *Nitzschia lecointei* was isolated from Antarctic bottom sea ice in the Amundsen Sea in 2011 by Torstensson et al. (2013). *N. lecointei* grows at temperatures of –2.3 to 8.3°C and salinities of 17 to 55 (Torstensson et al., 2013, 2019) with the highest growth rate measured at 5.1°C. Axenic stock cultures were established and maintained at –1°C and salinity 32 in 0.2 µm filtered artificial seawater (Enriched Seawater, Artificial Water, ESAW, Harrison et al., 1980) enriched with f/2 nutrients with silica (Guillard, 1975). Cultures were illuminated with cool-white lights on a 20:4 h light:dark cycle at 20–25 µmol photons m^{-2} s^{-1} of photosynthetically active radiation (PAR). Strict aseptic technique was used in order to maintain axenic cultures. Prior to experimental manipulations, cultures were checked for bacterial presence using DAPI fluorescent staining.

For experiments, cultures were grown in acid-washed, combusted borosilicate glass culture tubes. Axenic cultures were inoculated at a density of 7,000 cells mL^{-1}. Desired salinity of media was achieved by dilution or concentration of ESAW salt mix and confirmed by refractometry. Triplicate cultures (each replicate consisting of two pooled samples of 35 mL for 70 mL total per replicate) were grown in a matrix of two temperatures (–1°C and 4°C) and two salinities (32 and

41). Cultures were grown at –1°C in a Percival Scientific LT-36VL Low Temperature Chamber. Cultures were grown at 4°C in a custom-built insulated aquarium tank. Both setups were side-illuminated with cool-white lights at saturating light levels, 20–25 µmol photons m^{-2} s^{-1} and 20:4 h light:dark cycle. Temperatures for both setups were monitored throughout the experiment using Onset HOBO pendant data loggers.

Growth was monitored by relative fluorescence units (RFU) and cultures were sampled for metabolomics during exponential phase on day 21 of growth. Using combusted glassware and gentle vacuum filtration, cells were filtered onto 47 mm 0.2 µm Omnipore Membrane PTFE filters. Samples were kept on ice during the filtration process. Filters were stored in combusted aluminum foil and immediately frozen at –80°C until extraction. In separate, but identical experiments, RFU was measured in triplicate along with cell diameter and photosynthetic efficiency while carbon and nitrogen content were measured in quadruplicate. The similarity of RFU values and growth phase upon sampling between both sets of experiments supported making direct comparisons between experiments. Based on the tight correlation between RFU and cell number from this identical replicate experiment ($R^2 > 0.9$; Supplementary Figure 2.1), we converted RFU values from the original experiment to cell numbers as needed for normalization (i.e., metabolite moles per cell, etc.). RFU was measured at the same time each day, after 15 min of dark incubation and brief gentle mixing, by a Turner Designs TD-700 fluorometer. Cell number and diameter were measured using a Beckman Coulter Z2 Coulter Counter. To prevent cell lysis or changes in cell size, subsamples were diluted in isohaline and isothermal media. Photosynthetic efficiency (F_v/F_m) was measured using PAM fluorometry on replicate glass culture tubes that were kept on ice in the dark for 15 min before measurements were taken in a darkened room. F_v/F_m was determined by measuring the minimum fluorescence (F_0) at a low light level and maximum fluorescence (F_m)

after a short saturation pulse of measuring light and calculating the variable fluorescence ($F_v = F_m - F_0$). Particulate organic carbon (POC) and nitrogen (PN) samples were filtered through combusted (450°C, 4 h) 25 mm glass fiber filters (GF/F, pore size 0.7 µm pre-combustion) and frozen. Total organic carbon, nitrogen, and hydrogen of these filters was determined using an Exeter Analytical CE-440 CHN analyzer.

2.3.2 *Field sampling*

Samples were collected from first-year fast sea ice of the Chukchi Sea near Utqiaġvik (formerly Barrow), AK (at 71°22'22.5"N, 156°30'26.3"W) on 08 May 2017. Snow depth was recorded prior to clearing snow from an area of ice approximately 1 m^2. Ice cores were collected using a Kovacs MARK II ice auger of 9-cm internal diameter. For metabolomics, three dedicated cores were collected and the bottom 5-cm sections were placed into acid-clean 3-L polycarbonate tubs. These sections were then allowed to melt in a cold room at 4°C into prefiltered (0.2 µm) artificial brine solution prepared from Sigma sea salts using the isothermal-isohaline approach of Junge et al. (2004) to avoid osmotic shock and cell lysis. Approximately 500 mL of meltwater was filtered for metabolomics as described for cultures. Filtering was performed in a cold room at 4°C. An additional three cores were taken to measure chlorophyll *a* (Chl *a*), F_v/F_m, POC and PN from the bottom 5 cm after isohaline melts, filtering onto combusted GF/F filters and processing as described for cultures. Chl *a* and phaeopigment analyses was performed using un-acidified and acidified samples to correct for phaeopigments (Welschmeyer, 1994) by extracting filters in 90% v/v acetone/water for 24 h in the dark at –20°C and reading Chl *a* concentrations on a Turner Designs TD-700 (UNESCO, 1994). Temperature and salinity profiles were measured from a separate physical core at 5-cm intervals. Nutrients (phosphate, silicate, nitrate, nitrite, and ammonia) were measured on samples from the bottom 5 cm of the same core after direct melt

filtered through 0.2 µm syringe filter into acid-cleaned 60-mL Nalgene bottles and frozen at –20°C. Photosynthetically active radiation (PAR) was measured at the time of sampling through a 45° angled core using a Walz US-SQS spherical quantum sensor and ULM-500 light meter. In addition, the bottom 15 cm of three ice cores collected two days prior from a nearby field site (located 50 m away from the primary site and similar in environmental and biological parameters) were used to measure particulate extracellular polysaccharides (EPS) using the phenol-sulfuric acid method as detailed in Krembs et al. (2011), with conversion from glucose-equivalents (standards based on glucose concentrations) to carbon-equivalents.

2.3.3 *Extraction and analysis of metabolites*

Metabolite extraction, analysis, and data processing were carried out as described in Boysen et al. (2018). Briefly, polar and nonpolar metabolites were extracted using a modified Bligh-Dyer extraction of 1:1 methanol:water for the aqueous phase and dichloromethane for the organic phase (Bligh and Dyer, 1959; Canelas et al., 2009). Only metabolites extracted in the aqueous phase were analyzed for this study. For normalization, some isotope-labeled internal standards were added before and some after extractions, as in Boysen et al. (2018) and listed in Supplementary Table 2.1. Samples were stored at –80°C after extraction and before analysis.

Analysis of metabolite extracts was performed using liquid chromatography-mass spectrometry (LC-MS) exactly as in Boysen et al. (2018). Compounds were separated via liquid chromatography with a Waters Acquity I-Class UPLC, using reversed phase (RP) and hydrophilic interaction liquid chromatography (HILIC). Mass spectrometry parameters for targeted analytes were optimized by infusion of a pure metabolite standard for each. Targeted mass spectrometry data were acquired using a Waters Xevo TQ-S triple quadrupole (TQS) with electrospray ionization (ESI) in selected reaction monitoring mode (SRM) with polarity switching. Untargeted

mass spectrometry data was acquired using a Thermo QExactive HF (QE) with ESI to quantify compounds that were overloaded on the TQS.

For all metabolite data, peaks were integrated using Skyline for small molecules (MacLean et al., 2010), and integrated peaks were run through an in-house quality control and normalized via best-matched internal standard (B-MIS) normalization as in Boysen et al. (2018). In the culture experiment, peak areas were normalized to RFU measured on the sample from which metabolites were extracted. Field sample data were normalized to moles of POC on each filter, calculated using the measured moles of carbon per liter of meltwater. For metabolites below detection in some but not all treatments, fold changes were calculated by assigning a value corresponding to the limit of detection (3 × peak area for that compound in the blank +100), which underwent B-MIS and biological normalization as above, as in Lu et al. (2019). These numbers therefore represent a conservative estimate of the fold change.

2.3.4 *Relative and absolute metabolite abundances*

LC-MS peak areas are influenced by both the amount of a compound injected and its ionization efficiency. Thus, the peak area of two compounds within a sample may differ even if their concentrations are the same. However, normalized peak areas of a given compound can be compared between similar samples, here referred to as relative abundance, as they are a measure of the abundance of a compound relative to the biomass in each sample (i.e., peak area per RFU). DMSP may volatilize during sample processing resulting in some loss of this compound. Good agreement among replicates suggests that losses are similar across samples and therefore our measured relative concentrations can be compared across culture treatments as a minimum value. For the majority of metabolites, relative abundance data were collected on the TQS. For a small subset of overloaded metabolites (arginine, DHPS, DMSP, GBT, glutamic acid, glutamine, and

proline), relative abundance data were collected on the QE. We were able to calculate absolute concentrations for select metabolites, including proline (in field and culture samples), for which isotopically-labeled standards were added to samples before or after extraction as a part of the internal standard suite (Supplementary Table 2.1). All of these calculations of absolute concentration were performed using data from the TQS except for proline, for which we used data from the QE. In addition, we calculated absolute concentrations of DHPS, GBT, and choline (in field and culture samples) as well as homarine, trigonelline, proline betaine, and hydroxyectoine (in field samples only) by standard additions in matrix using the TQS. We express absolute concentrations in culture in terms of femtomole per cell, using the relationship between RFU and cell numbers ($R^2 > 0.9$, Supplementary Figure 2.1), as millimolar intracellular concentration, using cell volume calculated from measured cell diameter (Supplementary Figure 2.2) and as a concentration per mole of particulate organic carbon (µmol mol C^{-1}) for field and culture comparisons.

2.3.5 *Statistical analysis*

Measures of general cell physiology (growth rate, photosynthetic efficiency, carbon content, C:N) and the abundance of individual metabolites were analyzed with two-factor analysis of variance (ANOVA) using R Statistical Software. Post-hoc Tukey's HSD (honestly significant difference) tests were used to explore significant relationships between all treatments when a significant interaction effect between temperature and salinity was observed. If no significant interaction was observed, comparisons were made between total averages of each temperature or salinity treatment (i.e., $n = 6$). Detailed statistics from ANOVA are listed in supplemental tables, as indicated throughout. For comparisons of metabolite abundances across the entire targeted metabolome of *N. lecointei*, fold changes and *p*-values were calculated using unpaired *t*-tests. For these univariate

statistics on the targeted metabolome, *p*-values were corrected for false discovery rate (Benjamini and Hochberg, 1995). A probability level of ≤ 0.05 was used in determining statistical significance in all analyses. For comparison of absolute concentrations of select metabolites between culture and field samples, a linear regression was used and regression results reported with the adjusted R^2 and *p*-value.

2.4 RESULTS

2.4.1 *General cell physiology of Nitzschia lecointei cultures at different temperatures and salinities*

Growth rates and photosynthetic efficiency (F_v/F_m) showed small responses over the range of temperature and salinity tested. Specific growth rates were on average ~10% higher at 4°C compared to –1°C and at lower salinity (32) compared to higher salinity (41) ($p < 0.05$; Figure 2.1a, Supplementary Table 2.2). Photosynthetic efficiency (F_v/F_m) was generally high in all treatments, approaching the theoretical optimum for marine microalgae (~0.6, Figure 2.1b; versus 0.65, Schreiber, 2004), though F_v/F_m was 6% higher in cultures grown at –1°C than those grown at 4°C ($p < 0.01$; Figure 2.1b, Supplementary Table 2.2). Carbon content per cell was, on average, 30% higher at warmer temperatures compared to colder temperatures, and 20% higher at lower salinity compared to high salinity ($p < 0.001$ and $p < 0.01$, respectively; Figure 2.1c, Supplementary Table 2.2). C:N ratios and cell size were also higher at warmer and fresher conditions, concurrent with increased cellular carbon content (Figure 2.1d, Supplementary Figure 2.2).

2.4.2 *Metabolome changes in Nitzschia lecointei at different temperatures and salinities*

A total of 84 metabolites (Supplementary Table 2.3) were detected in *N. lecointei* with our targeted approach. A full list of targeted analytes searched can be found in Boysen et al. (2018). Of the 84 metabolites detected, 35 were significantly different (unpaired *t*-test, $p < 0.05$) between temperature treatments (Figure 2.2a). Most (30) of these metabolites only responded significantly to temperature under one salinity condition, while five metabolites responded to temperature under both salinity treatments. The direction of change was approximately evenly split, with 20 metabolites increased in the cold (–1°C) and 15 increased in the warm (4°C). In comparison, only three metabolites showed a significant difference between salinity treatments (Figure 2.2b). For these three compounds, relative abundance was significantly higher at salinity 32 when grown at –1°C (Figure 2.3).

The bulk of significant metabolite pool changes were due to changes in temperature at a salinity of 32 (Figure 2.3). Overall, there were more metabolites with a statistically significant change in relative abundance and with a greater magnitude of change with a temperature difference of 5°C than with a salinity change of 9. Of the five metabolites that responded to temperature at both salinities, UDP-glucose and homoserine increased at cold temperatures, whereas methylthioadenosine, aconitic acid, and carnitine decreased.

Many of the metabolites that were enriched under subzero conditions are known to act as compatible solutes for cryo- and osmoprotection (e.g., proline and DMSP) or are precursors of compatible solutes (e.g., methionine, choline, and glutamate), while some well-known compatible solutes, e.g. GBT, did not show significant changes in abundance using our strict definition. Many cofactors (NADP, ADP, NAD, AMP, and FAD) were also enriched. Higher abundances of the coenzyme B_{12} suggests higher uptake from the media since diatoms do not biosynthesize this

cofactor. Depleted metabolites at cold temperatures include those involved in the citric acid cycle (e.g., ketoglutaric acid and aconitic acid), along with sulfur-containing metabolites that have been associated with bacterial-algal interactions such as taurine, hypotaurine, and sulfolactic acid (Di Martino et al., 2013; Amin et al., 2015; Landa et al., 2017; Durham et al., 2019; Spietz et al., 2019). Metabolites whose relative abundance differed significantly with salinity did not change significantly with temperature. Isoleucine, N-acetyl-lysine, and tyrosine were all reduced at high salinity at subzero temperature (Figure 2.3).

2.4.3 *Comparison of sea-ice diatom metabolomes from cultures and the field*

To determine whether a metabolomic analysis of *N. lecointei* cultures could be representative of sea-ice diatom communities, we compared our axenic laboratory culture of *N. lecointei* with a diatom-dominated sea-ice community collected from first-year sea ice near Utqiaġvik, AK, in May 2017 (Figure 2.4a). A dense algal layer was visible within the bottom 5 cm of ice (Figure 2.4b). Light microscopy revealed a diatom-dominated community, with the predominant species being *Nitzschia frigida* (Figure 2.4c), a commonly observed and abundant pennate diatom in both Arctic and Antarctic sea ice (Hsiao, 1980; Horner and Schrader, 1982; Grossi and Sullivan, 1985; Aletsee et al., 1992; Michel et al., 2002), and the same genus as used in our laboratory study. Field data were compared to the *N. lecointei* culture grown at a salinity of 32 and temperature of –1°C, as this treatment experienced conditions closest to the in situ conditions of temperature (–1.3°C), salinity (30). In addition, light intensity (10–50 µmol photons m^{-2} s^{-1}) in the bottom sea ice at the time of collection (morning) closely matched our cultures. F_v/F_m were similar (0.50 ± 0.02 in the field and 0.58 ± 0.02 in cultures) (Table 2.1 and Figure 2.1b), as were C:N ratios (9.1 ± 0.1 in the field versus 8.6 ± 0.2 in culture) (Table 2.1 and Figure 2.1d).

Within our targeted compounds, more metabolites (104) were detected in the field samples than in the cultures (84) (Figure 2.5 inset), though the majority (74) were observed in both sample types. A complete comparison of compounds detected by sample type is provided in Supplementary Table 2.4. While we are unable to compare directly the relative abundances of metabolites between field and culture samples due to different matrix effects in the samples that affect ionization and the challenge of determining biomass in the field where detritus is present, we compare a subset of metabolites for which we obtained absolute concentrations normalized to either cell carbon in culture or moles of POC in the field (Figure 2.5 and Table 2.2). We found a strong correlation ($R^2 = 0.87$, $p = 3 \times 10^{-7}$, Figure 2.5), with most metabolites generally 2-fold enriched relative to carbon in the culture than in the field, and compatible solutes DHPS, proline, and GBT were 5- to 8-fold more enriched with respect to carbon in the culture than the field (Table 2.2). Notable exceptions were the metabolites taurine and isethionic acid, which were at higher concentrations in the field than in the culture samples (Figure 2.5). Homarine was at a lower concentration than GBT in the field (see Table 2.2) but was near the detection limit and could not be quantified in the cultures (Figure 2.5). Other potential N- and S-containing compatible solutes that were detected in field samples but were either not detected or quantifiable in culture samples included trigonelline, proline betaine, and hydroxyectoine (Table 2.2), though all at comparatively low concentrations (<15 μmol mol C^{-1}). Variation between triplicate cores was high in the field (Table 2.2), likely due to heterogeneity of algal biomass within sea ice.

2.4.4 *A closer look at highly abundant compatible solutes at varying temperature and salinity*

Metabolites with the highest measured absolute concentrations in culture and in the field (proline, GBT, and DHPS), and those that fall furthest from the regression line between culture and field samples (isethionic acid, taurine, methionine) are all S-containing compatible solutes or their

precursors. It is worth noting that though we did not calculate absolute concentrations of DMSP due to the possibility of evaporation during sample processing, its peak area and estimated ionization efficiency suggest that DMSP could be as or more concentrated than DHPS.

Within our targeted metabolome analysis in Figure 2.2, few metabolites showed significant differences in relative abundance due to salinity. However, this test was highly conservative due to the large number of metabolites analyzed and may have masked more nuanced responses. A closer inspection of the highly abundant compatible solutes (GBT, proline, DHPS and DMSP) using a two-way ANOVA revealed enrichment at both subzero temperatures and higher salinities (Figure 2.6, Supplementary Table 2.5) but the pattern and significance of abundance varied between compatible solutes.

Proline, which had intracellular concentrations of 10–50 mM (Table 2.3), responded to both temperature and salinity with no interaction between the two variables. Proline abundance was 142% higher at salinity 41 as compared to salinity 32 ($p < 0.0001$) and 62% higher at –1°C as compared to 4°C ($p < 0.01$; Figure 2.6a, Supplementary Table 2.5). Intracellular concentrations of GBT ranged from 30 to 70 mM (Table 2.3) and displayed an interactive response to temperature and salinity (Figure 2.6b). GBT concentration doubled at salinity 41 as compared to 32 when grown at 4°C ($p < 0.001$, Supplementary Table 2.5) but not at –1°C. GBT abundance also increased (33%) at warmer temperatures but only at a salinity of 41 ($p < 0.05$; Supplementary Table 2.5), not 32. The precursor to GBT, choline, was only significantly more abundant in response to subzero temperature (Figure 2.3) and was detected at a much lower intracellular concentrations (0.5–1 mM; Table 2.3) than GBT.

DHPS was detected in *N. lecointei* at intracellular concentrations ranging from 45 to 85 mM depending on the treatment, making it the most abundant quantified metabolite (Table 2.3).

There was a significant interaction between temperature and salinity for DHPS abundance (Supplementary Table 2.5). DHPS abundance was 55% higher at salinity 41 compared to 32 when grown at 4°C (Figure 2.6d, $p < 0.05$; Supplementary Table 2.5). DHPS abundance was also 81% higher when grown at –1°C as compared to 4°C at a salinity of 32 ($p < 0.01$; Supplementary Table 2.5).

The relative abundance of DMSP followed the same general pattern of response to temperature and salinity as DHPS (Figure 2.6c). Changes in DMSP across treatments showed comparatively high abundance in all treatments compared to the warmer and less salty treatment. DMSP abundance was 89% higher at salinity 41 as compared to 32 when grown at 4°C ($p < 0.01$; Supplementary Table 2.5) but not at –1°C. DMSP abundance was also 81% higher when cells were grown at –1°C as compared to 4°C at a salinity of 32 ($p < 0.01$; Supplementary Table 2.5) but not at 41. The intracellular concentration of methionine (a precursor to DMSP) was significantly higher in the subzero treatment (Figure 2.3) and its concentration was 0.1–0.2 mM (data not shown).

2.5 DISCUSSION

2.5.1 *Experimental conditions tested and general cell physiology*

Arrigo and Sullivan (1992) suggested that while temperature and salinity are physically co-varying in sea ice, the physiological responses to each factor is independent, for they found that temperature and salinity had a multiplicative but independent effect on Antarctic sea-ice microalgal growth and photophysiology. Our matrix of temperatures (–1°C vs 4°C) and salinities (32 vs 41) reflect conditions sea-ice diatoms may experience in bottom sea ice flushed with seawater and in the water column upon melt, and intentionally included a treatment not matched to the sea-ice environment (4°C and 41) to allow us to disentangle the individual influences of

temperature and salinity on metabolite abundances in *N. lecointei*. Our conditions allowed for similar growth in all treatments such that we could examine the impacts of temperature and salinity, rather than growth rate, on metabolite concentrations.

The range of temperature and salinity in our experimental matrix had little effect on growth rate and photophysiology. While a 10% increase in growth rate with a 5°C increase in temperature was smaller than expected based on Arrhenius equations, a growth response curve by Torstensson et al. (2013) suggests that *N. lecointei* has a broad optimum temperature range that may encompass the temperatures we tested. Alternatively, cells may have increased in size at the warmer temperature rather than increasing growth rate, as we observed significant increases in carbon per cell and cell size (Figure 2.1 and Supplementary Figure 2.2), which could be due to an actual increase in cell size or an increase in the production of cell-associated EPS. EPS production is sensitive to both temperature and salinity for sea-ice microbes (Krembs et al., 2002; Torstensson et al., 2019). We measured pEPS at high concentrations in the field (78 µM carbon; Table 2.1), and when used to correct C:N ratios in our field samples, the mean values were closer to Redfield (7.9 versus 9.1).

2.5.2 *Broad metabolome changes in environmental context*

The metabolome of *N. lecointei* differed among treatments despite the relatively small changes in cell growth. In particular, 2- to 3-fold changes in millimolar concentrations of compatible solutes highlight the importance of considering the metabolic response of sea-ice algae to changing environments. Temperature had a much greater effect on the metabolome than salinity, which could be due to the direct, and exponential, effect that temperature has on all biochemical reactions via enzyme kinetics, whereas cells respond to external changes in salinity by altering key processes to maintain a constant internal osmotic pressure (Yancey et al., 1982). Some compatible solutes

can mitigate both temperature and osmotic stress but do so in different ways: cryoprotectants prevent cell freezing via freezing point depression, but do not actively control cell temperature, whereas osmoprotectants actively alter internal osmotic pressure. The stronger response to temperature at 32 salinity compared to 41 may be due to the multiplicative effect of both temperature and salinity; i.e., if metabolites had already responded to high salinity, they might not show as large a response to temperature.

The metabolites with significantly different relative abundances in response to colder temperature, compatible solutes and their precursors, as well as various cofactors, were generally increased. In contrast, those metabolites reduced in abundance were involved in the mobilization of energy reserves (e.g carnitine) and energy production in the citric acid cycle (e.g., ketoglutaric acid and aconitic acid). Also, a number of metabolites implicated in algal-bacterial interaction and nutrient exchange (e.g., tryptophan, taurine, hypotaurine, sulfolactic acid) decreased at the colder temperature. Metabolite pools can change via altered metabolite production or consumption. For metabolites that provide cryoprotection, an increase in pool size would enhance cell survivability, while increases in enzyme cofactors may compensate for slow biochemical reactions at subzero temperatures. Many other organosulfur compounds involved in algal-bacterial interactions may be depleted as resources are redirected to the production of the organosulfur compatible solutes DHPS and DMSP at subzero temperatures. The temperature sensitivity of metabolites that have been associated with algal-bacterial interaction highlights the role temperature may play in dictating these compound-specific interactions in sea-ice environments. Whether the decrease in metabolites involved in energy metabolism is due to slower production or faster depletion of the metabolite pools at cold temperatures is not clear, but, their responses to changing temperature and salinity

may help explain how *N. lecointei* is able to maintain its growth rate while challenged with a fluctuating environment.

2.5.3 *Complex response of compatible solutes to environmental change*

Compatible solutes with N and S could be significant components of the seasonal cycling of N and S in sea ice. Other compatible solutes, such as many small carbohydrates, are not the focus of this study but could also be important for cryo- and osmoprotection (Greenway and Setter, 1979; Reed et al., 1984; Warr et al., 1984; Ferjani et al., 2003). For example, glucosylglycerol doubled in abundance at the colder culture temperature while sucrose was not significantly affected by either temperature or salinity. We did not quantify these compounds in absolute terms, so cannot comment on their relative contribution to compatible solute pools.

We found GBT, proline, and DHPS in high concentration (μmol mol C–1) in both our culture and field samples. GBT and proline, along with DMSP can act as osmolytes and/or cryoprotectants in polar diatoms (Dieckmann and Thomas, 2002; Krell et al., 2007; Boroujerdi et al., 2012; Lyon and Mock, 2014; Lyon et al., 2016). We detected two other compatible solutes known to occur in diatoms, homoserine (Bromke et al., 2013) and isethionic acid (Boroujerdi et al., 2012), in *N. lecointei*. DMSP, proline, DHPS and GBT had different patterns in response to temperature and salinity which may be due to other metabolic roles beyond osmo- and cryoprotection, constitutive versus inducible regulation, and/or preferential use dependent on cellular resource allocation. The nuanced response of these compounds suggests compatible solutes may play multiple and unique roles in the cell.

In our study, proline showed the largest response, > 4-fold higher at –1°C and salinity 41 compared to 4°C and salinity 32. Even with the 30% salinity increase alone we observed > 2-fold increase in proline. This magnitude of change is comparable to the 4.5-fold increase in proline

concentration in *F. cylindrus* in response to a hypersaline shock (a salinity increase of ~100% from 34–70 at 0°C), which was stressful enough to arrest growth temporarily (Krell et al., 2007). Perhaps the large response by *N. lecointei* to seasonal temperature changes may be an important adaptation enabling its success in sea ice. However, while the magnitude of change in proline concentration is similar, intracellular concentrations of proline varied between the two studies — the observed 4-fold increase of proline in *F. cylindrus* estimated as a 30–150 mM increase in intracellular concentration compared to 10–50 mM in N. lecointei (Table 2.3). While *N. lecointei* has lower intracellular concentrations of proline, its larger cell size (Olenina et al., 2006; Torstensson et al., 2019) and ability to form dense mats within sea ice means that *N. lecointei* proline production could still be important for biogeochemical cycling.

GBT had intracellular concentrations similar to proline (~30 mM) but was less responsive, doubling in abundance at higher salinity but only at 4°C and no clear response to temperature. GBT may be regulated constitutively or act only as an osmoprotectant in *N. lecointei*. Other evidence implicates GBT as an osmoprotectant in diatoms (Boroujerdi et al., 2012; Torstensson et al., 2019) but as a cryoprotectant only in plants (Chen and Murata, 2002). Torstensson and colleagues found that GBT is taken up from the environment to a greater extent under hypersaline conditions and rapidly expelled from *N. lecointei* during a hypo-osmotic shock (Torstensson et al., 2019), further highlighting the potential import of GBT in biogeochemical cycling.

The two abundant, sulfur-containing compatible solutes, DMSP and DHPS, showed similar patterns of increase with colder temperature and higher salinity, though the response does not appear to be additive. DMSP responds to salinity in other polar microalgae (Lyon et al., 2016) and to temperature in polar macroalgae (Karsten et al., 1996), but little is known about the role of DHPS in polar algae. While we did not quantify the absolute concentration of DMSP in this study,

concentrations of 15 mM have been reported in *F. cylindrus* grown at 0°C and a salinity of 35 (Lyon et al., 2016). Surprisingly, the concentrations of DHPS in *N. lecointei* are very high (70–85 mM at salinity 41), approximately 5- to 10-fold greater than has been measured in mesophilic diatom species (Durham et al., 2019) and 2- and 3-fold higher than we measured for GBT and proline, respectively. DHPS was also the most abundant metabolite we quantified in our field samples.

Recent work highlighted the importance of DHPS in sulfur cycling and carbon flux in the surface ocean (Durham et al., 2015, 2017, 2019; Landa et al., 2017, 2019), and its increased abundance with salinity has been noted in the chemoautotrophic bacteria *Sulfurimonas denitrificans* (Götz et al., 2018) and mesophilic diatom *Thalassiosira pseudonana* (Durham et al., 2019). Considering the apparent similarities in the role of DMSP and DHPS as cryo- and osmoprotectants, further investigation is needed to determine whether DHPS production and use could impact the production and release of DMSP, and ultimately the production of the climate-active gas, DMS (Kirst et al., 1991; Welsh, 2000; Lyon et al., 2011; Vancoppenolle et al., 2013). DHPS production may also be connected with the production and use of isethionic acid, as the biosynthesis routes for both compounds in eukaryotic phytoplankton are linked (Durham et al., 2019). Interestingly, isethionic acid is abundant in *F. cylindrus* (Boroujerdi et al., 2012) and in our field samples, despite its low concentration in *N. lecointei*, suggesting species-specific compatible solute use, even within polar diatoms.

2.5.4 *Relevance of sea-ice algal culture work to the sea-ice community*

The metabolome in our axenic *N. lecointei* culture showed strong similarities with a sea-ice community dominated by *N. frigida*, with the majority of metabolites found in both sample types and a similar pattern of expression in the subset of metabolites we were able to quantify (for

example, DHPS is approximately 3-fold more abundant than proline and GBT, which are of similar concentrations). A notable exception was isethionic acid, and to a lesser extent homarine, which were considerably higher in the field than the *N. lecointei* cultures (near the detection limit). Homarine and isethionic acid may be produced by other diatoms or sea-ice organisms (Nothnagel, 1995; Keller et al., 2004; Boroujerdi et al., 2012; Gebser and Pohnert, 2013; Scholz and Liebezeit, 2012; Fenizia et al., 2020). The lower absolute concentrations of metabolites in the field were likely due to differences in comparing an exponentially growing culture with a mixed sea-ice community that included non-*Nitzschia* diatoms, other organisms, and detrital material collected on a 0.2 µm filter (Horner, 1985; Arrigo et al., 2014; van Leeuwe et al., 2018; Tedesco et al., 2012) that may have diluted the metabolite signals. The overall similarities observed here suggest that results from culture studies can be applied to the field, making targeted metabolomics a powerful approach to tease apart the fine-scale effects of temperature and salinity on the metabolism of sea-ice diatoms.

2.5.5 *Potential impact of compatible solutes on N cycling in sea ice*

Fluctuations in the intracellular concentration of N-rich compatible solutes in response to environmental shifts could be a significant source/sink of available nitrogen within bottom sea ice. In the case of a sudden salinity downshift, as occurs during ice melt, cold-adapted bacteria have been shown to release compatible solutes rapidly, on subsecond timescales (Firth et al., 2016). Additionally, *N. lecointei* expelled 85% of the intracellular pool of GBT within 68 h following a sudden salinity downshift from 31 to 17 (Torstensson et al., 2019). Assuming proline and homarine have a similar response to salinity downshifts as GBT, an 85% efflux of the intracellular pool of these three compounds, as measured here in the field, during ice melt would equal ~1 µM of compatible solute derived organic nitrogen being released into the equivalent water parcel of a

melted 5 cm × 9 cm ice section (see Supplementary Table 2.6 for calculation). This concentration of organic nitrogen is about one-tenth of the inorganic nitrate concentration in our field samples (Table 2.1). There are few existing measures of dissolved organic nitrogen (DON) in sea ice, but Retelletti Brogi et al. (2018) measured ~10–15 µM DON in the bottom 15 cm of sea ice in Cambridge Bay (Canadian Arctic) during April–May.

While our estimated organic nitrogen input may be a liberal estimation, it suggests that the release during ice melt of three N-containing compatible solutes alone (less the undefined total pool of nitrogen-containing compatible solutes capable of such efflux) could impact N cycling and heterotrophic production in sea ice considerably, for they could be taken up readily by other organisms and used as compatible solutes (Kiene and Hoffmann Williams, 1998; Spielmeyer et al., 2011; Firth et al., 2016; Torstensson et al., 2019) or as carbon, nitrogen or energy sources (Welsh, 2000; Cherrier and Bauer, 2004). Additionally, respiration of N-containing compatible solutes by sea-ice bacteria may alter the available ammonium pool in sea ice and fuel nitrification (Firth et al., 2016). The release and recycling of N-containing compatible solutes is likely to be more important to N cycling in oligotrophic regions of the Arctic than the coastal regions (where our samples were collected), or the Antarctic, where nitrate concentrations in sea ice are generally higher (up to 8 µM in bottom sections and up to 27 µM in gap layers of ice floes; Kattner et al., 2004). As sea-ice algae are likely producing and releasing these compounds continuously throughout their lives either constitutively or in response to frequent environmental shifts, their cumulative contribution to the dissolved organic matter (DOM) pool may be much larger than the concentration we observe from an instantaneous metabolomic measurement. Characterizing the suite of algal compatible solutes and quantifying their release into the DOM pool is key to fully assessing their importance in biogeochemical cycling in sea ice.

2.6 CONCLUSIONS

Temperature and salinity change dramatically with the seasonal cycling of sea ice, yet little is known about how sea-ice diatoms are physiologically adapted to survive these changes. Here we have shown that an Antarctic sea-ice diatom, *Nitzschia lecointei*, maintains a differentially regulated suite of compatible solutes when grown under temperature and salinity variations well within what they would experience over a seasonal cycle. Many of these compatible solutes were found in similar abundance ratios in a natural bottom sea-ice community, showing the relevance of model organisms in teasing apart complex interactions of factors within sea ice. The varied sensitivity of compatible solute responses suggests that a complex suite of osmo- and cryoprotectant compounds are utilized concurrently to mitigate environmental stress, which in turn may impact biogeochemical cycling and ecosystem dynamics in sea ice over the season. This work highlights that detailed analyses of intracellular composition, such as the metabolomic approach used here, are needed to estimate accurately the impact of cell-level physiological responses of sea-ice algae to temperature and salinity on the surrounding community and environment.

2.7 DATA ACCESSIBILITY STATEMENT

Metabolomics data are available in Metabolomics Workbench under Study ID ST001393 (https://www.metabolomicsworkbench.org/data/index.php).

2.8 ACKNOWLEDGEMENTS

This work was funded by the Beatrice Crosby Booth Endowed Fellowship (HMD), University of Washington Graduate Top Scholar Award (HMD), grants from the National Science Foundation (174465, HMD and JNY; OCE-1228770, AEI; GRFP to AKB and KRH) and the Simons Foundation (SF Award ID 385428, AEI; Award ID 598819, KRH), and JNY Start-up funds from

the University of Washington, School of Oceanography. The opportunity to sample Arctic sea ice was provided by Jody W. Deming through funding from the Gordon and Betty Moore Foundation, Grant 5488. We would like to thank Jody W. Deming for insightful discussion and the opportunity to sample sea ice; Anders Torstensson for providing the axenic culture strain of *N. lecointei*, field photography, and for useful discussions; Bryndan P. Durham for helpful discussions about the role of DHPS; the Ukpeaġvik Iñupiat Corporation Science team for essential logistical support for sea-ice collection; the members of our larger field team for support: Shelly Carpenter, Anders Torstensson, Max Showalter, and Zac Cooper; Regina Lionheart, Alexa Weid, and Natalie Kellogg for assistance with lab work; Viviana Castillo for assistance with lab work; Aaron Morello and the UW Marine Chemistry Lab for assistance with CHN and Chlorophyll analysis; and Megan Schatz and E. Virginia Armbrust for assistance with PAM fluorometry measurements.

References

Aletsee, L and Jahnke, J. 1992. Growth and productivity of the psychrophilic marine diatoms *Thalassiosira antarctica* Comber and *Nitzschia frigida* Grunow in batch cultures at temperatures below the freezing point of sea water. *Polar Biol* 11(8): 643–647. DOI: https://doi.org/10.1007/BF00237960

Amin, SA, Hmelo, LR, van Tol, HM, Durham, BP, Carlson, LT, Heal, KR, Morales, RL, Berthiaume, CT, Parker, MS, Djunaedi, B, Ingalls, AE, Parsek, MR, Moran, MA and Armbrust, EV. 2015. Interaction and signaling between a cosmopolitan phytoplankton and associated bacteria. *Nature* 522(7554): 98–101. DOI: https://doi.org/10.1038/ nature14488

Arrigo, KR. 2014. Sea ice ecosystems. *Ann Rev Mar Sci* 6(1): 439–467. DOI: https://doi.org/10.1146/ annurev-marine-010213-135103

Arrigo, KR. 2016. Sea ice as a habitat for primary producers. In: Thomas, D (ed.), *Sea ice*, 3rd ed., 352–369. Chichester, UK; Hoboken, NJ: John Wiley & Sons. DOI: https://doi.org/10.1002/9781118778371.ch14

Arrigo, KR, Brown, ZW and Mills, MM. 2014. Sea ice algal biomass and physiology in the Amundsen Sea, Antarctica. *Elem Sci Anthr* 2: 000028. DOI: https:// doi.org/10.12952/journal.elementa.000028

Arrigo, KR and Sullivan, CW. 1992. The influence of salinity and temperature covariation on the photophysiological characteristics of Antarctic sea ice microalgae. *J Phycol* 28(6): 746–756. DOI: https:// doi.org/10.1111/j.0022-3646.1992.00746.x

Azam, F and Malfatti, F. 2007. Microbial structuring of marine ecosystems. *Nat Rev Microbiol* 5(10): 782– 791. DOI: https://doi.org/10.1038/nrmicro1747

Benjamini, Y and Hochberg, Y. 1995. Controlling the false discovery rate: A practical and powerful approach to multiple testing. *J R Stat Soc* 57(1): 289 –300. DOI: https://doi.org/10.1111/j.2517-6161.1995.tb02031.x

Bligh, EG and Dyer, WJ. 1959. A rapid method of total lipid extraction and purification. *Can J Biochem Physiol* 37(8): 911–917. DOI: https://doi.org/10.1139/ o59-099

Boroujerdi, AFB, Lee, PA, DiTullio, GR, Janech, MG, Vied, SB and Bearden, DW. 2012. Identification of isethionic acid and other small molecule metabolites of *Fragilariopsis cylindrus* with nuclear magnetic resonance. *Anal Bioanal Chem* 404(3): 777–784. DOI: https://doi.org/10.1007/s00216-012-6169-2

Boysen, AK, Heal, KR, Carlson, LT and Ingalls, AE. 2018. Best-matched internal standard normalization in liquid chromatography-mass spectrometry metabolomics applied to

environmental samples. *Anal Chem* 90(2): 1363–1369. DOI: https://doi.org/10.1021/acs.analchem.7b04400

Bromke, MA, Giavalisco, P, Willmitzer, L and Hesse, H. 2013. Metabolic analysis of adaptation to short-term changes in culture conditions of the marine diatom *Thalassiosira pseudonana*. *PLoS One* 8(6): e67340. DOI: https://doi.org/10.1371/journal.pone.0067340

Canelas, AB, ten Pierick, A, Ras, C, Seifar, RM, van Dam, JC, van Gulik, WM and Heijnen, JJ. 2009. Quantitative evaluation of intracellular metabolite extraction techniques for yeast metabolomics. *Anal Chem* 81(17): 7379–7389. DOI: https://doi. org/10.1021/ac900999t

Chen, THH and Murata, N. 2002. Enhancement of tolerance of abiotic stress by metabolic engineering of betaines and other compatible solutes. *Curr Opin Plant Biol* 5(3): 250–257. DOI: https://doi. org/10.1016/S1369-5266(02)00255-8

Cherrier, J and Bauer, JE. 2004. Bacterial utilization of transient plankton-derived dissolved organic carbon and nitrogen inputs in surface ocean waters. *Aquat Microb Ecol* 35(3): 229–241. DOI: https:// doi.org/10.3354/ame035229

Dickson, DMJ and Kirst, GO. 1987. Osmotic adjustment in marine eukaryotic algae: the role of inorganic ions, quaternary ammonium, tertiary sulfonium and carbohydrate solutes. 2. Prasinophytes and Hapto- phytes. *New Phytol* 106(4): 657–666. DOI: https://doi.org/10.1111/j.1469-8137.1987.tb00166.x

Di Martino, ML, Campilongo, R, Casalino, M, Micheli, G, Colonna, B and Prosseda, G. 2013. Polyamines: Emerging players in bacteria-host interactions. *Int J Med Microbiol* 303(8): 484–491. DOI: https://doi. org/10.1016/j.ijmm.2013.06.008

Dieckmann, GS and Thomas, DN. 2002. Antarctic sea ice–a habitat for extremophiles. *Science* 295(5555): 641–644. DOI: https://doi.org/10.1126/science. 1063391

Durham, BP, Boysen, AK, Carlson, LT, Groussman, RD, Heal, KR, Cain, KR, Morales, RL, Coesel, SN, Morris, RM, Ingalls, AE and Armbrust, EV. 2019. Sulfonate-based networks between eukaryotic phytoplankton and heterotrophic bacteria in the surface ocean. *Nat Microbiol* 4(10): 1706–1715. DOI: https://doi.org/10.1038/s41564-019-0507-5

Durham, BP, Dearth, SP, Sharma, S, Amin, SA, Smith, CB, Campagna, SR, Armbrust, EV and Moran, MA. 2017. Recognition cascade and metabolite transfer in a marine bacteria-phytoplankton model system. *Environ Microbiol* 19(9): 3500–3513. DOI: https://doi.org/10.1111/1462-2920.13834

Durham, BP, Sharma, S, Luo, H, Smith, CB, Amin, SA, Bender, SJ, Dearth, SP, Van Mooy, BAS, Campagna, SR, Kujawinski, EB, Armbrust, EV and Moran, MA. 2015. Cryptic carbon and sulfur cycling between surface ocean plankton. *Proc Natl Acad Sci* 112(2): 453–457. DOI: https://doi. org/10.1073/pnas.1413137112

Eicken, H. 1992. Salinity profiles of Antarctic sea ice: Field data and model results. *J Geophys Res* 97(92): 15545– 15557. DOI: https://doi.org/10.1029/92JC01588

Ewert, M and Deming, JW. 2014. Bacterial responses to fluctuations and extremes in temperature and brine salinity at the surface of Arctic winter sea ice. *FEMS Microbiol Ecol* 89(2): 476–489. DOI: https://doi. org/10.1111/1574-6941.12363

Fenizia, S, Thume, K, Wirgenings, M and Pohnert, G. 2020. Ectoine from bacterial and algal origin is a compatible solute in microalgae. *Mar Drugs* 18(1), 42: 1–13. DOI: https://doi.org/10.3390/ md18010042

Ferjani, A, Mustardy, L, Sulpice, R, Marin, K, Suzuki, I, Hagemann, M and Murata, N. 2003. Glucosylglycerol, a compatible solute, sustains cell division under salt stress. *Plant Physiol* 131(4): 1628–1637. DOI: https://doi.org/10.1104/pp.102.017277

Fiala, M, Kuosa, H, Kopczyńska, EE, Oriol, L and Delille, D. 2006. Spatial and seasonal heterogeneity of sea ice microbial communities in the first-year ice of Terre Adélie area (Antarctica). *Aquat Microb Ecol* 43(1): 95–106. DOI: https://doi.org/10.3354/ame043095

Firth, E, Carpenter, SD, Sørensen, HL, Collins, RE and Deming, JW. 2016. Bacterial use of choline to tolerate salinity shifts in sea-ice brines. *Elem Sci Anthr* 4: 000120. DOI: https://doi.org/10.12952/journal.elementa.000120

Fulda, S, Hagemann, M and Libbert, E. 1990. Release of glucosylglycerol from the cyanobacterium *Synechocystis* spec. SAG 92.79 by hypoosmotic shock. *Arch Microbiol* 153(4): 405–408. DOI: https://doi.org/10.1007/BF00249013

Gebser, B and Pohnert, G. 2013. Synchronized regulation of different zwitterionic metabolites in the osmoadaption of phytoplankton. *Mar Drugs* 11(6): 2168–2182. DOI: https://doi.org/10.3390/md11062168

Götz, F, Longnecker, K, Kido Soule, MC, Becker, KW, Mcnichol, J, Kujawinski, EB and Sievert, SM. 2018. Targeted metabolomics reveals proline as a major osmolyte in the chemolithoautotroph *Sulfurimonas denitrificans*. *MicrobiologyOpen* 7(4): e00586. DOI: https://doi.org/10.1002/mbo3.586

Greenway, H and Setter, TL. 1979. Accumulation of proline and sucrose during the first hours after transfer of *Chlorella emersonii* to high NaCl. *Funct Plant Biol* 6(1): 69–79. DOI: https://doi.org/10.1071/PP9790069

Grossi, SM and Sullivan, CW. 1985. Sea ice microbial communities: The vertical zonation of diatoms in an Antarctic fast ice community. *J Phycol* 21(3): 401– 409. DOI: https://doi.org/10.1111/j.0022-3646.1985.00401.x

Guillard, RRL. 1975. Culture of phytoplankton for feeding marine invertebrates. In: Smith, WL and Chanley, MH (eds.), *Cult of Mar Invert Anim*, 26–60. New York, USA: Plenum Press. DOI: https://doi. org/10.1007/978-1-4615-8714-9_3

Günther, S and Dieckmann, GS. 2001. Vertical zonation and community transition of sea-ice diatoms in fast ice and platelet layer, Weddell Sea, Antarctica. *Ann Glaciol* 33: 287–296. DOI: https://doi.org/ 10.3189/172756401781818590

Harrison, PJ, Waters, RE and Taylor, FJR. 1980. A broad spectrum artificial sea water medium for coastal and open ocean phytoplankton. *J Phycol* 16(1): 28–35. DOI: https://doi.org/10.1111/j.0022-3646.1980.00028.x

Horner, RA. (ed.) 1985. *Sea ice biota*. Boca Raton, FL: CRC Press.

Horner, RA and Schrader, GC. 1982. Relative contributions of ice algae, phytoplankton, and benthic microalgae to primary production in nearshore regions of the Beaufort Sea. *Arctic* 35(4): 485–503. DOI: https://doi.org/10.14430/arctic2356

Hsiao, SIC. 1980. Quantitative composition, distribution, community structure and standing stock of sea ice microalgae in the Canadian Arctic. *Arctic* 33(4): 768–793. DOI: https://doi.org/10.14430/arctic2595

Junge, K, Eicken, H and Deming, JW. 2004. Bacterial Activity at –2 to –20°C in Arctic wintertime sea ice. *Appl Environ Microbiol* 70(1): 550–557. DOI: https://doi.org/10.1128/AEM.70.1.550-557.2004

Karsten, U, Kück, K, Vogt, C and Kirst, GO. 1996. Dimethylsulfoniopropionate production in phototrophic organisms and its physiological functions as a cryoprotectant. In: Kiene, RP, Vissher, PT, Keller, MD and Kirst, GO (eds.), *Biological and environmental chemistry of DMSP and related sulfonium compounds*, 143–153. Boston, MA: Springer US. DOI: https://doi.org/10.1007/978-1-4613-0377-0_13

Kattner, G, Thomas, DN, Haas C, Kennedy, H and Dieckmann, GS. 2004. Surface ice and gap layers in Antarctic sea ice: highly productive habitats. *Mar Ecol Prog Ser* 277: 1–12. DOI: https://doi.org/10.3354/meps277001

Keller, MD, Matrai, PA, Kiene, RP and Bellows, WK.
2004. Responses of coastal phytoplankton populations to nitrogen additions: dynamics of cell-associated dimethylsulfoniopropionate (DMSP), glycine betaine (GBT), and homarine. *Can J Fish Aquat Sci* 61(5): 685–699. DOI: https://doi.org/10.1139/f04-058

Kiene, RP and Hoffmann Williams, LP. 1998. Glycine betaine uptake, retention, and degradation by microorganisms in seawater. *Limnol Oceanogr* 43(7): 1592–1603. DOI: https://doi.org/10.4319/ lo.1998.43.7.1592

Kirst, GO, Thiel, C, Wolff, H, Nothnagel, J, Wanzek, M and Ulmke, R. 1991. Dimethylsulfoniopropionate (DMSP) in ice algae and its possible biological role. *Mar Chem* 35(1–4): 381–388. DOI: https://doi. org/10.1016/S0304-4203(09)90030-5

Kohlbach, D, Lange, BA, Schaafsma, FL, David, C, Vortkamp, M, Graeve, M, van Franeker, JA, Krumpen, T and Flores, H. 2017. Ice algae-produced carbon is critical for overwintering of Antarctic krill *Euphausia superba*. *Front Mar Sci* 4: 310. DOI: https://doi.org/10.3389/fmars.2017.00310

Kottmeier, ST and Sullivan, CW. 1987. Late winter primary production and bacterial production in sea ice and seawater west of the Antarctic Peninsula. *Mar Ecol Prog Ser* 36(3): 287–298. DOI: https://doi. org/10.3354/meps036287

Krell, A, Funck, D, Plettner, I, John, U and Dieckmann, G. 2007. Regulation of proline metabolism under salt stress in the psychrophilic diatom *Fragilariopsis cylindrus* (Bacillariophyceae). *J Phycol* 43(4): 753–762. DOI: https://doi.org/10.1111/j. 1529-8817.2007.00366.x

Krembs, C, Eicken, H and Deming, JW. 2011. Exopolymer alteration of physical properties of sea ice and implications for ice habitability and biogeochemistry in a warmer Arctic. *PNAS* 108(9): 3653–3658. DOI: https://doi.org/10.1073/pnas. 1100701108

Krembs, C, Eicken, H, Junge, K and Deming, JW. 2002. High concentrations of exopolymeric substances in Arctic winter sea ice: Implications for the polar ocean carbon cycle and cryoprotection of diatoms. *Deep Res Part I Oceanogr Res Pap* 49(12): 2163–2181. DOI: https://doi.org/10.1016/ S0967-0637(02)00122-X

Landa, M, Burns, AS, Durham, BP, Esson, K, Nowinski, B, Sharma, S, Vorobev, A, Nielsen, T, Kiene, RP and Moran, MA. 2019. Sulfur metabolites that facilitate oceanic phytoplankton–bacteria carbon flux. *ISME J* 13(10): 2536–2550. DOI: https://doi. org/10.1038/s41396-019-0455-3

Landa, M, Burns, AS, Roth, SJ and Moran, MA. 2017. Bacterial transcriptome remodeling during sequential co-culture with a marine dinoflagellate and diatom. *ISME J* 11(12): 2677–2690. DOI: https:// doi.org/10.1038/ismej.2017.117

Lizotte, MP. 2001. The contributions of sea ice algae to Antarctic marine primary production. *Am Zool* 41(1): 57–73. DOI: https://doi.org/10.1093/icb/ 41.1.57

Lu, X, Heal, KR, Ingalls, AE, Doxey, AC and Neufeld, JD. 2019. Metagenomic and chemical characterization of soil cobalamin production. *ISME J* 14(1): 53–66. DOI: https://doi.org/10.1038/ s41396-019-0502-0

Lyon, BR, Bennett-Mintz, JM, Lee, PA, Janech, MG and Ditullio, GR. 2016. Role of dimethylsulfo- niopropionate as an osmoprotectant following gradual salinity shifts in the

sea-ice diatom *Fragilariopsis cylindrus*. *Environ Chem* 13(2): 181–194. DOI: https://doi.org/10.1071/EN14269

Lyon, BR, Lee, PA, Bennett, JM, DiTullio, GR and Janech, MG. 2011. Proteomic analysis of a sea-ice diatom: Salinity acclimation provides new insight into the dimethylsulfoniopropionate production pathway. *Plant Physiol* 157(4): 1926–1941. DOI: https://doi.org/10.1104/pp.111.185025

Lyon, BR and Mock, T. 2014. Polar microalgae: New approaches towards understanding adaptations to an extreme and changing environment. *Biology* 3(1): 56–80. DOI: https://doi.org/10.3390/biology 3010056

MacLean, B, Tomazela, DM, Shulman, N, Chambers, M, Finney, GL, Frewen, B, Kern, R, Tabb, DL, Liebler, DC and MacCoss, MJ. 2010. Skyline: An open source document editor for creating and analyzing targeted proteomics experiments. *Bioinformatics* 26(7): 966–968. DOI: https://doi. org/10.1093/bioinformatics/btq054

Michel, C, Nielsen, TG, Nozais, C and Gosselin, M. 2002. Significance of sedimentation and grazing by ice micro- and meiofauna for carbon cycling in annual sea ice (northern Baffin Bay). *Aquat Microb Ecol* 30(1): 57–68. DOI: https://doi.org/10.3354/ame030057

Nothnagel, J. 1995. The effects of salinity and light intensity on the osmolyte concentrations, cell volumes and growth rates of the Antarctic sea-ice diatoms *Chaetoceros* sp. and *Navicula* sp. with emphasis on the amino acid proline [dissertation]. Bremen, DE: University of Bremen, Dept. of Biology/Chemistry and Marine Botany. *Rep Polar Res* 161.

O'Brien, DP. 1987. Direct observations of the behavior of *Euphausia superba* and *Euphausia crystallorophias* (Crustacea: Euphausiacea) under pack ice during the Antarctic spring of 1985. *J Crustacean Biol* 7(3): 437–448. DOI: https://doi.org/10.2307/1548293

Olenina, I, Hajdu, S, Edler, L, Andersson, A, Wasmund, N, Göbel, J, Huttunen, M, Jaanus, A, Legaine, I, Huseby, S and Niemkiewicz, E. 2006. Biovolumes and size-classes of phytoplankton in the Baltic Sea. *HELCOM Balt Sea Environ Proc* 106: 1–144.

Reed, RH, Richardson, DL, Warr, SRC and Stewart, WDP. 1984. Carbohydrate accumulation and osmotic stress in cyanobacteria. *J Gen Microbiol* 130(1): 1–4. DOI: https://doi.org/10.1099/00221287-130-1-1

Retelletti Brogi, S, Ha, SY, Kim, K, Derrien, M, Lee, YK and Hur, J. 2018. Optical and molecular characteriza- tion of dissolved organic matter (DOM) in the Arctic ice core and the underlying seawater (Cambridge Bay, Canada): Implication for increased autochthonous DOM during ice melting. *Sci Total Environ* 627: 802–811. DOI: https://doi.org/10.1016/j. scitotenv.2018.01.251

Riaux-Gobin, C, Poulin, M, Dieckmann, G, Labrune, C and Vétion, G. 2011. Spring phytoplankton onset after the ice break-up and sea-ice signature (Adélie Land, East Antarctica). *Polar Res* 30(1): 5910. DOI: https://doi.org/10.3402/polar.v30i0.5910

Scholz, B and Liebezeit, G. 2012. Compatible solutes in three marine intertidal microphytobenthic Wadden Sea diatoms exposed to different salinities. *Eur J Phycol* 47(4): 393–407. DOI: https://doi.org/10.10 80/09670262.2012.720714

Slama, I, Abdelly, C, Bouchereau, A, Flowers, T and Savouré, A. 2015. Diversity, distribution and roles of osmoprotective compounds accumulated in halophytes under abiotic stress. *Ann Bot* 115(3): 433–447. DOI: https://doi.org/10.1093/aob/mcu239

Spielmeyer, A, Gebser, B and Pohnert, G. 2011. Investigations of the uptake of dimethylsulfoniopropionate by phytoplankton. *ChemBioChem* 12(15): 2276–2279. DOI: https://doi.org/10.1002/cbic.201100416

Spielmeyer, A and Pohnert, G. 2012. Influence of temperature and elevated carbon dioxide on the production of dimethylsulfoniopropionate and glycine betaine by marine phytoplankton. *Mar Environ Res* 73: 62–69. DOI: https://doi.org/10.1016/j.marenvres.2011.11.002

Spietz, RL, Lundeen, RA, Zhao, X, Nicastro, D, Ingalls, AE and Morris, RM. 2019. Heterotrophic carbon metabolism and energy acquisition in *Candidatus* Thioglobus singularis strain PS1, a member of the SUP05 clade of marine *Gammaproteobacteria*. *Environ Microbiol* 21(7): 2391–2401. DOI: https://doi.org/10.1111/1462-2920.14623

Tedesco, L, Vichi, M and Thomas, DN. 2012. Process studies on the ecological coupling between sea ice algae and phytoplankton. *Ecol Modell* 226: 120–138. DOI: https://doi.org/10.1016/j.ecolmodel.2011.11.011

Torstensson, A, Hedblom, M, Andersson, J, Andersson, MX and Wulff, A. 2013. Synergism between elevated *p*CO2 and temperature on the Antarctic sea ice diatom *Nitzschia lecointei*. *Biogeosciences* 10(10): 6391–6401. DOI: https://doi.org/10.5194/ bg-10-6391-2013

Torstensson, A, Young, JN, Carlson, LT, Ingalls, AE and Deming, JW. 2019. Use of exogenous glycine betaine and its precursor choline as osmoprotectants in Antarctic sea-ice diatoms. *J Phycol* 70: 1–13. DOI: https://doi.org/10.1111/jpy.12839

UNESCO. 1994. Protocols for the joint global ocean flux study (JGOFS) core measurements. *IOC Manuals and Guides* 29.

van Leeuwe, MA, Tedesco, L, Arrigo, KR, Assmy, P, Campbell, K, Meiners, KM, Rintala, J-M, Selz, V, Thomas, DN and Stefels, J. 2018. Microalgal community structure and primary production in Arctic and Antarctic sea ice: A synthesis. *Elem Sci Anth* 6. DOI: https://doi.org/10.1525/elementa.267

Vancoppenolle, M, Meiners, KM, Michel, C, Bopp, L, Brabant, F, Carnat, G, Delille, B, Lannuzel, D, Madec, G, Moreau, S, Tison, JL and van der Merwe, P. 2013. Role of sea ice in global biogeochemical cycles: Emerging views and challenges. *Quat Sci Rev* 79: 207–230. DOI: https://doi.org/10.1016/j.quascirev.2013.04.011

Warr, SRC, Reed, RH and Stewart, WDP. 1984. Osmotic adjustment of cyanobacteria: The effects of NaCl, KCl, sucrose and glycine betaine on glutamine synthetase activity in a marine and a halotolerant strain. *J Gen Microbiol* 130(9): 2169–2175. DOI: https://doi.org/10.1099/00221287-130-9-2169

Welschmeyer, NA. 1994. Fluorometric analysis of chlorophyll a in the presence of chlorophyll b and pheopigments. *Limnol Oceanogr* 39(8): 1985–1992. DOI: https://doi.org/10.4319/lo.1994.39.8.1985

Welsh, DT. 2000. Ecological significance of compatible solute accumulation by micro-organisms: from single cells to global climate. *FEMS Microbiol Rev* 24(3): 263–290. DOI: https://doi.org/10.1111/j.1574-6976.2000.tb00542.x

Yancey, PH. 2005. Organic osmolytes as compatible, metabolic and counteracting cytoprotectants in high osmolarity and other stresses. *J Exp Biol* 208(15): 2819–2830. DOI: https://doi.org/10.1242/jeb.01730

Yancey, PH, Clark, ME, Hand, SC, Bowlus, RD and Somero, GN. 1982. Living with water stress: Evolution of osmolyte systems. *Science*. 217(4566): 1214–1222. DOI: https://doi.org/10.1126/science.7112124

2.9 TABLES AND FIGURES

Table 2.1. Environmental parameters of the bottom sea-ice sections from the Utqiaġvik, AK field site at the time of sampling.

Sampling Date	8-May-2017
Snow thickness (cm)	7–10
Ice thickness (cm)	125–128
Ice section sampled	Bottom 5 cm (algal band)
Temperature (°C)	–1.3
Salinity	29.9
Light intensity (µmoles photons m^{-2} s^{-2})	10–50
$\boldsymbol{F_v/F_M}$[a]	0.50 ± 0.02
Chl a (mg m^{-3})[a]	348 ± 34
POC (mM C)[a]	1.7 ± 0.1
C:N (mol:mol)[a]	9.1 ± 0.1
DOC (µM C)[a]	621 ± 386
NO_3^- (µM)[c]	10.19 ± 0.01
pEPS (µM C)[b]	78

[a] Values are mean ± SD, $n = 3$.

[b] Measured from the bottom 15 cm of ice cores and estimated that all came from the bottom 5 cm.

[c] Values are mean ± SD, $n = 2$.

Table 2.2. Absolute intracellular concentrations of selected metabolites in the *Nitzschia lecointei* culture grown at –1°C and salinity 32 and the Utqiaġvik, AK bottom sea-ice sections.

Compound	Concentration (µmol mol C^{-1})[a]		Fold difference (culture/field)
	Culture	Field	
DHPS	3100 ± 81	390 ± 100	8
GBT	1200 ± 99	230 ± 97	5
Proline	960 ± 80	180 ± 110	5
Alanine	190 ± 17	120 ± 67	2
Choline	61 ± 6.7	26 ± 17	2
Cysteic acid	27 ± 2.2	15 ± 5.0	2
Valine	24 ± 1.4	13 ± 9.5	2
Histidine	14 ± 1.2	6.8 ± 4.0	2
Phenylalanine	8.5 ± 0.15	4.7 ± 2.4	2
Methionine	6.9 ± 0.5	12 ± 8.9	0.6
Taurine	5.9 ± 1.1	24 ± 17	0.2
Isoleucine	5.8 ± 0.43	2.4 ± 0.83	2
Tryptophan	4.9 ± 0.2	3.0 ± 1.4	2
Isethionic acid	2.9 ± 0.35	120 ± 51	0.02
Sulfolactic acid	1.5 ± 0.61	0.72 ± 0.36	2
Homarine	dl[b]	13 ± 5.3	–
Proline betaine	nd[c]	13 ± 5.7	–
Trigonelline	dl	1.1 ± 0.58	–
Hydroxyectoine	nd	1.1 ± 0.44	–

[a] Values are mean ± SD, n = 3. An additional 20% error based on particulate carbon measurement may be present.

[b] At or below detection limit.

[c] Not detected.

Table 2.3. Intracellular concentrations[a] of quantified compatible solutes in cultures of two different sea-ice diatoms at different temperatures and salinities.

	Treatment	Proline		DHPS		GBT		Choline	
Algal taxon	**(S, T)**	**(fmol cell^{-1})**	**(mM)**	**(fmol cell^{-1})**	**(mM)**	**(fmol cell^{-1})**	**(mM)**	**(fmol cell^{-1})**	**(mM)**
N. lecointei	31, –1°C[b]	–[c]	–	–	–	6.0 ± 0.4	31.7 ± 2	0.68 ± 0.09	3.6 ± 0.5
N. lecointei	32, –1°C[d]	3.4 ± 0.28	22 ± 1.9	11 ± 0.27	71 ± 1.8	4.3 ± 0.34	28 ± 2.2	0.21 ± 0.023	1.4 ± 0.15
N. lecointei	41, –1°C[d]	7.7 ± 1.2	52 ± 7.3	9.9 ± 1.6	67 ± 11	7.2 ± 0.97	67 ± 11	0.16 ± 0.028	1.1 ± 0.19
N. lecointei	32, 4°C[d]	2.3 ± 0.3	11 ± 1.5	9.1 ± 1.1	45 ± 5.3	6.6 ± 0.55	33 ± 2.8	0.11 ± 0.0087	0.53 ± 0.043
N. lecointei	41, 4°C[d]	5.9 ± 1.1	30 ± 5.8	17 ± 1.7	84 ± 8.5	11 ± 1.6	54 ± 8.2	0.1 ± 0.023	0.53 ± 0.12
F. cylindrus	34, 0°C[e]	3.4	33	–	–	–	–	–	–
F. cylindrus	70, 0°C[e]	15	150	–	–	–	–	–	–
F. cylindrus	70, –4°C[e]	14	130	–	–	–	–	–	–

[a] Values are mean metabolite concentrations ± SD, $n = 3$ unless otherwise noted.

[b] GBT and choline measurements from Torstensson et al. (2019), after 140-h incubation, $n = 2$.

[c] Not reported.

[d] Data from this study, where mM concentrations for *Nitzschia lecointei* were based on cell diameter (Supplementary Figure 2.2) by Coulter Counter and assumed spherical volume. An additional 5% error based on cell volume estimate may be present.

[e] Proline measurements from Krell et al. (2007), after 20-d incubation, $n = 3$; concentrations calculated using *Fragilariopsis cylindrus* cell volume and carbon content from Olenina et al. (2006).

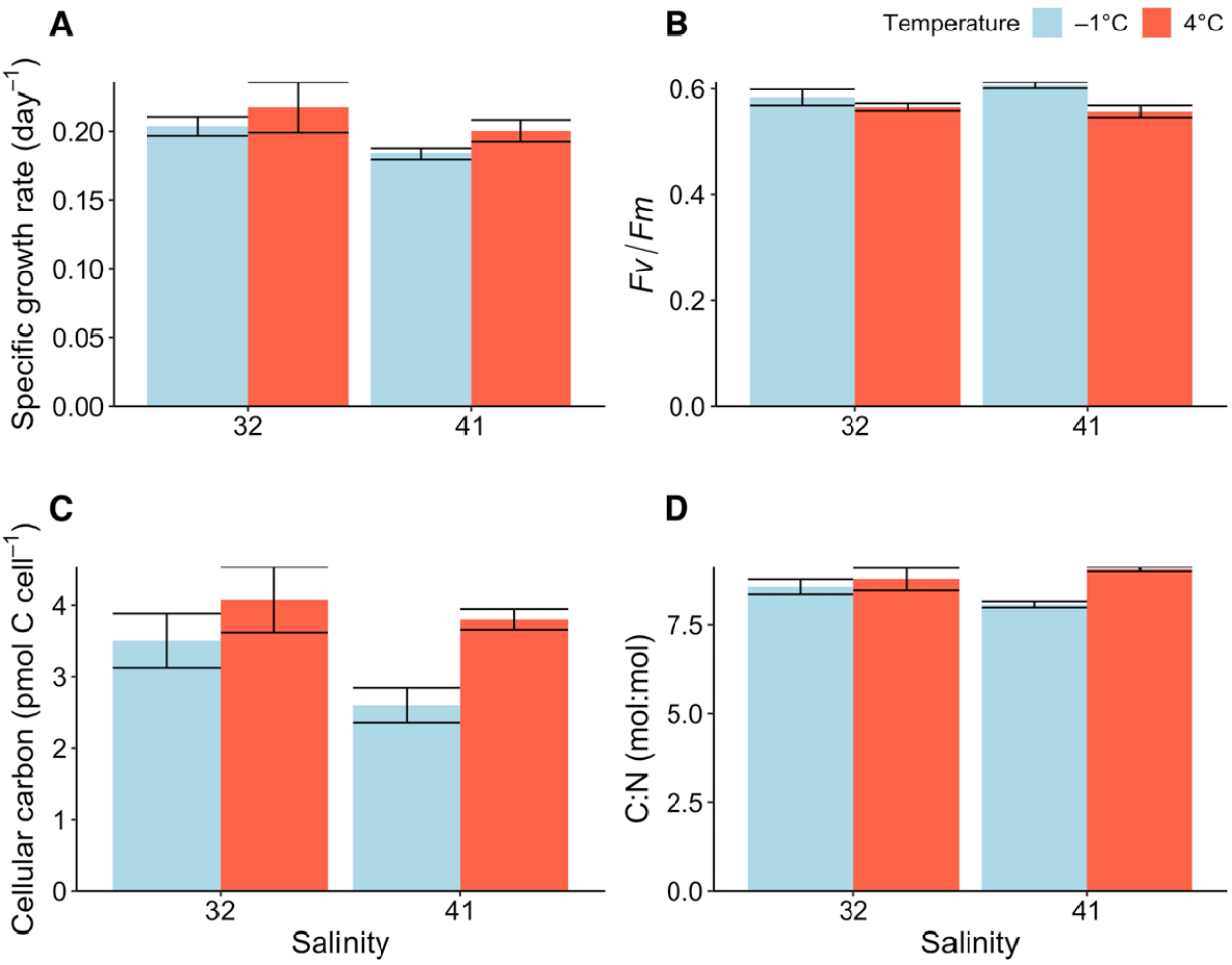

Figure 2.1. General cell physiology of *Nitzschia lecointei* cultures. a) Specific growth rate (day^{-1}, n = 3), b) maximum quantum yield (F_v/F_m, n = 3, except for 4°C and 32 salinity, where n = 2), c) carbon per cell (pmol cell^{-1}, n = 4), and d) molar ratio of C:N (n = 4). Error bars represent SD. Statistics from two-way ANOVAs are provided in Supplementary Table 2.2.

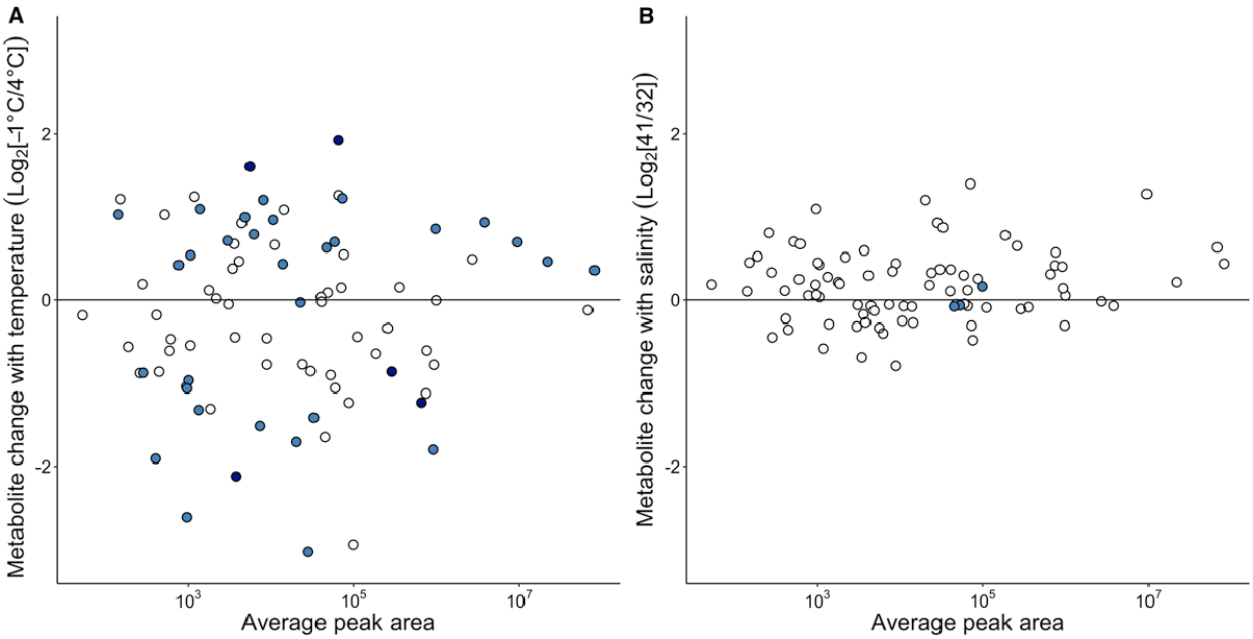

Figure 2.2. Fold change in relative concentration of metabolites with temperature and salinity. Results of targeted metabolomic analysis of *Nitzschia lecointei*, where treatment effect is expressed as $\log_2$[fold change] in metabolite abundance with (a) temperature, at –1°C compared to 4°C, and (b) salinity, at 41 compared to 32. Each circle represents a detected metabolite plotted according to its averaged normalized peak area. Compound peak areas were normalized to relative fluorescence units (RFU) before analysis. X-axis is log-scaled. Light blue circles indicate compounds significantly different only under one matching treatment ($p < 0.05$); e.g., in (a), significant differences with temperature at either 32 or 41 salinity. Dark blue circles indicate compounds significantly different under both matching treatments ($p < 0.05$); white circles, no significant differences.

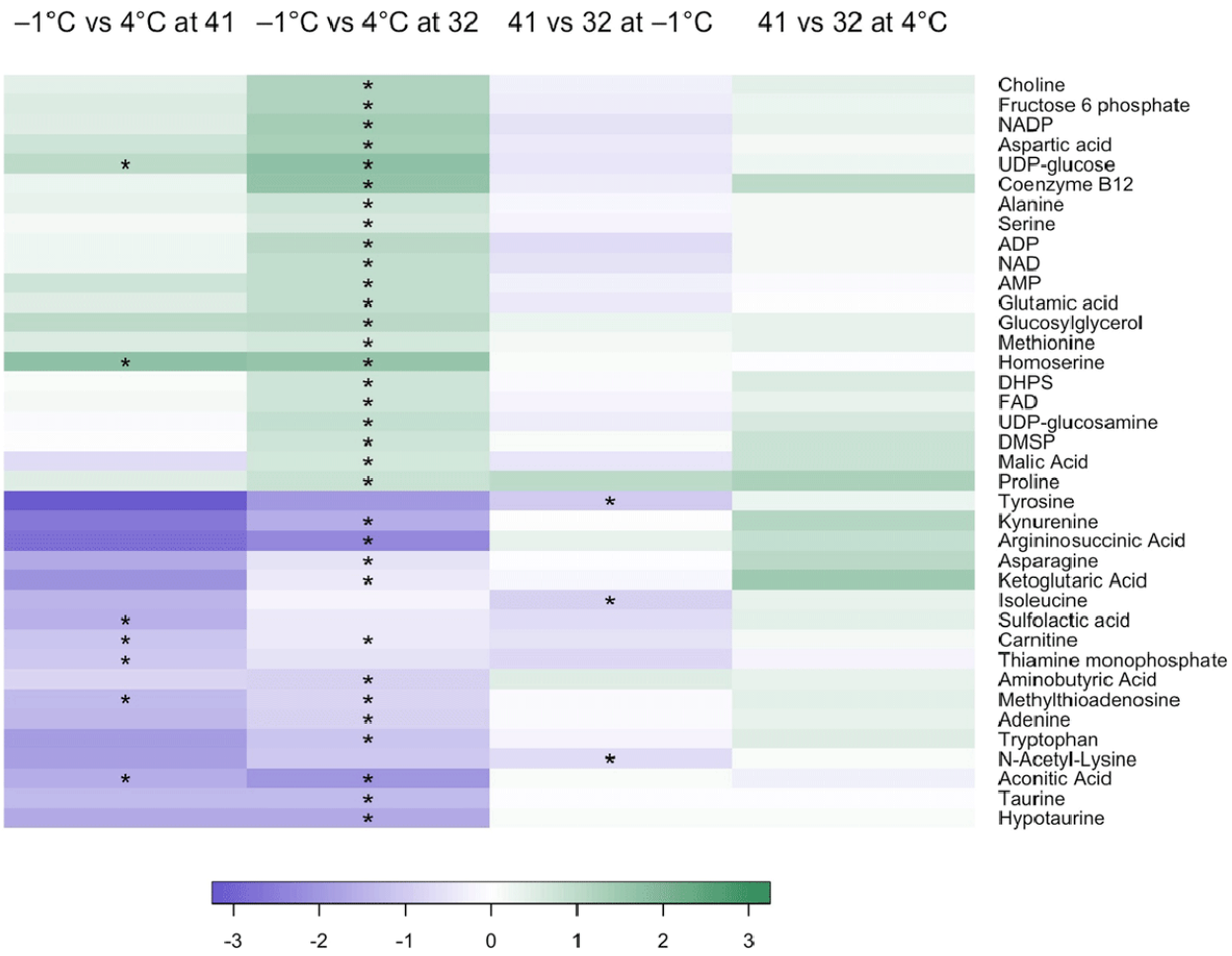

Figure 2.3. Significant fold changes in relative concentration of metabolites between treatment conditions. Log_2[fold change] of metabolite abundances (normalized metabolite area per relative fluorescence unit) between treatment conditions in *Nitzschia lecointei* cultures for those compounds with one or more significant comparisons (Figure 2.2), where an asterisk denotes significance ($p < 0.05$). Cell coloration is the log_2[fold change] of average peak size between the different treatments as shown in color key; i.e., average peak size at salinity 41/average peak size at salinity 32 at each temperature, or average peak size at –1°C/average peak size at 4°C at each salinity, as indicated by column name. Thus, green indicates compounds of higher abundance in the –1°C or salinity 41 treatments and purple indicates those of higher abundance in the 4°C or salinity 32 treatments.

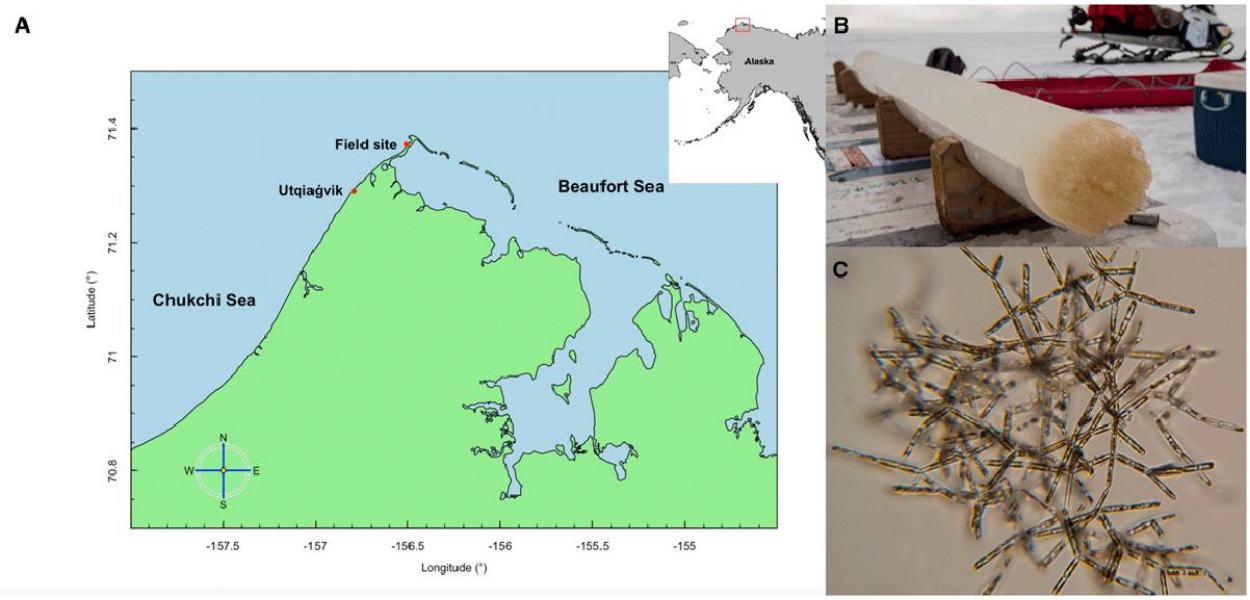

Figure 2.4. Geographic location and imagery of field site for sea-ice samples collected. (a) Map of field site location near Utqiaġvik with zoom-out inset of Alaska; (b) photo by A. Torstensson of sampled ice core with visible bottom algal layer; and (c) microscopic image by A. Torstensson of *Nitzschia frigida*, the dominant alga present by visual identification.

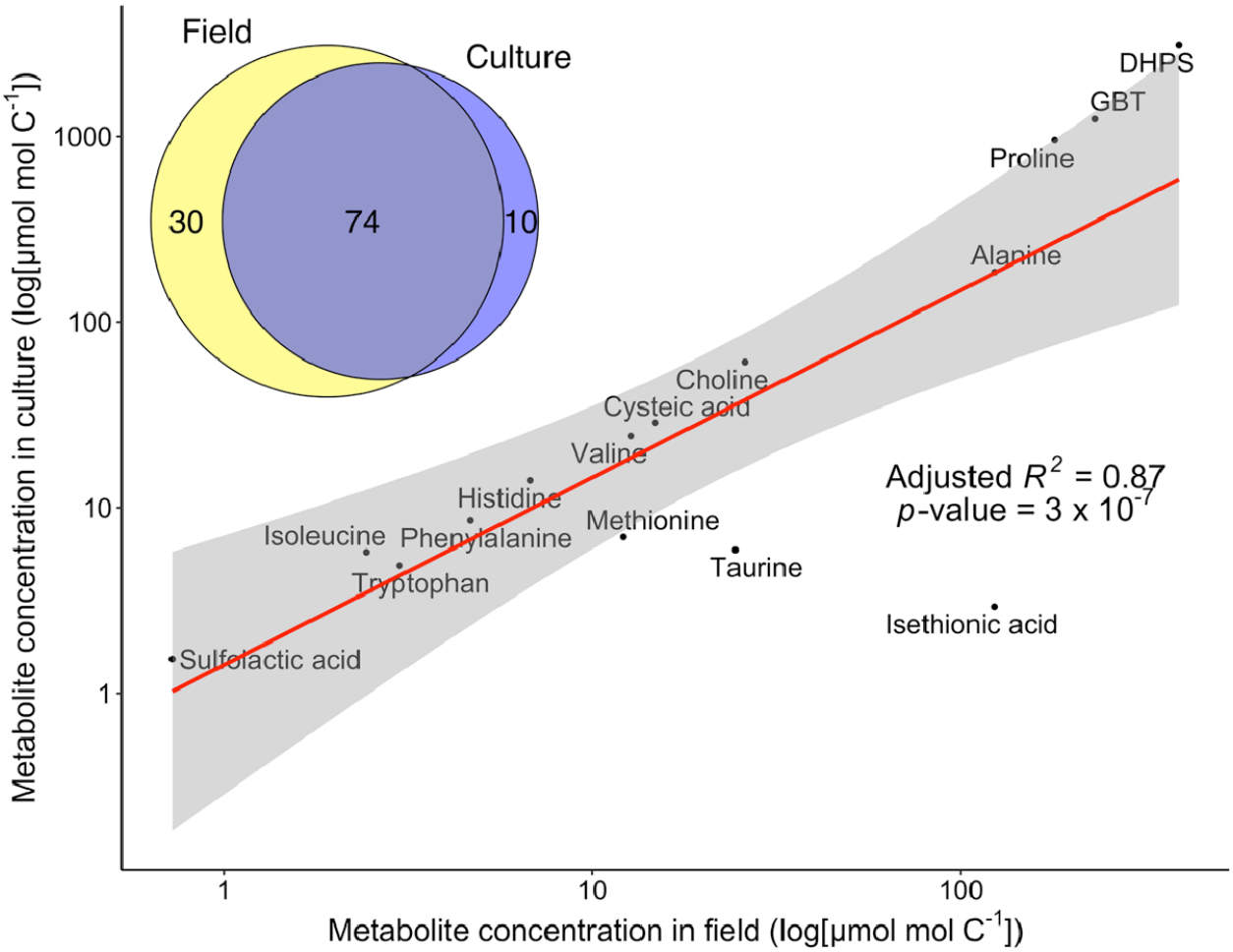

Figure 2.5. Comparison of culture and field metabolomes. Intracellular concentrations of quantified compatible solutes in *Nitzschia lecointei* cultures grown at salinity 32 and –1°C and field samples of the diatom-dominated mixed community in the bottom 5 cm of sea-ice cores collected from Utqiaġvik, AK. Values are means (n = 3) for all compounds in the culture and field samples. Homarine and trigonelline are not included in this analysis as their concentrations were near the detection limit and not determined in the culture samples, as discussed in the text. Their concentrations in the field samples are available in Table 2.2. Linear regression statistics are provided on the plot. The shaded area represents a pointwise 95% confidence interval of the fitted values. Axes are log-scaled. Inset is a Venn diagram of targeted metabolites detected in the same *N. lecointei* cultures and field samples.

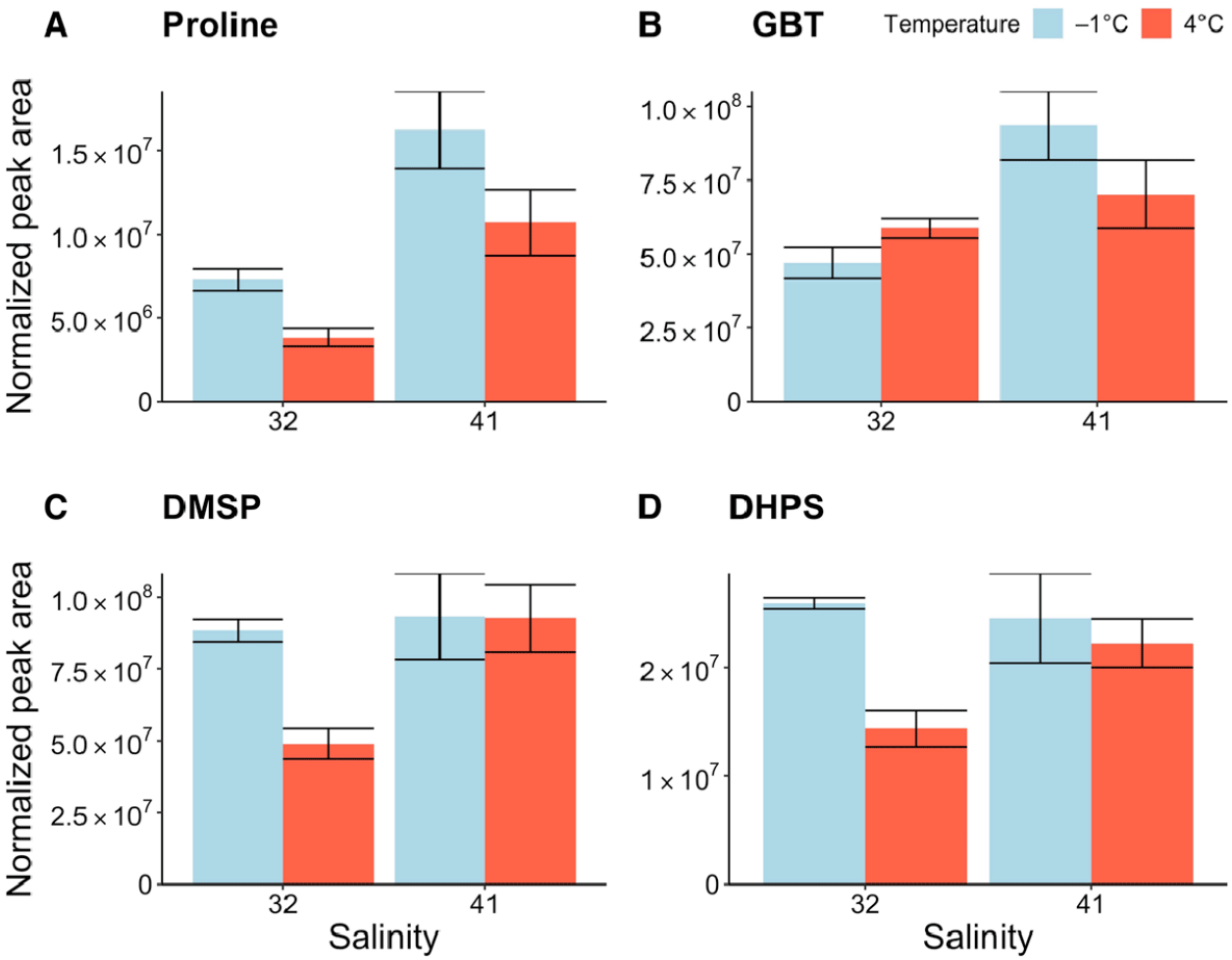

Figure 2.6. Compatible solute relative concentration changes in response to temperature and salinity. Normalized peak areas (normalized metabolite area per relative fluorescence unit) of compatible solutes in *Nitzschia lecointei* cultures, grouped by each treatment, for a) proline, b) GBT, c) DMSP, and d) DHPS. Blue indicates –1°C; orange indicates 4°C. Error bars represent SD (n = 3).

2.10 Supplementary Tables and Figures

Supplementary Table 2.1. Internal standard suite used in B-MIS normalization. Bolded standards were used for absolute quantification of compounds for comparison between field and culture samples as the non-labeled compounds were detected in both sample types. This table is provided as a separate file.

Supplementary Table 2.2. Full two-factor ANOVA statistics from general cell physiology measures from *Nitzschia lecointei* culture study. Average and standard deviation per treatment for each measure also listed. This table is provided as a separate file.

Supplementary Table 2.3. Full results from targeted metabolomics analysis of *Nitzschia lecointei*, including univariate statistics for comparisons between treatments, with *p*-value, *q*-value with false discovery rate correction (Benjamini and Hochberg, 1995), $\log_2$ fold change (FC), sample average peak areas, and reported significance (T/F). Reported peak areas per replicate are adjusted via B-MIS normalization (Boysen et al., 2018) and normalized to RFU. This table is provided as a separate file.

Supplementary Table 2.4. Full comparison of compounds detected in field and culture samples from targeted metabolomics analysis of *Nitzschia lecointei* grown at –1°C and salinity 32 and samples of bottom sea ice from Utqiaġvik, AK. This table is provided as a separate file.

Supplementary Table 2.5. Full two-factor ANOVA statistics from compatible solute (proline, GBT, DMSP and DHPS) relative abundances (normalized peak area per RFU) from *Nitzschia lecointei* cultures. This table is provided as a separate file.

Supplementary Table 2.6. Calculation of potential compatible solute-based organic nitrogen release into the sea-ice environment. This table is provided as a separate file.

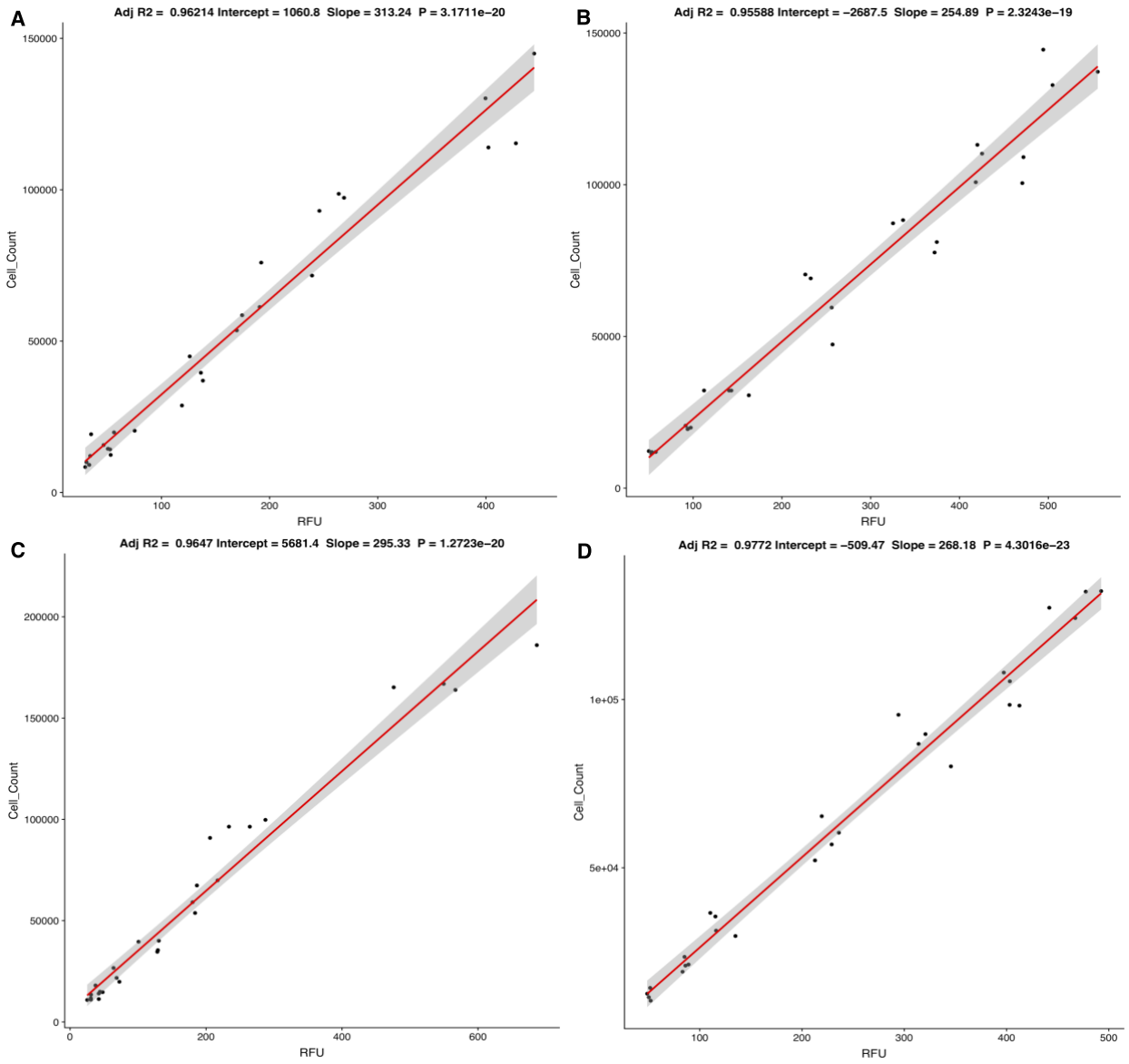

Supplementary Figure 2.1. Correlation between cell counts and relative fluorescence units (RFU). Biomass density of *Nitzschia lecointei* cultures grown at a) salinity 32 and –1°C, b) salinity 32 and 4°C, c) salinity 41 and –1°C, and d) salinity 41 and 4°C as measured by (RFU) and cell density (cells mL^{-1}). Values are individual measures of individual tubes (no error). Linear regression statistics shown on plot.

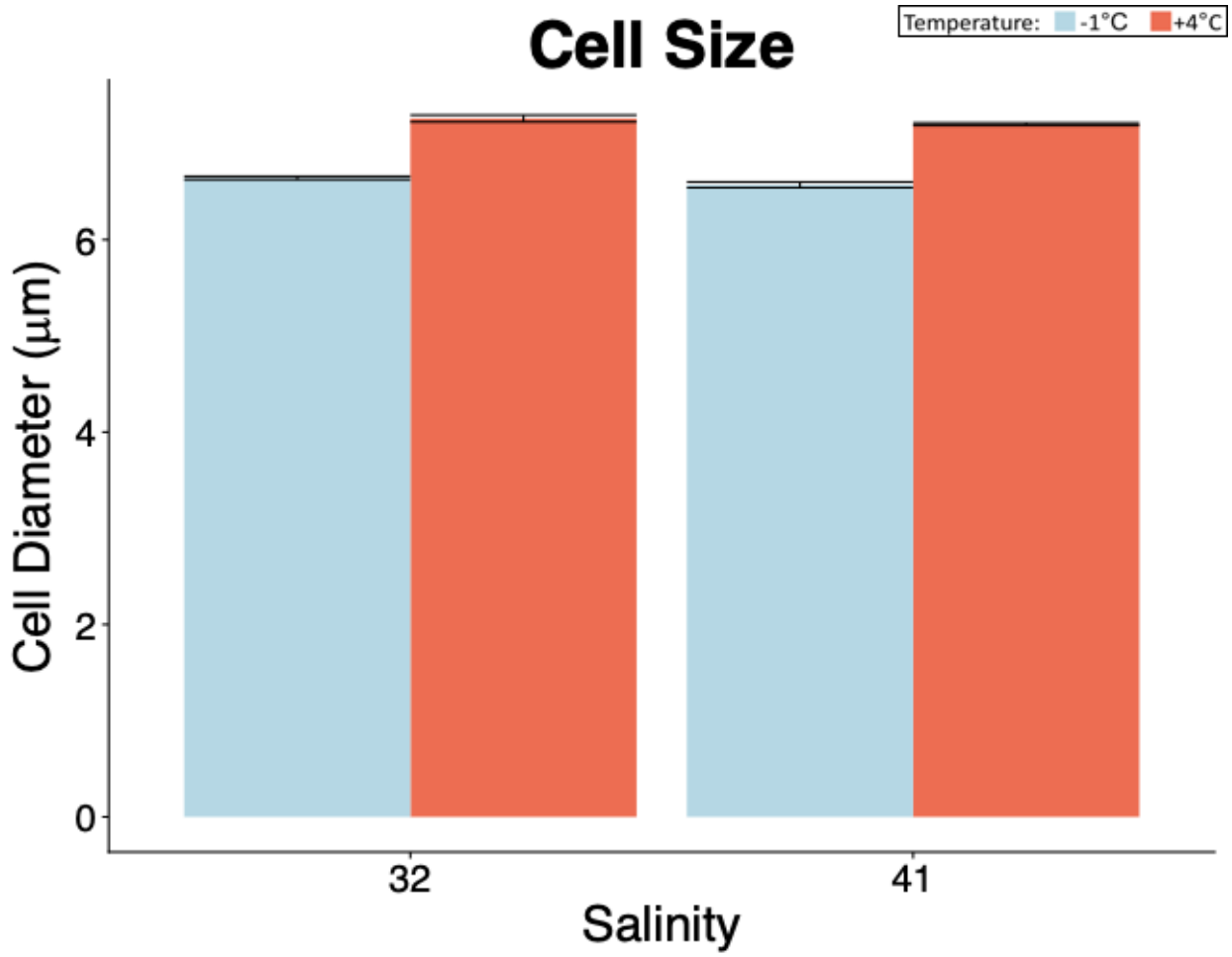

Supplementary Figure 2.2. Cell size of *Nitzschia lecointei* cultures during exponential growth, estimated as cell diameter (µm) by Coulter Counter. Blue indicates –1°C; orange indicates 4°C. Error bars represent SD (n = 3). Detailed statistics of two-factor ANOVA are provided in Supplementary Table 2.2.

Chapter 3. LARGE DIVERSITY IN NITROGEN- AND SULFUR-CONTAINING COMPATIBLE SOLUTE PROFILES IN POLAR AND TEMPERATE DIATOMS

A version of this chapter has been previously published as:

Dawson H.M., Heal K.R., Torstensson A., Carlson L.T., Ingalls A.E., Young J.N. (2020). Large diversity in nitrogen- and sulfur-containing compatible solute profiles in polar and temperate diatoms. *Integr Comp Biol*. 60(6): 1401–1413. https://doi.org/10.1093/icb/icaa133

3.1 ABSTRACT

Intense bottom-ice algal blooms, often dominated by diatoms, are an important source of food for grazers, organic matter for export during sea ice melt, and dissolved organic carbon. Sea-ice diatoms have a number of adaptations, including accumulation of compatible solutes, that allows them to inhabit this highly variable environment characterized by extremes in temperature, salinity, and light. In addition to protecting them from extreme conditions, these compounds present a labile, nutrient-rich source of organic matter, and include precursors to climate active compounds (e.g., dimethyl sulfide [DMS]), which are likely regulated with environmental change. Here, intracellular concentrations of 45 metabolites were quantified in three sea-ice diatom species and were compared to two temperate diatom species, with a focus on compatible solutes and free amino acid pools. There was a large diversity of metabolite concentrations between diatoms with no clear pattern identifiable for sea-ice species. Concentrations of some compatible solutes (isethionic acid, proline) approached 1 M in the sea-ice diatoms, *Fragilariopsis*

cylindrus and *Navicula* cf. *perminuta*, but not in the larger sea-ice diatom, *Nitzschia lecointei* or in the temperate diatom species. The differential use of compatible solutes in sea-ice diatoms suggests different adaptive strategies and highlights which small organic compounds may be important in polar biogeochemical cycles.

3.2 INTRODUCTION

Intense algal blooms within sea ice are often dominated by diatoms and can account for 55–65% of Antarctic coastal primary production (McMinn et al. 2010; Torstensson et al. 2015) and can reach densities up to 10 gm^{-3} of chlorophyll (Arrigo 2016). High heterogeneity, difficulties in sampling, and paucity of data make modeling sea-ice primary production difficult. However, under-ice and within-ice microalgal blooms likely contribute to the export of organic carbon and other nutrients during seasonal ice melt (Roukaerts et al. 2016; Kim et al. 2019). Ice-algae are also known to be an essential overwintering food source for grazers (Graeve et al. 2018). As ice melts, rapid recycling of ice algal biomass may provide inorganic nutrients that fuel spring phytoplankton blooms.

While measurements of biomass, taxonomy, and primary production rates in sea ice exist (van Leeuwe et al. 2018), the influence of the unique physiology of sea-ice algae on polar ecosystems is poorly understood. Sea-ice diatoms have a number of adaptations to survive subzero temperatures, fluctuating salinity, and low light (Thomas and Dieckmann 2003). The strong seasonal cycle requires microalgae to regulate their cellular composition in response to large shifts in their environment (notably temperature, salinity, pH, nutrients, and light) with implications for biogeochemical cycling and ecosystem nutrition (Leu et al. 2015; Torstensson et al. 2019). Adaptations include elevated protein and ribosome concentrations or increased flexibility of enzyme tertiary structure to maintain cellular rates at low temperatures (Gianese et al. 2001; Toseland et al. 2013; DasSarma et al. 2013), elevated concentrations of polyunsaturated fatty acids to increase membrane fluidity, production of ice-binding proteins, and exopolymers to alter ice crystal structure and changes in intra- and extra-cellular compatible solute pools (for review, see Deming and Young 2017; Young and Schmidt 2020).

3.2.1 *Compatible solutes*

All organisms have compatible solutes within their cells. Compatible solutes are small compounds that can accumulate to high intracellular concentrations and form hydration shells that stabilize the tertiary structure of proteins and maintain cell metabolism in high salt environments (Anton 2011). Compatible solutes can be a variety of compounds such as free amino acids and derivatives, quaternary ammonium compounds, tertiary sulfonium compounds, sugars, and sugar alcohols (Slama et al. 2015). These compounds can have a variety of roles in the cell, including cryoprotection, osmoprotection, and mitigation of reactive oxygen species. Well-known compatible solutes in polar marine diatoms include dimethylsulfoniopropionate (DMSP; Kameyama et al. 2020; Sheehan and Petrou 2020), isethionic acid (Boroujerdi et al. 2012), glycine betaine (GBT), proline, and homarine (Krell et al. 2007; Boroujerdi et al. 2012; Dawson et al. 2020). Intracellular concentrations of these compounds increase (up to 3- to 4-fold) with decreasing temperature and increasing salinity (Krell et al. 2007; Lyon et al. 2016). In addition to *in situ* biosynthesis, the Antarctic sea-ice diatoms *Nitzschia lecointei*, *Navicula* cf. *perminuta*, and *Fragilariopsis cylindrus* can take up GBT from the environment under high salinity (Torstensson et al. 2019). Unlike in bacteria (Firth et al. 2016), *N. lecointei* does not respire this acquired GBT or convert it to larger macromolecules. Instead, any GBT taken up by *N. lecointei* is retained as a small, soluble molecule in the cell, presumably for exclusive use as a compatible solute (Torstensson et al. 2019).

Characterization and quantification of compatible solutes in marine algae, and sea-ice algae, in particular, is still understudied. Most research has focused on one or two diatom species and a few known compatible solutes (Krell et al. 2007; Lyon et al. 2016; Boroujerdi et al. 2012). While some compatible solutes are likely in high abundance in many diatoms, the wide range of

compounds that can be utilized as compatible solutes suggests there is large variation among phytoplankton groups and even between diatom species. For example, isethionic acid was shown to be important in *F. cylindrus* (Boroujerdi et al. 2012) though it was not detected in high abundance in the sea-ice diatom, *N. lecointei* (Dawson et al. 2020). Likewise, homarine has been detected in mesophilic diatoms (Heal et al. 2019) and in *Nitzschia*-dominated, bottom sea-ice samples from the Arctic but was not detected in cultures of *N. lecointei* (Dawson et al. 2020). Recently, the compound, 2,3-dihydroxypropane-1-sulfonate (DHPS), was found to be a potential compatible solute in diatoms (Durham et al. 2019) and at high concentrations in *N. lecointei* (Dawson et al. 2020). Many of these compatible solutes contain nitrogen and sulfur; therefore, the rapid regulation, uptake, and release of these compounds in response to changing temperature and salinity likely have an impact on biogeochemical cycles. Nitrogen-containing compatible solutes could be an important organic source for heterotrophic catabolism, which would provide regenerated nitrogen within the upper water column to support phytoplankton growth. Volatile sulfur compounds originating from compatible solutes (e.g., DMS) can impact climate and may structure interspecies interactions (Bullock et al. 2017). Thus, nitrogen- and sulfur-containing compatible solutes were characterized in a range of sea-ice diatoms, to determine if their profiles significantly differ from more temperate species.

3.2.2 *Approach*

This study quantifies intracellular concentrations of a range of nitrogen- and sulfur-containing compatible solutes and free amino acids in three sea-ice diatoms (*Nitzschia lectointei*, *Fragilariopsis cylindrus*, and *Navicula* cf. *perminuta*) and two temperate diatom species (*Thalassiosira pseudonana* and *Navicula pelliculosa*). Cultures and metabolomic extractions were

leveraged from previous studies (Heal 2018; Heal et al. 2019; Dawson et al. 2020; Torstensson et al. 2019), and samples were reanalyzed with an entirely new question in mind: does adaptation to the extreme sea-ice environment fundamentally change compatible solute composition in diatoms? This work will help characterize the organic composition of sea-ice diatoms with the aim of better understanding their role in organic matter cycling and ecology in polar ecosystems.

3.3 METHODS

3.3.1 *Culture maintenance and growth conditions*

Axenic cultures of three Antarctic sea-ice diatoms (*N. lecointei*, *N.* cf. *perminuta*, and *F. cylindrus*) and two temperate diatoms (*T. pseudonana* and *N. pelliculosa*) were chosen for study. The exact cultures presented here were examined in previous studies as follows: *N. lecointei*, *N.* cf. *perminuta*, and *F. cylindrus* in Torstensson et al. (2019), *T. pseudonana* in Heal et al. (2019), and *N. pelliculosa* in Heal (2018). *Nitzschia lecointei* and *N.* cf. *perminuta*, were isolated from Antarctic bottom sea ice in 2011 (Torstensson et al. 2013; Aguirre et al. 2018). *Fragilariopsis cylindrus* strain CCMP1102, *T. pseudonana* CCMP1335, and *N. pelliculosa* CCMP 543 were purchased from NCMA Bigelow.

Antarctic species were grown at −1°C and a PAR irradiance of 45 μmol photons $m^{-2}s^{-1}$ (16:8 light: dark cycle) using cool white lights. Temperate species were grown at 13°C and a PAR irradiance of 120 μmol photons $m^{-2}s^{-1}$ (12:12 light: dark cycle). In both cases, light was saturating. All cultures were grown in 50 mL borosilicate glass tubes with 35 mL of filter sterilized artificial seawater media with f/2 nutrients (Guillard 1975). Cultures were grown in artificial seawater (ESAW, salinity 31, for Antarctic species, and Instant Ocean, salinity ~35 for temperate species). Cobalamin (vitamin B_{12}), replete in all cultures, was included in the Antarctic culture media as per the f/2 recipe but was added separately at 200 pM to the temperate culture media

(Heal 2018; Heal et al. 2019). Antarctic species were confirmed to be axenic via DAPI fluorescent staining and temperate cultures were confirmed to be axenic via marine purity test broth (Saito et al. 2002).

For the Antarctic species, growth rate ($n = 2$) and cell biovolume (Hillebrand et al. 1999) were determined using light microscopy as described in Torstensson et al. (2019). For the temperate species, growth rates were determined for cultures ($n = 9$) via the increase in relative fluorescence units (RFUs) using a Turner fluorometer (Heal 2018; Heal et al. 2019) and confirmed by cell counts for *T. pseudonana* using a Beckman Coulter Z2 Particle Count and Size Analyzer (Beckman Coulter) and light microscopy for *N. pelliculosa* as it is a colonial species (Lund et al. 1958). There was good agreement between RFU and cell counts ($R^2 > 0.9$), so RFU was converted to cell density on filters at the day of harvest for the temperate species (Heal 2018; Heal et al. 2019).

To explore the effect of growth conditions on metabolic profiles using nonmetric dimensional scaling (NMDS) analysis, samples were included of *N. lecointei* grown at temperatures −1°C and 4°C, and salinities 32 and 41 (Dawson et al. 2020) and *T. pseudonana* was grown under cobalamin and/or light limitation (Heal et al. 2019). Culture maintenance and growth condition details for these cultures are discussed in detail in Heal et al. (2019) and Dawson et al. (2020). Data processing and analysis for these intraspecific variation samples were carried out exactly as detailed below for the present samples.

3.3.2 *Metabolite extraction and LC-MS methods*

Cells were harvested during exponential growth onto 47 mm 0.2 μm PTFE filters (Omnipore) using combusted glassware and gentle filtration and stored at –80°C until extraction. For each biological replicate ($n = 2$ for Antarctic species, $n = 3$ for temperate species), two 35 mL cultures

were harvested onto each filter. An un-inoculated media blank was prepared and treated in the same manner as samples. Cellular metabolites were extracted using a modified Bligh Dyer extraction (Bligh and Dyer 1959) as described in detail in Boysen et al. (2018), which resulted in a nonpolar organic fraction and a polar aqueous fraction. In this study, metabolites of interest were in the polar fraction and so only this fraction was analyzed. To aid in normalization, a cocktail of internal standards was added (listed in Supplementary Tables 3.1 and 3.2, depending on sample as listed in Supplementary Table 3.3) before and after extraction (Boysen et al. 2018). Metabolites were analyzed by liquid chromatography–mass spectrometry using a Waters Acquity I-Class UPLC fitted with a SeQuant ZIC-pHILIC column. Mass spectrometry data were acquired using a Thermo QExactive HF (QE) with electrospray ionization with polarity switching (full method in Boysen et al. 2018). Data were acquired in two separate runs, as noted in Supplementary Table 3.3. A pooled sample was injected at full and half strength throughout the run to monitor instrument stability and train downstream normalization. In addition, a mix of standards in water and a representative matrix at known concentrations was injected at the start and end of the run for quantification, as detailed below.

3.3.3 *Data processing*

Masses of ions corresponding to metabolites (as listed in Supplementary Table 3.4) were integrated using Skyline for small molecules (MacLean et al. 2010), and integrated peaks were run through in-house quality control (QC) and best-matched internal standard (B-MIS) normalization as in Boysen et al. (2018). Full and abbreviated compound names are listed in Supplementary Table 3.4. Abbreviated names are used in figures throughout. Leucine and isoleucine did not chromatographically separate well, so were integrated as a combined signal, referred to here as (iso)leucine. For QC, peaks that did not meet minimum criteria set to ensure correct compound

identification and peak quality (listed in Supplementary Table 3.5) were excluded from further analysis and referred to as "not detected". Glycine is referred to as "not measured" in *T. pseudonana* since glycine has a *m/z* below the *m/z* scan range used in the associated data acquisition run and thus could not be detected or quantified in those samples. For peaks that passed through QC, a 30% improvement to the relative standard deviation (RSD) of each compound in a pooled sample was used as the criteria to apply normalization for the sea-ice diatom and *N. pelliculosa* data, using tools in the B-MIS normalization package to determine this value (Boysen et al. 2018). A 20% improvement threshold was used to apply normalization for *T. pseudonana* data, exactly as in Heal et al. (2019). Any compounds with a raw RSD of <10% across the raw pooled areas were not normalized, similar to previous work (Heal et al. 2019). For B-MIS normalization, samples were only adjusted within the same run, not between runs.

3.3.4 *Metabolite abundances*

Intracellular concentrations were calculated from peak areas for the compounds presented here using three approaches. For metabolites where isotopically-labeled standards were added to samples as a part of the internal standard suite (Supplementary Tables 3.1 and 3.2, depending on sample as listed in Supplementary Table 3.3) concentrations were calculated directly (labeled "isotopologue" in quantification method of Supplementary Table 3.6). For compounds without isotopologues, a compound-specific response factor (RF) and RF ratio (RF_{ratio}, as in Boysen et al. 2018) were calculated and used to correct for ion suppression using authentic standards mixed into water and a representative matrix (details outlined in supplemental methods of Heal 2018; Boysen et al. 2020 and labeled "direct RF and RF_{ratio}" in quantification methods of Supplementary Table 3.6). For a final set of compounds for measured before acquiring authentic standards, an RF for the compound was estimated using a proxy standard that had been run in all sample sets that share

the same column, ionization, and structural similarity (assuming a consistent relative RF between the proxy compound and analyte). For these later-acquired compounds, RF_{ratio} was calculated from a later run once an authentic standard was acquired in the same manner as above (labeled "relative RT and RF_{ratio}" in quantification methods of Supplementary Table 3.6). For example, the *T. pseudonana* data were acquired before the standard for trigonelline was acquired; for those samples, an established homarine RF was used (another aromatic betaine) to estimate a RF assuming a similar homarine/trigonelline ratio in RFs. Then, the RF_{ratio} calculated for trigonelline in the later run, which included a trigonelline standard in a comparable matrix, was used for the *T. pseudonana* run. For any compound in which the ambient matrix signal was larger than the signal of the authentic standard in representative matrix, a RF_{ratio} of one was assumed rather than using the calculated value (labeled "RF_{ratio} assumed" in quantification methods of Supplementary Table 3.6). For detailed compound and sample set quantification details, see Supplementary Table 3.6.

Intracellular concentrations in culture were expressed in terms of millimolar intracellular concentration, using cell volume as estimated by microscopy following Hillebrand et al. (1999) for Antarctic species (Torstensson et al. 2019) and from literature values for temperate species (Durham et al. 2019), as listed in Table 3.1. Cell volumes used for the additional experimental growth conditions are exactly as in Heal et al. (2019) and Dawson et al. (2020). DMSP may volatilize during sample processing resulting in some loss of this compound (Spielmeyer and Pohnert 2010). Good agreement among replicates suggests that losses are similar across samples and therefore estimated intracellular concentrations can be taken as a minimum value.

3.3.5 *Statistical approaches*

For multivariate analysis, intracellular concentrations were standardized to the maximum intracellular concentration observed for each compound across all samples. A nonmetric approach

was used to accommodate for the high variable to sample ratio and the non-normal distribution of peak areas across samples. An NMDS analysis (Kruskal and Wish 1978) was used based on a Euclidean distance matrix of standardized peak areas to visualize overall differences between samples; dimensionality of the NMDS was assessed by examining a scree plot and calculated the probability with a Monte-Carlo permutation. Data transformation, standardization and NMDS were performed in R using the vegan (version 2.5-6), and MASS (version 7.3.51.5) packages in R (version 4.0-0).

3.4 RESULTS

3.4.1 *Growth rates and cell volume of different diatoms*

All samples for metabolomic analysis were collected during exponential growth under replete conditions and were previously analyzed for other studies (Heal 2018; Heal et al. 2019; Torstensson et al. 2019). Culture growth rates and cell volumes for the sea-ice diatoms are published (Torstensson et al. 2019). Growth rates for the temperate diatoms were published in Heal (2018) and Heal et al. (2019). Cell volumes for temperate species were previously reported in Durham et al. (2019). This information is summarized in Table 3.1.

All sea-ice diatoms grown at −1°C had specific growth rates close to 0.2 d^{-1} (Torstensson et al. 2019) whereas the temperate diatoms grown at 13°C had specific growth rates of ∼0.7 d^{-1} and 0.5 d^{-1} for *T. pseudonana* and *N. pelliculosa*, respectively (Heal 2018; Heal et al. 2019). Measured cell volumes for polar diatoms ranged from 22, 75, and 190 μm^3 for *F. cylindrus, N.* cf. *perminuta*, and *N. lecointei*, respectively (Torstensson et al. 2019), whereas both temperate diatoms had reported cell volumes in the middle of this range, 60 and 50 μm^3 for *T. pseudonana* and *N. pelliculosa*, respectively (Durham et al. 2019).

3.4.2 *Metabolite overview*

A total of 45 metabolites could be quantified and are ranked according to their abundance averaged across all species in Figure 3.1. Many well-known compatible solutes (e.g., proline, DHPS, glutamic acid, homarine and DMSP) are the most abundant though their concentrations vary widely between species. Full quantification data are shown in Supplementary Table 3.7.

Stacked intracellular concentrations of 45 quantified metabolites for each diatom species is shown in Figure 3.2. *Fragilariopsis cylindrus and Navicula* cf. *perminuta* had considerably higher total measured metabolite pools (~3 and ~2 M, respectively) compared to *N. lecointei* (500 mM) and the temperate diatoms. This is predominantly driven by large intracellular pools of 3–4 metabolites. In both *F. cylindrus* and *N.* cf. *perminuta*, glutamic acid is highly abundant. *N.* cf. *perminuta* also has a high concentration of proline, whereas *F. cylindrus* has high concentrations of ornithine and isethionic acid. While at lower concentrations, major metabolites in *N. lecointei* include DMSP and DHPS, in *T. pseudonana* include glutamic acid and proline and in *N. pelliculosa* include arginine and proline.

NMDS based on the proportional concentrations of all measured metabolites was used to explore the relationships between different species (full list of metabolites and concentrations shown in Supplementary Table 3.7). To compare interspecific variation in metabolite pools with intraspecific variation under different growth conditions, data from experimental growth conditions of *N. lecointei* (temperatures −1°C and 4°C, and salinities 32 and 41, Dawson et al. 2020) and *T. pseudonana* (cobalamin and/or light limitation, Heal et al. 2019) were also included. While separation within a species due to growth conditions could be observed in nondimensional space, all species were clearly separated from each other regardless of growth conditions (Figure 3.3).

3.4.3 *Sulfur-containing compatible solutes*

Cellular concentrations of select S-containing compatible solutes and metabolites involved in cell-cell interactions are shown in Table 3.2. DMSP was present in all strains except *N. pelliculosa*. Within the sea-ice diatoms, *F. cylindrus* is noticeable in lacking DHPS but has high concentrations of isethionic acid (~1 M) and taurine (~340 mM), which are both at sub-millimolar concentrations or below detection in the other diatom species tested (here and Durham et al. 2019). *Navicula* cf. *perminuta* has high concentrations of DHPS (~200 mM) and cysteic acid (~40 mM), whereas DHPS is the only sulfonated compatible solute tested that had a high concentration in *N. lecointei* (~75 mM).

3.4.4 *Nitrogen-containing compatible solutes*

Nitrogen-containing metabolites, particularly quaternary amines, are known to be important compatible solutes in sea-ice diatoms, though few studies have quantified intracellular concentrations. Table 3.3 shows selected nitrogenous compounds known to function as compatible solutes. *Fragilariopsis cylindrus* is enriched in ornithine (~700 mM). *Navicula* cf. *perminuta* is enriched in proline (>600 mM). Of the selected N-containing metabolites in Table 3.3, only GBT and proline are of a reasonably high concentration in *N. lecointei.* Interestingly, GBT is a widely used compatible solute and has a similar concentration (~20 mM) across all species with the exception of *N. pelliculosa*, where it was not detected. Other possible nitrogenous compatible solutes, such as ectoine (Fenizia et al. 2020) and proline betaine (Bashir et al. 2014), were not found in high concentrations.

3.4.5 *Free amino acid pools*

A selection of free proteinogenic amino acids was quantified (concentrations in Supplementary Table 3.7). *Navicula* cf. *perminuta* and *F. cylindrus* (pools totaling ~1.5 and ~1 M, respectively) had higher free amino acids compared to the other species (<400 mM) (Figure 3.4). Besides proline, glutamic acid is a major pool and to a lesser extent alanine, arginine and aspartic acid. In addition, lysine and tyrosine were also significant pools in *F. cylindrus*.

3.5 DISCUSSION

3.5.1 *Diversity in compatible solute profiles is indicative of multiple functions and complementary pathways*

Isethionic acid was the most abundant metabolite measured, ~1 M in *Fragilariopsis cylindrus*, though <1 mM in the other two sea-ice diatoms and not detected in either temperate species. Its precursor, taurine, is also highly abundant (340 mM) in *F. cylindrus* compared to the other diatoms (<1 mM). A survey of marine phytoplankton and bacterial cultures by Durham et al. (2019) found isethionic acid in temperate diatoms, *Pseudo-nitzschia pungens* (20 mM) and *Cyclotella meneghiniani* (4 mM), though not in any of the other cultures. The prevalence of *F. cylindrus* in both sea ice and pelagic polar environments, coupled with high concentrations of isethionic acid found within *F. cylindrus* cultures (this study and qualitatively in Boroujerdi et al. 2012) and environmental sea-ice samples (Dawson et al. 2020), suggest that isethionic acid may be potentially important in polar biogeochemical cycles.

In contrast to isethionic acid, another sulfonate, DHPS, was not detected in *F. cylindrus*, despite being widespread in other diatoms and coccolithophores (this study and Durham et al. 2019), and within seawater and sea ice (Durham et al. 2015; Boysen et al. 2020; Dawson et al. 2020). While intracellular concentrations of DHPS in *Nitzschia lecointei* and *Navicula*

pelliculosa matched those published in Durham et al. (2019) and Dawson et al. (2020), respectively, concentrations in *Thalassiosira pseudonana* were ~10-fold higher than measured by Durham et al. (2019), possibly due to differing culture conditions. In addition to their roles as compatible solutes, isethionic acid, taurine, and DHPS (and DMSP) are involved in algal–bacterial interactions (Mayer et al. 2010; Amin et al. 2015; Durham et al. 2015; Landa et al. 2019). These different sulfonated pathways may possibly fulfill complementary roles in cell homeostasis and cryptic sulfur cycling.

Of the nitrogen-containing compatible solutes we measured, homarine was higher in both *F. cylindrus* and *N.* cf. *perminuta*, as was ornithine in *F. cylindrus*. The dinoflagellate *Amphidinium carterae* and haptophyte *Emiliania huxleyi* had 0.2 and 0.5 mM homarine, respectively (Keller et al. 1999), though another study by Gebser and Pohnert (2013) found 20 mM in *E. huxleyi* increasing to 47 mM with a doubling of salinity. Homarine is prevalent in the marine environment, including sea-ice communities (Dawson et al. 2020) and tropical surface waters (Keller et al. 2004; Boysen et al. 2020), and could potentially be an important organic substrate in marine biogeochemical cycles.

Ornithine is known to act as a compatible solute in higher plants (Slama et al. 2015) but is mostly associated with salt stress in the sea-ice diatom *F. cylindrus* as an alternative precursor to glutamate for proline synthesis (Krell et al. 2007). In diatoms, ornithine is also an important component of the ornithine-urea cycle, which can be used for recycling nitrogen within the cell (Allen et al. 2011). In addition, diatoms use ornithine and its decarboxylated product to anchor polyamines that provide the organic scaffolding for silica frustule synthesis (Kröger et al. 2000). The high concentrations of ornithine in *F. cylindrus* suggest that it is used directly as a major

compatible solute though questions remain whether this high concentration also impacts proline synthesis, urea cycling or frustule biosynthesis.

Proline was highly abundant in *N.* cf. *perminuta* (>600 mM). Both Krell et al. (2007) and Dawson et al. (2020) found >4-fold variation in proline concentrations in response to salinity in *N. lecointei* and *F. cylindrus*, respectively. In contrast, GBT, a well-known compatible solute across many different organisms, has moderate and similar intracellular concentrations across all species tested (except *N. pelliculosa* in which it was absent). Dawson et al. (2020) found no clear pattern of regulation in response to temperature and salinity in *N. lecointei*. GBT also modulates methylation of gene promoters to regulate gene expression (Figuerosa-Soto and Valenzuela-Soto 2018), and at vacuolar concentrations >0.1 M can enhance diatom buoyancy (Boyd and Gradmann 2002). GBT abundance is strongly regulated in response to cobalamin availability in *T. pseudonana* (Heal et al. 2019) and between exponential and stationary growth in other eukaryotic algae (Keller et al. 1999). While GBT is an effective compatible solute in sea-ice diatoms via uptake, retention, and release, as shown for *N. lecointei* in Torstensson et al. (2019), its *de novo* synthesis may not be strongly regulated by temperature and salinity in sea-ice diatoms.

3.5.2 *Free amino acid pools*

The free amino acid pool can be utilized for protein synthesis, as stores of metabolic intermediates and as compatible solutes in their own right (Clark et al. 1972). In *N.* cf. *perminuta* and *F. cylindrus*, elevated levels of free amino acid pools of alanine, arginine, glutamic acid, and aspartic acid were found, which are all elevated in plants under abiotic stress (Mansour 2000). Glutamic acid was particularly large in these species; it is known to act as a compatible solute and is a precursor for proline synthesis (Fujii et al. 1995). High tyrosine in *F. cylindrus* compared to other

species (33 mM compared to ≤1 mM in others) could be related to the role of tyrosine kinases in regulating cell volume during salt stress (Pasantes-Morales et al. 2006).

3.5.3 *Environment and cell size likely factor into the requirement of high intracellular concentrations of compatible solutes*

The large variability in intracellular metabolite concentrations across different diatom species suggests no preference of particular compatible solutes by sea-ice diatoms. Perhaps the general flexibility of diatom metabolism overrides any sea-ice-specific response. Alternatively, the similar salinities in our cultures may have masked any sea-ice response, which may only be identifiable under salt stress. Nonetheless, N- and S-containing compatible solute concentrations approaching 1 M in the sea-ice diatoms *F. cylindrus* and *N.* cf. *perminuta* are among the highest concentrations measured in eukaryotic algae although there are few data available. DMSP can reach ∼1 M in some dinoflagellates and prymnesiophytes (McParland and Levine 2019) and GBT can reach close to 1 M in halophilic bacteria (Imhoff and Rodriguez-Valera 1984). Adaptation to a permanently cold, fluctuating salinity environment may have resulted in these two species maintaining high intracellular concentrations of compatible solutes compared to temperate diatoms.

High concentrations of some potential compatible solutes and free amino acids in *F. cylindrus* and *N.* cf. *perminuta* contrasted with the third sea-ice diatom analyzed, *N. lecointei,* that had no uniquely high concentrations of any measured compatible solutes. This could be due to a number of factors: *N. lecointei* may use compatible solutes that we were unable to quantify, may have different intracellular concentrations/pumping of cations (K^+/Na^+), or employ other strategies (e.g., EPS, Steele et al. 2014). *Nitzschia lecointei* is considerably larger (190 μm^3) compared to *F. cylindrus* (22 μm^3). An overestimation of cell cytosol volume (e.g., to the presence of large vacuoles) would result in calculated lower intracellular concentrations, though this is unlikely as

there is not a consistent trend across all metabolites. The smaller surface area: volume in *N. lecointei* may reduce the need for large intracellular pools of compatible solutes although more species and more conditions are needed before any conclusions can be drawn. Cell size and intracellular concentrations of metabolites are not fixed, and can vary in response to environmental stress. Gebser and Pohnert (2013) found that the haptophye, *E. huxleyi*, will change cell size but maintain compatible solute ratios in response to salinity shifts whereas the dinoflagellate *Prorocentrum minimum* changes compatible solute ratios while maintaining volume. Both Krell et al. (2007) and Dawson et al. (2020) found a 3- to 4-fold increase in proline concentrations in response to an upshift in salinity of 36 for *F. cylindrus* and 10 for *N. lecointei*, respectively. Dawson et al. (2020) also found an increase in a number of other compatible solutes, responding to both temperature and salinity, in conjunction with a small change in cell size. This study provides one of the first surveys of baseline intracellular concentrations of a variety of compatible solutes and amino acids in sea-ice diatoms under nutrient replete, exponential growth, highlighting the diversity in composition. Further research is needed to determine how these profiles may be regulated under varying environmental conditions, as has been shown for other marine environments (Boysen et al. 2020).

3.5.4 *Environmental implications*

Little is known about the intentional release of compatible solutes during normal growth or rates of cell lysis, but some compatible solutes can be rapidly ejected from the cell in response to a hypoosmotic shock (Torstensson et al. 2019) producing dissolved organic carbon. Dawson et al. (2020) used "back-of-the-envelope" calculations based on *N. lecointei* and field samples to demonstrate that a large release of the nitrogenous compatible solutes due to ice melt could be a significant source of labile dissolved organic nitrogen. Considering that *N. lecointei* had some of

the lowest compatible solute concentrations that were measured here, regulation and release of compatible solutes by a mix of sea-ice algal species (and thus the community composition) could be an important missing component of the nitrogen cycling budget in polar oceans.

3.6 Data Availability Statement

The data underlying this study are available in the published article's online supplementary material (https://doi.org/10.1093/icb/icaa133), and available in Metabolomics Workbench (https://www.metabolomicsworkbench.org/data/ index.php) study ID ST001480. *T. pseudonana* data are available in Metabolights (https://www.ebi.ac.uk/metabolights/) under study ID S703.

3.7 Acknowledgements

This work was supported by grants from the National Science Foundation (OPP 1744645, J.N.Y.) and the Simons Foundation (561645 to J.N.Y.; 385428 and 329108 to A.E.I.; 598819 to K.R.H.). We would like to thank Natalie Kellogg, Regina Lionheart and Alec Meyers for assistance in the culturing, microscopic counts, and extraction of *T. pseudonana* and *N. pelliculosa* cultures and Alec Meyers for LC-MS run set up. Thanks also to the National Science Foundation (OPP 1925160 to Jim McClintock); the Society of Integrative and Comparative Biology, including its divisions of Comparative Physiology and Biochemistry, Ecology and Evolution, and Invertebrate Zoology; the American Microscopical Society; and The Crustacean Society for support of the Antarctic Symposium. We appreciate the helpful comments of two anonymous reviewers.

References

Aguirre LE, Ouyang L, Elfwing A, Hedblom M, Wulff A, Inganäs O. 2018. Diatom frustules protect DNA from ultraviolet light. Sci Rep 8:5138.

Allen AE, Dupont CL, Oborník M, Horák A, Nunes-Nesi A, McCrow JP, Zheng H, Johnson DA, Hu H, Fernie AR, et al. 2011. Evolution and metabolic significance of the urea cycle in photosynthetic diatoms. Nature 473:203–7.

Amin SA, Hmelo LR, van Tol HM, Durham BP, Carlson LT, Heal KR, Morales RL, Berthiaume CT, Parker MS, Djunaedi B, et al. 2015. Interaction and signaling between a cosmopolitan phytoplankton and associated bacteria. Nature 522:98–101.

Antón J. 2011. Compatible solute. In: Gargaud M, Amils R, Quintanilla JC, Cleaves HJ, Irvine WM, Pinti D, Viso M, editors. Encyclopedia of astrobiology. Berlin, Heidelberg, Germany: Springer.

Arrigo KR. 2016. Sea ice as a habitat for primary producers. In: Thomas DN, editor. Sea ice. 3rd ed. Hoboken (NJ): John Wiley and Sons Ltd. P. 352–69.

Bashir A, Hoffmann T, Kempf B, Xie X, Smits SHJ, Bremer E. 2014. Plant-derived compatible solutes proline betaine and betonicine confer enhanced osmotic and temperature stress tolerance to *Bacillus subtilis*. Microbiology 160:2283–94.

Bligh EG, Dyer WJ. 1959. A rapid method of total lipid extraction and purification. Can J Biochem Physiol 37:911–7.

Boroujerdi AFB, Lee PA, DiTullio GR, Janech MG, Vied SB, Bearden DW. 2012. Identification of isethionic acid and other small molecule metabolites of *Fragilariopsis cylindrus* with nuclear magnetic resonance. Anal Bioanal Chem 404:777–84.

Boyd CM, Gradmann D. 2002. Impact of osmolytes of marine phytoplankton. Mar Biol 141:605–18.

Boysen AK, Carlson LT, Durham BP, Groussman RD, Aylward FO, Ribalet F, Heal KR, DeLong EF, Armbrust EV, Ingalls AE. 2020. Diel oscillations of particulate metabolites reflect synchronized microbial activity in the North Pacific subtropical gyre. bioRxiv. 2020.05.09.086173

Boysen AK, Heal KR, Carlson LT, Ingalls AE. 2018. Best-matched internal standard normalization in liquid chromatography–mass spectrometry metabolomics applied to environmental samples. Anal Chem 90:1363–9.

Bullock HA, Luo H, Whitman WB. 2017. Evolution of dimethylsulfoniopropionate metabolism in marine phytoplankton and bacteria. Front Microbiol 8:637.

Clark VL, Peterson DE, Bernlohr RW. 1972. Changes in free amino acid production and intracellular amino acid pools of *Bacillus licheniformis* as a function of culture age and growth media. J Bacteriol 112:715–25.

DasSarma S, Capes MD, Karan R, DasSarma P. 2013. Amino acid substitutions in cold-adapted proteins from *Halorubrumlacus profundi*, an extremely halophilic microbe from Antarctica. PLoS One 8: e58587.

Dawson HM, Heal KR, Boysen AK, Carlson LT, Ingalls AE, Young JN, Helmig D, Arrigo K. 2020. Potential of temperature- and salinity-driven shifts in diatom compatible solute concentrations to impact biogeochemical cycling within sea ice. Elem Sci Anth 8:25.

Deming JW, Young JN. 2017. The role of exopolysaccharides in cold-adaptation. In: Margesin R, editor. Psychrophiles: from biodiversity to biotechnology. 2nd ed. Berlin, Heidelberg, Germany: Springer-Verlag. p. 259–84.

Durham BP, Boysen AK, Carlson LT, Groussman RD, Heal KR, Cain KR, Morales RL, Coesel SN, Morris RM, Ingalls AE, Armbrust EV. 2019. Sulfonate-based networks between eukaryotic phytoplankton and heterotrophic bacteria in the surface ocean. Nat Microbiol 4:1706–15.

Durham BP, Sharma S, Luo H, Smith CB, Amin SA, Bender SJ, Dearth SP, Van Mooy BAS, Campagna SR, Kujawinski EB, et al. 2015. Cryptic carbon and sulfur cycling between surface ocean plankton. Proc Natl Acad Sci U S A 112:453–7.

Fenizia S, Thume K, Wirgenings M, Pohnert G. 2020. Ectoine from bacterial and algal origin is a compatible solute in microalgae. Mar Drugs 18:42.

Figueroa-Soto CG, Valenzuela-Soto EM. 2018. Glycine betaine rather than acting only as an osmolyte also plays a role as regulator in cellular metabolism. Biochimie 147:89–97.

Firth E, Carpenter SD, Sørensen HL, Collins RE, Deming JW. 2016. Bacterial use of choline to tolerate salinity shifts in sea-ice brines. Elem Sci Anthr 4:000120.

Fujii S, Nishimoto N, Notoya A, Hellebust JA. 1995. Growth and osmoregulation of *Chaetoceros muelleri* in relation to salinity. Plant Cell Physiol 36:759–64.

Gebser B, Pohnert G. 2013. Synchronized regulation of different zwitterionic metabolites in the osmoadaption of phytoplankton. Mar Drugs 11:2168–82.

Gianese G, Argos P, Pascarella S. 2001. Structural adaptation of enzymes to low temperatures. Protein Eng 14:141–8.

Graeve M, Kohlbach D, Vortkamp M, van Franeker JA, Brandt A, Flores H, Schaafsma FL, Lange BA, David C. 2018. Dependency of Antarctic zooplankton species on ice algae-

produced carbon suggests a sea ice-driven pelagic ecosystem during winter. Glob Chang Biol 24:4667–81.

Guillard RRL. 1975. Culture of phytoplankton for feeding marine invertebrates. In: Smith WL, Chanley MH, editors. Culture of marine invertebrate animals. Boston (MA): Springer. p. 29–60.

Heal KR. 2018. The power and promise of direct measurements of metabolites in marine systems. [Ph. D thesis]. [Seattle (WA)]: University of Washington.

Heal KR, Kellogg NA, Carlson LT, Lionheart RM, Ingalls AE. 2019. Metabolic consequences of cobalamin scarcity in the diatom *Thalassiosira pseudonana* as revealed through metabolomics. Protist 170:328–48.

Hillebrand H, Dürselen CD, Kirschtel D, Pollingher U, Zohary T. 1999. Biovolume calculation for pelagic and benthic microalgae. J Phycol 35:403–24.

Imhoff JF, Rodriguez-Valera F. 1984. Betaine is the main compatible solute of halophilic eubacteria. J Bacteriol 160:478–9.

Kameyama S, Otomaru M, McMinn A, Suzuki K. 2020. Ice melting can change DMSP production and photosynthetic activity of the haptophyte *Phaeocystis antarctica* 1. J Phycol 56:761–74.

Keller MD, Kiene RP, Matrai PA, Bellows WK. 1999. Production of glycine betaine and dimethylsulfoniopropionate in marine phytoplankton. II. N-limited chemostat cultures. Mar Biol 135:249–57.

Keller MD, Matrai PA, Kiene RP, Bellows WK. 2004. Responses of coastal phytoplankton populations to nitrogen additions: dynamics of cell-associated dimethylsulfoniopropionate (DMSP), glycine betaine (GBT), and homarine. Can J Fish Aquat Sci 61:685–99.

Kim M, Yang EJ, Kim D, Jeong JH, Kim HJ, Park J, Jung J, Ducklow HW, Lee S, Hwang J. 2019. Sinking particle flux and composition at three sites of different annual sea ice cover in the Amundsen Sea, Antarctica. J Mar Syst 192:42–50.

Krell A, Funck D, Plettner I, John U, Dieckmann G. 2007. Regulation of proline metabolism under salt stress in the psychrophilic diatom *Fragilariopsis cylindrus* (Bacillariophyceae). J Phycol 43:753–62.

Kröger N, Deutzmann R, Bergsdorf C, Sumper M. 2000. Species-specific polyamines from diatoms control silica morphology. Proc Natl Acad Sci U S A 97:14133–8.

Kruskal JB, Wish M. 1978. Multidimensional scaling. In: Uslaner E, editor. Paper series on quantitative applications in the social sciences. Vol. 07–011. Beverly Hills and London: Sage Publications. p. 7–28.

Landa M, Burns AS, Durham BP, Esson K, Nowinski B, Sharma S, Vorobev A, Nielsen T, Kiene RP, Moran MA. 2019. Sulfur metabolites that facilitate oceanic phytoplankton–bacteria carbon flux. ISME J 13:2536–50.

Leu E, Mundy CJ, Assmy P, Campbell K, Gabrielsen TM, Gosselin M, Juul-Pedersen T, Gradinger R. 2015. Arctic spring awakening – steering principles behind the phenology of vernal ice algal blooms. Prog Oceanogr 139:151–70.

Lund JWG, Kipling C, Le Cren ED. 1958. The inverted microscope method of estimating algal numbers and the statistical basis of estimations by counting. Hydrobiologia 11:143–70.

Lyon BR, Bennett-Mintz JM, Lee PA, Janech MG, Ditullio GR. 2016. Role of dimethylsulfoniopropionate as an osmoprotectant following gradual salinity shifts in the sea-ice diatom *Fragilariopsis cylindrus*. Environ Chem 13:181–94.

MacLean B, Tomazela DM, Shulman N, Chambers M, Finney GL, Frewen B, Kern R, Tabb DL, Liebler DC, MacCoss MJ. 2010. Skyline: an open source document editor for creating and analyzing targeted proteomics experiments. Bioinformatics 26:966–8.

Mansour MMF. 2000. Nitrogen containing compounds and adaptation of plants to salinity stress. Biol Plant 43:491–500.

Mayer J, Huhn T, Habeck M, Denger K, Hollemeyer K, Cook AM. 2010. 2,3-Dihydroxypropane-1-sulfonate degraded by *Cupriavidus pinatubonensis* JMP134: purification of dihydroxypropanesulfonate 3-dehydrogenase. Microbiology 156:1556–64.

McMinn A, Martin A, Ryan K. 2010. Phytoplankton and sea ice algal biomass and physiology during the transition between winter and spring (McMurdo Sound, Antarctica). Polar Biol 33:1547–56.

McParland EL, Levine NM. 2019. The role of differential DMSP production and community composition in predicting variability of global surface DMSP concentrations. Limnol Oceanogr 64:757–73.

Pasantes-Morales H, Lezama RA, Ramos-Mandujano G. 2006. Tyrosine kinases and osmolyte fluxes during hyposmotic swelling. Acta Physiol 187:93–102.

Roukaerts A, Cavagna AJ, Fripiat F, Lannuzel D, Meiners KM, Dehairs F. 2016. Sea-ice algal primary production and nitrogen uptake rates off East Antarctica. Deep Sea Res Part II Top Stud Oceanogr 131:140–9.

Saito MA, Moffett JW, Chisholm SW, Waterbury JB. 2002. Cobalt limitation and uptake in *Prochlorococcus*. Limnol Oceanogr 47:1629–36.

Sheehan CE, Petrou K. 2020. Dimethylated sulfur production in batch cultures of Southern Ocean phytoplankton. Biogeochemistry147:53–69.

Slama I, Abdelly C, Bouchereau A, Flowers T, Savouré A. 2015. Diversity, distribution and roles of osmoprotective compounds accumulated in halophytes under abiotic stress. Ann Bot 115:433–47.

Spielmeyer A, Pohnert G. 2010. Direct quantification of dimethylsulfoniopropionate (DMSP) with hydrophilic interaction liquid chromatography/mass spectrometry. J Chromatogr B Anal Technol Biomed life Sci 878:3238–42.

Steele DJ, Franklin DJ, Underwood GJC. 2014. Protection of cells from salinity stress by extracellular polymeric substances in diatom biofilms. Biofouling 30:987–98.

Thomas DN, Dieckmann G. 2003. Sea Ice: an introduction to its physics, chemistry, biology and geology. Hoboken (NJ): Blackwell Science Ltd.

Torstensson A, Dinasquet J, Chierici M, Fransson A, Riemann L, Wulff A. 2015. Physicochemical control of sea ice microbial communities. Environ Microbiol 17:3869–81.

Torstensson A, Hedblom M, Andersson J, Andersson MX, Wulff A. 2013. Synergism between elevated pCO_2 and temperature on the Antarctic sea ice diatom *Nitzschia lecointei*. Biogeosciences 10:6391–401.

Torstensson A, Young JN, Carlson LT, Ingalls AE, Deming JW. 2019. Use of exogenous glycine betaine and its precursor choline as osmoprotectants in Antarctic sea-ice diatoms. J Phycol 675:663–75. o.

Toseland A, Daines SJ, Clark JR, Kirkham A, Strauss J, Uhlig C, Lenton TM, Valentin K, Pearson GA, Moulton V, et al. 2013. The impact of temperature on marine phytoplankton resource allocation and metabolism. Nat Clim Change 3:979–84.

van Leeuwe MA, Tedesco L, Arrigo KR, Assmy P, Campbell K, Meiners KM, Rintala J-M, Selz V, Thomas DN, Stefels J, Deming JW. 2018. Microalgal community structure and primary production in Arctic and Antarctic sea ice: a synthesis. Elem Sci Anth 6:4.

Young JN, Schmidt K. 2020. It's what's inside that matters: physiological adaptations of high-latitude marine microalgae to environmental change. New Phytol 227:1307–18.

3.8 TABLES AND FIGURES

Table 3.1. Specific growth rate of axenic diatom cultures.

Diatom species	Growth temp (°C)	Specific growth rate (d^{-1})	Cell volume (μm^3)
Fragilariopsis cylindrus[a]	−1	0.19 ± 0.001	22
Nitzschia lecointei[a,c]	−1	0.22 ± 0.005	190
Navicula cf. *perminuta*[a,c]	−1	0.22 ± 0.006	75
Thalassiosira pseudonana[b,c]	13	0.66 ± 0.01	60
Navicula pelliculosa[b]	13	0.47 ± 0.01	50

Data show mean ± SD (n = 2) unless noted.

[a] Antarctic diatom cultures grown for 140 h at 31 ppt salinity and −1˚C. Cell volume as measured by microscopy in Torstensson et al. (2019).

[b] Mesophilic diatom cultures grown for 120 and 144 h, respectively, at 35 ppt salinity and 13˚C, n = 9. Cell volume based on previously reported values of cell dimension and size as reported in Durham et al. (2019).

[c] Growth rates for this species under additional experimental culture conditions can be found in Supplementary Table 3.3.

Table 3.2. Cellular concentrations of select S-containing compatible solutes.

Diatom species	DHPS (mM)	Cysteic acid (mM)	Sulfolactate (µM)	Isethionic acid (mM)	Taurine (mM)	DMSP (+/−)
Fragilariopsis cylindrus[a]	ND	0.200 ± 0.028	6 ± 2	973 ± 90	342 ± 1	+
*Nitzschia lecointe*i[a]	76 ± 6	2.2 ± 0.5	40 ± 4	0.94 ± 0.9	0.33 ± 0.3	+
Navicula cf. *Perminuta*[a]	211 ± 9	43 ± 6	6 ± 1	0.26 ± 0.1	ND	+
Thalassiosira pseudonana[b]	78 ± 8	0.005 ± 0.001	3 ± 0.3	ND	0.002 ± 0.0001	+
Navicula pelliculosa[b]	4.4 ± 3	ND	ND	ND	ND	−

[a] Sea-ice diatoms.

[b] Temperate diatoms.

ND, not detected.

Table 3.3. Cellular concentrations of select nitrogenous compatible solutes.

Diatom species	**GBT (mM)**	**Choline (mM)**	**Homarine (mM)**	**Homoserine (mM)**	**Ornithine (mM)**	**Proline (mM)**
Fragilariopsis cylindrus	37 ± 8	4 ± 1	37 ± 9	17 ± 5	685 ± 108	126 ± 23
Nitzschia lecointei	20 ± 0.2	4 ± 0.5	0.06 ± 0.04	1 ± 0.1	4 ± 1	49 ± 0.9
Navicula cf. *perminuta*	25 ± 2	49 ± 4	42 ± 4	16 ± 3	43 ± 3	627 ± 170
Thalassiosira pseudonana	18 ± 1	15 ± 2	12 ± 1	1.1 ± 0.2	7 ± 2	104 ± 13
Navicula pelliculosa	ND	0.05 ± 0.01	ND	ND	10 ± 0.6	86 ± 11

ND, not detected.

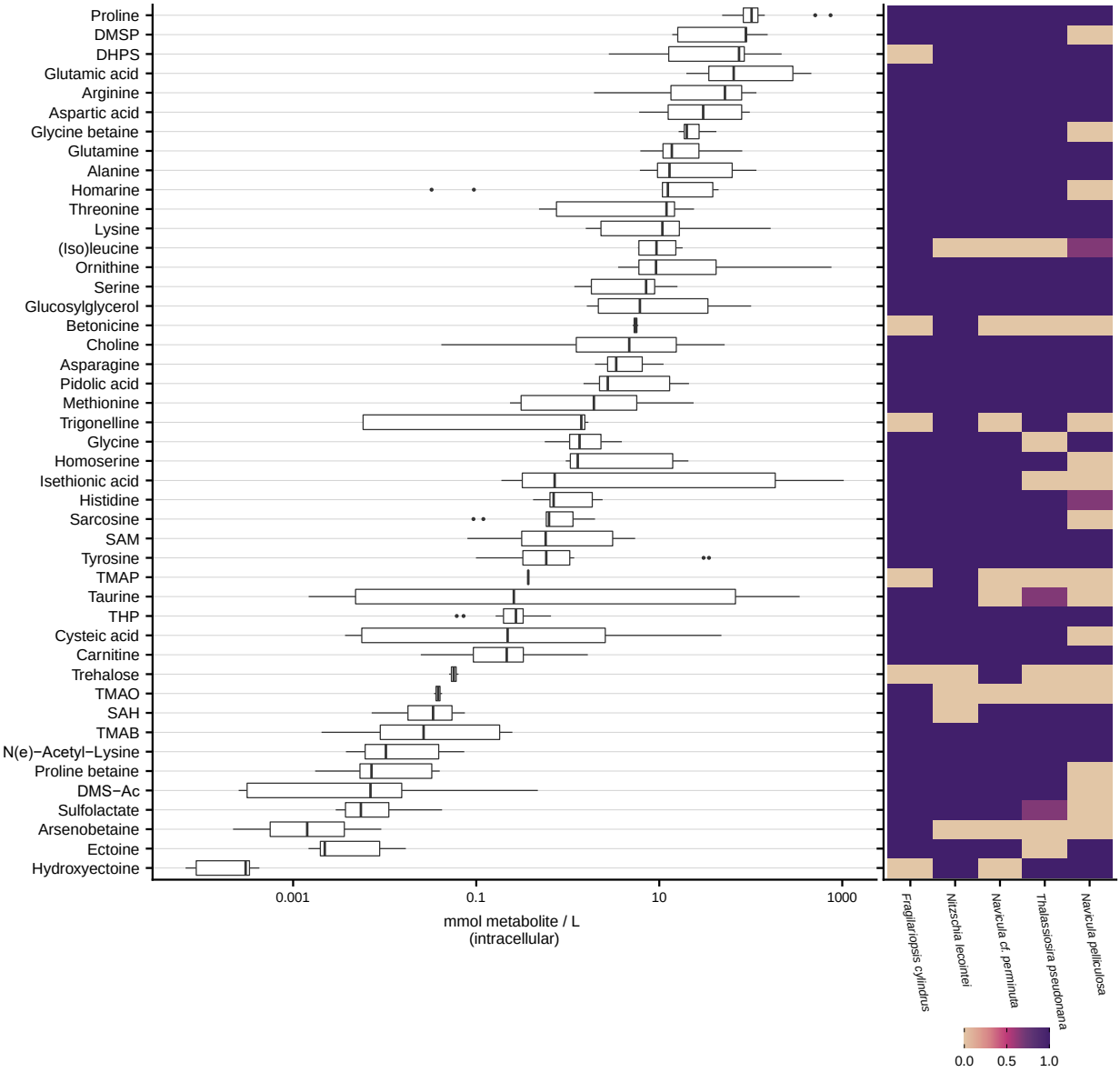

Figure 3.1. Left panel: Box and whisker plot of intracellular concentrations of quantifiable metabolites averaged across all species and replicates under optimal growth. The X-axis is log-scaled. Right panel: Presence/absence of a metabolite across replicates for each species. A value of 0 indicates it was not detected in that species, 1.0 indicates present in all replicates, and between

0 and 1 it was detected in some but not all replicates. Data are summarized in Supplementary Table 3.7.

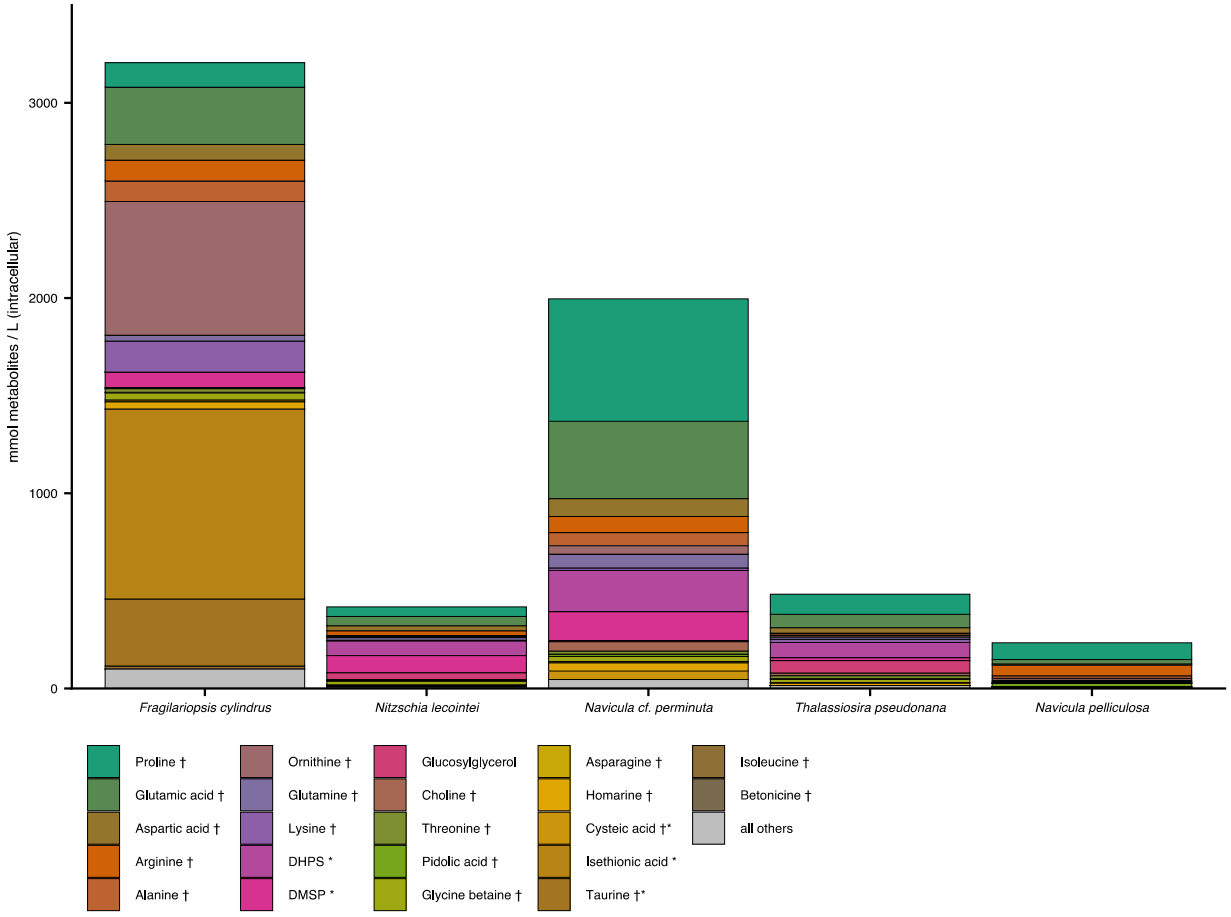

Figure 3.2. Intracellular concentrations of select metabolites across the five diatom species. Average of triplicates for *Thalassiosira pseudonana* and *Navicula pelliculosa* and duplicates for the three sea-ice diatoms. The most abundant 22 molecules for each organism are shown, with compounds that do not fall into this criterion depicted as a summed amount in gray. Crosses and asterisk denote N- and S-containing metabolites, respectively.

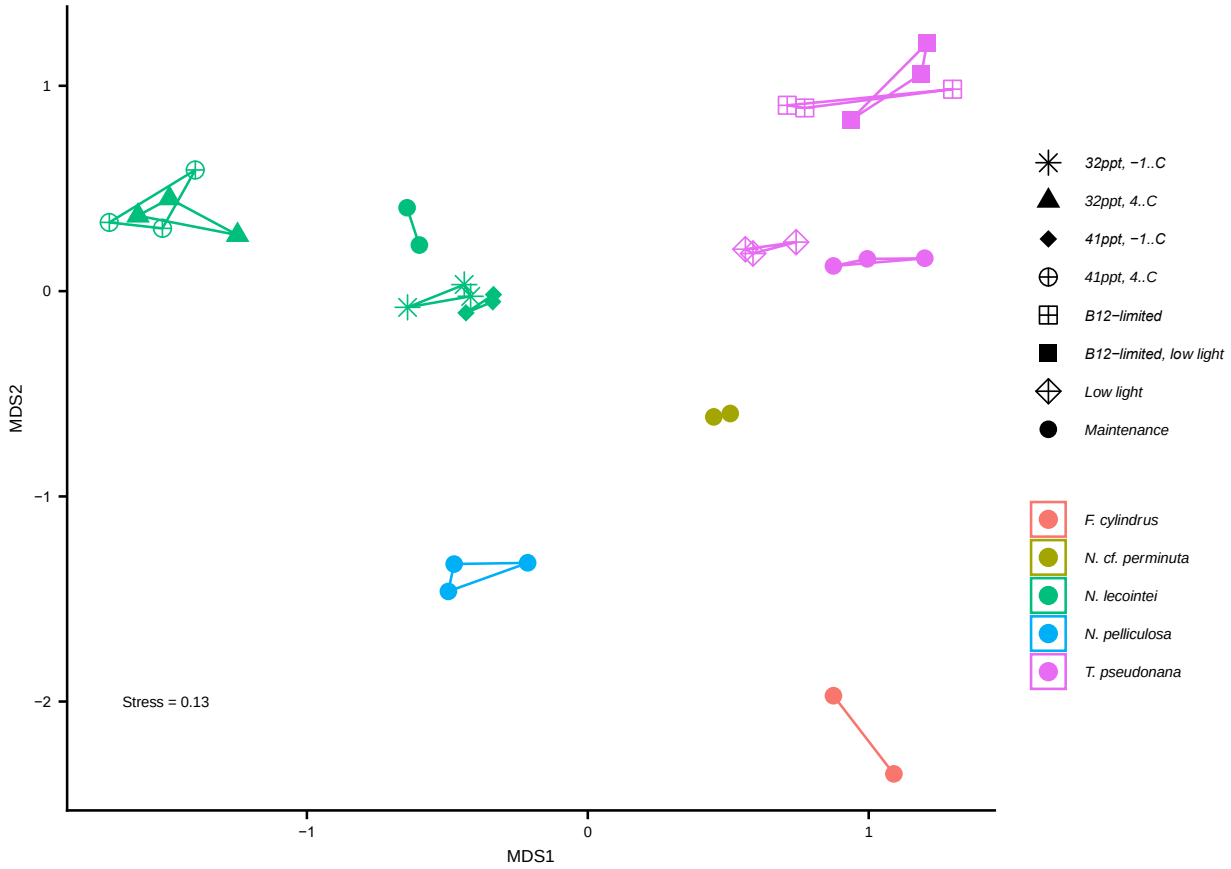

Figure 3.3. Nonmetric multidimensional scaling comparing the metabolite composition of five diatom species. Metabolite concentrations are scaled to the total measured metabolite pool for each replicate. Colors match different species and symbols indicate replicates under different growth conditions. Culture information and growth rates for all samples can be found in Supplementary Table 3.3. Metabolites included and raw intracellular concentrations for each can be found in Supplementary Table 3.7.

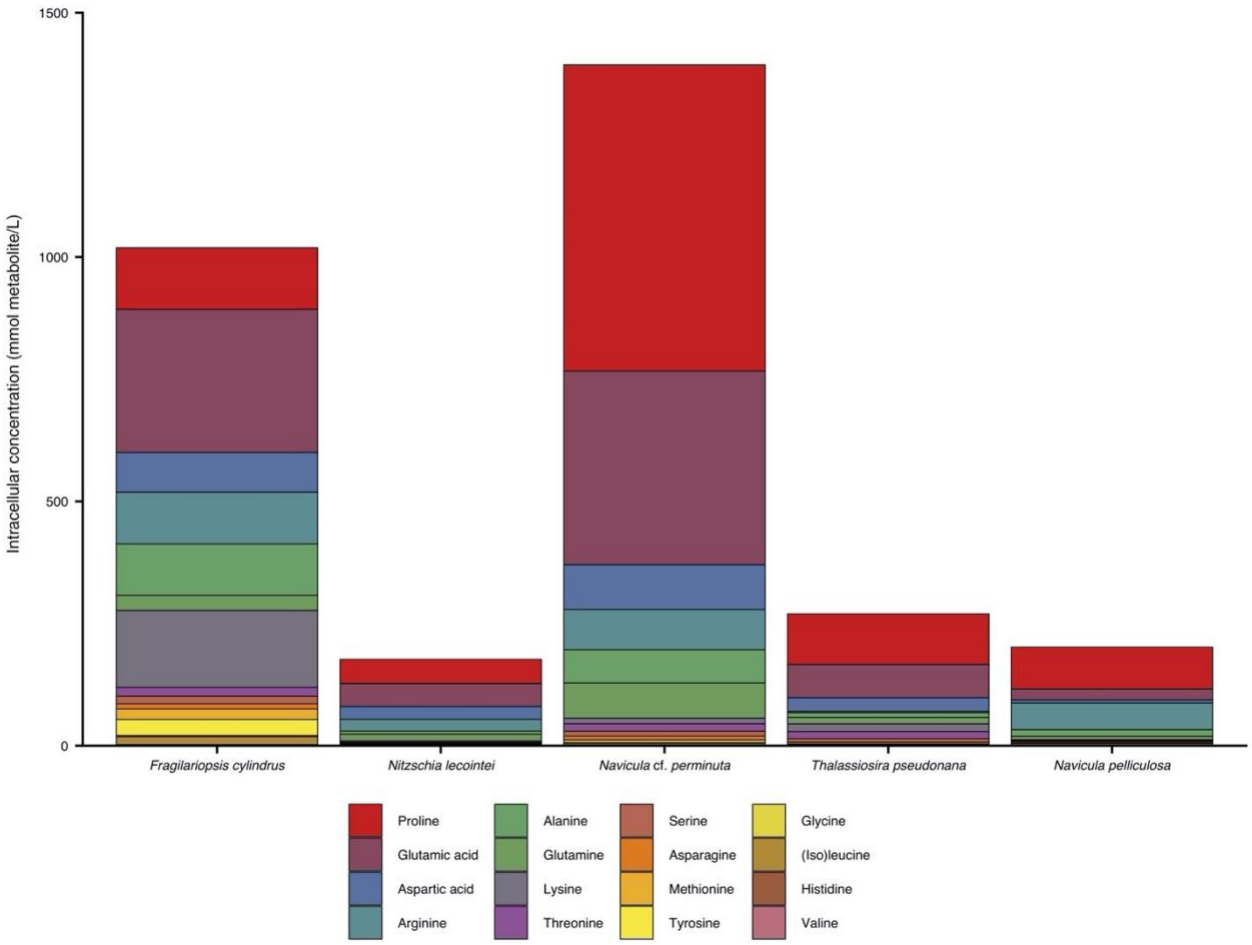

Figure 3.4. Stacked bar chart of intracellular concentrations of quantified free proteinogenic amino acids. Average of triplicates for *Thalassiosira pseudonana* and *Navicula pelliculosa*, and duplicates for *Nitzschia lecointei, Fragilariopsis cylindrus,* and *Navicula* cf. *perminuta.* Concentration data for each species is in Supplementary Table 3.7.

3.9 SUPPLEMENTARY TABLES

Supplementary Table 3.1. Isotopically-labeled internal standards used in B-MIS normalization and isotopologue quantification for *Fragilariopsis cylindrus*, *Nitzschia lecointei*, and *Navicula* cf. *perminuta* samples. The column, ion mode (z), injection concentration, and extracted *m*/*z* used for analysis for each standard. This table is provided as a separate file.

Supplementary Table 3.2. Isotopically-labeled internal standards used in B-MIS normalization and isotopologue quantification for *Navicula pelliculosa* and *Thalassiosira pseudonana* samples. The column, ion mode (z), injection concentration, and extracted *m*/*z* used for analysis for each standard. This table is provided as a separate file.

Supplementary Table 3.3. Sample details for cultures used in this study. Species, strain (if available), number of replicates (*n*), growth condition if different from maintenance growth condition listed in Table 3.1 (culture condition), culture condition abbreviation as used throughout supplemental tables, specific growth rate, data acquisition date (run date), internal standard suite used as listed in Supplementary Tables 3.1 and 3.2, and previous publication data appeared in for each sample. This table is provided as a separate file.

Supplementary Table 3.4. Compounds screened for presence, and further quantified if present, in this study. Full compound name, abbreviated compound name, *m*/*z*, average sample retention time (min), and charge (z) are listed for each compound screened. For quantifiable compounds (detected, passed through quality control parameters as listed in Supplementary Table 3.5) the number samples in which it was quantified, species in which it was quantified, and the

concentration range quantified across samples (mM) are listed. Experimental growth conditions for *Nitzschia lecointei* and *Thalassiosira pseudonana* are not included in this table. This table is provided as a separate file.

Supplementary Table 3.5. Quality control (QC) parameters used following peak integration and preceding B-MIS normalization. Peaks were removed from the data set (marked NA) if they did not meet the listed limits for minimum area to qualify as a real peak (Areamin), maximum fraction media blank can be of a sample (BlankRatiomax), parts per million mass error flexibility (ppmflex), minimum signal/noise ratio (SNmin), and minimum number of replicates detected (Repmin). Peaks were also removed if the retention time within a sample was greater than the allowed RT flexibility (RTflex) around the range of retention time of the compound in our concurrently run mix of standards. This table is provided as a separate file.

Supplementary Table 3.6. Quantification method for each quantified metabolite in each sample set. Full and abbreviated compound names are listed for each metabolite. Proxy compound (when applicable) is the compound by which a relative response factor (RF) was calculated. Details of quantification methods are provided in methods. Experimental growth conditions for *Nitzschia lecointei* and *Thalassiosira pseudonana* are included in this table. This table is provided as a separate file.

Supplementary Table 3.7. Full results of quantification in the present study for *Fragilariopsis cylindrus* (Fc), *Nitzschia lecointei* (Nl), *Navicula* cf *perminuta* (Nperm), *Navicula pelliculosa* (Npell), and *Thalassiosira pseudonana* (Tp). Nl and Tp experimental growth conditions are noted

after species ID if other than optimal. Reported concentrations were calculated from QC-filtered and B-MIS normalized peak areas using the quantification methods detailed in the methods section and summarized in Supplementary Table 3.6. Concentrations are mmol metabolite L^{-1} of intracellular volume, using cell volumes reported in Table 3.1 for normalization. Full and abbreviated compound names are provided for each metabolite. Mean and standard deviation are listed per compound per organism, denoted by the ending "_ave" and "_sd", respectively. This table is provided as a separate file.

Chapter 4. METABOLOME RESPONSES IN MICROBIAL COMMUNITIES ALONG THE WESTERN ANTARCTIC PENINSULA TO CHANGES IN TEMPERATURE AND SALINITY

A version of this chapter has been submitted for review to The ISME Journal as: Dawson, H.M., Connors, E., Erazo, N., Sacks, J.S., Mierzejewski, V., Rundell, S., Carlson, L.T., Deming, J.W., Ingalls, A.E., Bowman, J., Young, J.N. Metabolome responses in microbial communities along the western Antarctic Peninsula to changes in temperature and salinity.

4.1 ABSTRACT

Seasonal cycles within the marginal ice zones in polar regions include large shifts in temperature and salinity that strongly influence microbial abundance and physiology. However, the combined effects of concurrent temperature and salinity change on microbial community structure and biochemical composition during transitions between seawater and sea ice are not well understood. Coastal marine communities along the western Antarctic Peninsula were sampled and surface seawater was incubated at combinations of temperature and salinity mimicking the formation (cold, salty) and melting (warm, fresh) of sea ice to evaluate how these factors may shape community composition and particulate metabolite pools during seasonal transitions. Bacterial and algal community structures were tightly coupled to each other and distinct across sea-ice, seawater, and sea-ice-meltwater, with unique metabolite profiles in each habitat. During short-term (approximately 10-day) incubations under different temperature and salinity conditions, community compositions changed minimally while metabolite pools shifted dramatically, strongly

accumulating compatible solutes like proline and glycine betaine under cold and salty conditions. Lower salinities reduced total metabolite concentrations in particulate matter, which may have altered the composition of the labile dissolved organic matter pool. Low salinity also increased acylcarnitine concentrations, suggesting a potential for fatty acid degradation and reduced nutritional value at the base of the food web during freshening. Our findings have consequences for food web dynamics, microbial interactions, and carbon cycling as polar regions undergo rapid climate change.

4.2 INTRODUCTION

Surface ocean temperatures along the western Antarctic Peninsula (WAP) have increased by > 1°C since the 1950s (1). Associated changes in sea-ice thickness, extent, and duration have also been observed, along with increased occurrence of freshwater melt ponds and under-ice melt lenses (2,3). Glacial ice-mass loss has also contributed to greater freshwater inputs into coastal regions (4), with an observed overall warming and freshening of Southern Ocean waters (5). The largest glacial ice-mass loss in Antarctica was observed along the WAP (6), where a reduction in sea-ice extent and shorter sea-ice season have also been observed (7–10).

With global air temperatures expected to rise at least 1–3°C over the next century (11), coastal Antarctic ecosystems will likely be exposed to further warming, freshening, and alterations to seasonal ice dynamics. These changes can be expected to alter the temporal and spatial extent of unique microbial habitats that are created and lost seasonally with the formation and melting of sea ice, from and into the surrounding seawater. Microbial community composition is distinct across these polar environments (12–14), but the mechanisms that drive the distinctions are not fully understood. In terms of biomass, ice-associated communities are usually dominated by sea-ice algae, which can account for 55–65% of coastal Antarctic primary production (15) and provide a concentrated source of fixed carbon to microbes and higher trophic levels, particularly during winter when primary production in the water column is nearly zero (16). Newly formed sea-ice algal communities generally resemble the mixed community in the source seawater, while older ice loses centric diatoms and becomes dominated by large pennate diatoms; spring ice shows increasingly mixed communities before diatoms are lost during ice melt, leaving many flagellates (14). Prokaryotic taxa are similarly distinct, with newly formed sea-ice communities often

dominated by Alphaproteobacteria and Archaea, resembling source seawater, and spring ice shifting to dominance by Gammaproteobacteria and Flavobacteriia (13,17,18).

Transitions between polar marine habitats are associated with shifts in light, nutrients, temperature, and salinity (19–22). However, the combined role of temperature and salinity in shaping community composition among polar microorganisms, and the organic matter they use and produce, has not been fully explored. Limited work in sea ice has shown that moderate differences in temperature (–1.8 to –0.5˚C), with associated changes in salinity, correlate with differences in community composition for protists and bacteria (17). Culture studies of polar microalgae have shown physiological adaptations to shifting environments, including changes in ribosome and protein abundance, enzyme activity, fatty acid content and composition, production of ice-binding proteins and exopolymers, and alterations in compatible solute concentrations (for review, see (23,24)), but observations from mixed natural communities remain limited.

Compatible solutes, or osmolytes, are small organic molecules in a cell's cytosol that maintain turgor pressure and stabilize enzymes; they also play other roles (25,26). For example, they act as cryoprotectants in polar microalgae by reducing the intracellular freezing point and maintaining protein hydration spheres (27). Polar diatoms in culture accumulate compatible solutes to high intracellular concentrations (approximately 1 M) in a taxon-specific manner and alter concentrations as a function of temperature or salinity (28–33). Direct measurements of compatible solutes in polar environments are rare, but previous work suggests that many are similarly abundant in diatom-dominated sea ice and sea-ice diatom cultures (30).

Compatible solutes contribute to the larger pool of intracellular metabolites. Although marine particulate organic matter is composed largely of macromolecules (34), small polar metabolites, including compatible solutes, are the main component of the aqueous cytosol of cells

in particulate organic matter (35). These metabolites are considered a currency of the microbial loop (36), with roughly half of annual net primary production in the ocean rapidly cycling through the microbial loop as labile dissolved organic carbon (DOC; e.g. metabolites)(37). Metabolites serve as carbon, nutrient, and energy sources for heterotrophic bacteria (38,39), but also mediate phytoplankton-bacteria interactions, serve as predator repellants, manage redox stress, and more (35,40,41). Measurements of the diversity and concentration of small polar metabolites in natural marine communities are limited (42–44), particularly for polar regions (30), and the plasticity of metabolite concentrations is largely unknown (45). Intracellular metabolite pools can shift substantially in response to microbial interactions (38), making measurements on whole communities valuable alongside single-organism laboratory studies. Thus, *in situ* measurement of particulate metabolites and their sensitivity to temperature and salinity change will enhance our understanding of microbial physiology during seasonal transitions between polar marine habitats and the resultant impacts on community membership and chemical composition of marine organic matter.

Here, we characterize community structure and particulate metabolite profiles of bacterial and protist communities in sea-ice meltwater, seawater, and sea ice during austral spring along the WAP, recognizing that both the taxonomic composition of microbial communities and the chemical inventory of metabolites impact the flux of carbon and energy though polar food webs. We also examine the flexibility of metabolite pools in the surface seawater community under temperature and salinity conditions that mimic the formation and melt of sea ice. As polar oceans experience rapid warming, increased freshwater inputs, and shifts in seasonal ice formation and melt, this research serves to deepen our understanding of the potential responses of the microbial communities.

4.3 METHODS

4.3.1 *Field sample collections*

Sea-ice meltwater, seawater, and sea-ice samples were collected near Palmer Station, Anvers Island, Antarctica in November of 2018 (Table 4.1). Surface (< 1 m) seawater samples were collected into acid-clean carboys at 5 intervals over an 11-day period (November 8–19) in open water off Bonaparte Point (Station B of the LTER sampling grid; (46)). Sea-ice meltwater was collected into acid-clean carboys as surface water adjacent (< 1 m) to a melting pan of landfast sea ice located in Hero Inlet next to Palmer Station and the Marr Glacier. Sea-ice cores were collected in this area from the R/V *Lawrence M. Gould* using a Kovacs MARK II ice auger. For all ice cores, the bottom 5-cm sections were melted in the dark at 4°C into prefiltered (0.2 μm) seawater to avoid osmotic shock and cell lysis. Final salinity of ice samples following this melt procedure are provided in Table 4.1.

4.3.2 *Temperature and salinity incubations*

On 12 November 2018 (sample SW_12), we collected additional seawater for incubation experiments that simulated temperature(T)-salinity(S) conditions of sea-ice meltwater (3˚C and 21 ppt, designated Meltwater_T-S), ambient seawater (0˚C and 35 ppt, SW_T-S), and sea ice (c3˚C and 52 ppt, Sea ice_T-S). Triplicate 10-L polycarbonate carboys were used for each treatment. All samples were enriched with f/2 nutrients with silica (47) and incubated for approximately 10 days at 100 μmol photons m^{-2} s^{-1} light on a 20:4 h light:dark cycle. Incubations were subsampled daily for growth and harvested during exponential growth for the measurements detailed below. For details on incubation set up and monitoring, see Supplementary information.

4.3.3 *Sample processing*

Field and incubation samples were processed for particulate metabolomics, DNA sequencing, chlorophyll *a* (Chl *a*), particulate organic carbon and nitrogen (POC, PN), DOC, particulate and dissolved extracellular polysaccharides (pEPS, dEPS), and major nutrients (NO_3^-, NO_2^-, NH_4, SiO_4, PO_4^{3-}). All methods for the collection and processing of these samples are described in Supplementary information. Temperature, salinity, and photosynthetically active radiation (PAR) were measured using a digital thermometer, refractometer, and Walz US-SQS/L spherical quantum sensor with ULM-500 light meter, respectively.

4.3.4 *Metabolite extraction and LC-MS analysis*

Metabolites were extracted from samples filters, separated via liquid chromatography with a Waters Acquity I-Class UPLC coupled to a Thermo Q-Exactive mass spectrometer, and data was acquired in full scan mode for compound quantification as modified from Boysen et al. (2018). Further details on metabolite extraction and LC-MS analysis are provided in Supplementary information.

4.3.5 *Metabolomic data processing*

Metabolite peaks obtained from mass spectrometry were integrated using Skyline for small molecules (49). Full and abbreviated compound names are listed in Supplementary Table 4.1, with abbreviated names used in figures throughout. Integrated peak areas were subject to quality control (Supplementary Table 4.2) and normalized to the peak area of internal standards (Supplementary Table 4.3) using best-matched internal standard normalization (48). For details, see Supplementary information.

4.3.6 *Metabolite concentration calculations*

Absolute concentrations of compounds were calculated or estimated from peak areas using commercially available standards run in the same batch as our samples, similar to previous work (31,42,44). Full quantification methods are provided in Supplementary information and summarized in Supplementary Table 4.1.

4.3.7 *DNA extraction, sequencing, and processing*

All methods for DNA extraction, Illumina MiSeq sequencing of the V3-V4 region of the 16S rRNA gene and V9 region of the 18S rRNA gene, and sequence analysis for unique amplicon sequence variants (ASVs) are given in Supplementary information. The Inverse Simpson alpha diversity index was calculated using the phyloseq package in R (50) following Callahan et al. (2016b).

4.3.8 *Statistical approaches*

All methods for evaluating statistical differences in community structure, metabolite composition, metabolite concentrations, and ancillary measurements between samples are described in Supplementary information. For all statistical analyses, a probability level of ≤ 0.05 was used to determine statistical significance with *p*-values corrected for false discovery rate (FDR) (52) where appropriate.

4.4 RESULTS

4.4.1 *Physical environment*

Temperature and salinity in our meltwater, seawater, and sea-ice samples were narrower in range than those imposed in the incubation treatments. Field temperatures for meltwater and seawater

ranged between –0.9 and 0˚C, while salinity was approximately 25 ppt and 35 ppt, respectively (Table 4.1). PAR varied substantially in the field, ranging from 305 to 1100 µmol photons m^{-2} s^{-1} (compared to 100 µmol photons m^{-2} s^{-1} in the treatments; Table 4.1). Though not measured directly in sea-ice samples, temperature and salinity are presumed to be close to seawater (53) and PAR is presumed to be lower than surface seawater due to the attenuation of light in ice. The final salinity of sea-ice samples following melt for sampling was lower than seawater (12–20 ppt; Table 4.1).

4.4.2 *Biological measurements*

After an initial lag, photosynthetic growth was detected in all incubation treatments with specific growth rates of approximately 0.3 d^{-1} for Meltwater_T-S and SW_T-S and 0.2 d^{-1} for Sea ice_T-S (Figure 4.1a and Supplementary Figure 4.1a). The seawater community sampled over the same period also showed an increase in biomass (Chl *a* and POC) with an estimated specific growth rate of approximately 0.2 d^{-1} (Figure 4.1a, Supplementary Figure 4.1b, Supplementary Table 4.4). A slight drawdown of nutrients over the sampling period was observed in both the seawater samples and the incubation treatments, though none reached limiting conditions (Supplementary Table 4.4). Meltwater had comparable biomass (POC, Figure 4.1b) and nutrient concentrations (Supplementary Table 4.4) to seawater. C:N ratios were generally low (5.2–5.6 in seawater and 6.2 in SW_T-S and Sea ice_T-S), with slightly higher values in meltwater and Meltwater_T-S (7.6 and 8, respectively; Figure 4.1c).

4.4.3 *Alpha diversity*

Eukaryotic diversity in seawater was initially high (Inverse Simpson’s index of 14 for the incubation inoculum SW_12) and decreased in throughout the field sampling period and in

incubation bottles as the incubation progressed (Figure 4.2a), reaching similarly low diversity (approximately 5) within a similar timeframe (7 and 8–9 days, respectively). Sea ice and meltwater diversity fell within the range found in seawater. The prokaryotic community did not show a clear change in diversity over the sampling period in either seawater or the incubation treatments (Figure 4.2b), and meltwater diversity was similar to that in seawater. The prokaryotic sea-ice community however, was considerably more diverse (Inverse Simpson's index of 30) than all other communities sampled ($p << 0.001$).

4.4.4 *Community composition*

Diatoms (Bacillariophyta) dominated the eukaryotic community numerically in all samples, regardless of habitat or treatment. The initial seawater community was approximately 50% diatoms, increasing to 80% over the sampling period for both seawater and incubation treatments (Supplementary Figure 4.2). The diatom *Rhizosolenia pungens* dominated in all treatments and increased in seawater (from SW_08 to SW_17), though the diatom *Corethron inerme* eventually dominated in seawater (SW_19; Figure 4.3a). In contrast, the taxonomic composition of sea ice was mixed, with higher proportions of the diatom *Fragilariopsis sublineata* and the dinoflagellate *Pentapharsodinium dalei*, while most meltwater samples were dominated by a raphid pennate diatom. The prokaryotic community was largely bacterial, with the classes Gammaproteobacteria, Alphaproteobacteria, and Flavobacteriia making up the majority of ASVs (Supplementary Figure 4.3). The genus *Polaribacter* was abundant across seawater (increasing in abundance with time), sea-ice, and all incubation samples (Figure 4.3b). *Polaribacter* ASVs were less abundant in the meltwater field samples, which were dominated by *Octadecabacter*. Seawater also had high contributions of *Candidatus* Pelagibacter and *Candidatus* Thioglobus (decreasing in abundance with time). Sea-ice bacterial communities were mixed, with large contributions from *Polaribacter*,

Sulfitobacter, and *Paraglaciecola.* Archaeal ASVs were rare, with all reads assigned to the domain making up 0.05–2% of total reads per sample, and dominated by the phylum Thaumarchaeota. Full ASV abundance data and taxonomic information for 18S and 16S rRNA sequencing, including archaeal ASVs, are available in Supplementary Tables 4.5 and 4.6, respectively.

4.4.5 *Interdependency of prokaryotic and eukaryotic community structures*

NMDS ordinations of community structure paired with ANOSIM tests displayed a clear separation of meltwater, seawater, and sea ice from one another (eukaryotic: R = 0.78, $p << 0.001$; prokaryotic: R = 0.79, $p << 0.001$), despite one meltwater replicate grouping with seawater (Figures 4.4a and b). Seawater samples grouped together in ordination space, though community structure changed significantly over the course of seawater sampling (eukaryotic: R = 0.67, $p << 0.001$; prokaryotic: R = 0.40, $p = 0.003$). Incubation community structures during harvest were distinct from the initial seawater (eukaryotic: R = 0.61, $p << 0.001$; prokaryotic: R = 0.88, $p << 0.001$) but did not differ between treatments (eukaryotic: R = –0.08, $p = 0.47$; prokaryotic: R = 0.12, $p = 0.23$). Full ANOSIM results for eukaryotic and prokaryotic data are listed in Supplementary Tables 4.7 and 4.8, respectively.

NMDS ordinations revealed similar patterns within the eukaryotic and prokaryotic community structures (Figures 4.4a and b). Symmetric Procrustes analysis revealed a strong, significant congruency among these communities ($m^2 = 0.14$, $p << 0.001$), whereby samples with similar eukaryotic community structures were likely to share similar prokaryotic community structures (Figure 4.4c). Correlation analyses indicated numerous inter-domain co-occurrences. Across the top 20 eukaryotic and prokaryotic ASVs in our sample set, 350 ASV pairings correlated significantly, with 189 correlating positively and 161 negatively (Supplementary Figure 4.4a, Supplementary Table 4.9). These pairings included positive correlations between abundant diatom

ASVs *Rhizosolenia pungens*.12 (ρ = 0.76, p = 3.49 x 10^{-7}) and *Chaetoceros neogracilis*.1 (ρ = 0.75, p = 9.98 x 10^{-7}) with *Polaribacter* sp. L3A8.31. Across our field samples, significant positive correlations between ASVs aligned largely by habitat type (Supplementary Figure 4.4b): taxa abundant in sea-ice and meltwater samples (*Sulfitobacter*, *Octadecabaceter*, *Fragilariopsis sublineata*, etc.) correlated with each other, while taxa abundant in seawater samples (*Candidatus* Pelagibacter, *Candidatus* Thioglobus, *R. pungens*, etc.) correlated with each other in a separate cluster. Full correlation results for all samples (incubation and field) and for field samples only can be found in Supplementary Tables 4.9 and 4.10, respectively.

4.4.6 *Metabolite pools in polar environments*

Particulate pools of 134 known metabolites were quantified (see Supplementary Table 4.11). NMDS ordinations paired with ANOSIM tests showed that metabolite profiles clearly separated the meltwater, seawater, and sea-ice samples from each other (R = 0.99, $p << 0.001$), including a weaker but significant shift over the seawater sampling period (R = 0.61, $p = 1x10^{-4}$; Figure 4.4d). This distinction by habitat followed the observed pattern in community structure, with samples similar in metabolite composition tending to be similar in eukaryotic and prokaryotic community structure as well (Supplementary Figure 5.5). Unlike community structure, metabolite profiles for incubated samples separated very strongly according to treatment (R = 0.97, p = 0.003), with the control treatment (SW_T-S) grouping closely with the *in situ* seawater samples. When grouped by salinity status, the samples ordered across MDS1, with fresher field samples (meltwater and sea ice) grouping significantly with the Meltwater_T-S samples as compared to the ambient-salinity seawater or high-salinity Sea ice_T-S samples (Supplementary Figure 4.6; R = 0.89, $p << 0.001$). Full ANOSIM results are provided in Supplementary Table 4.12.

Total particulate metabolite concentration (as molar carbon concentration, nM C) ranged broadly between field sample types, from approximately 170 nM C in meltwater to 315–1325 nM C in seawater (Supplementary Figure 4.7; Supplementary Table 4.14). In our seawater samples, this equates to 2.6–4.0% of POC and 3.1–5.1% of PN, with no clear pattern over the sampling period (Figure 4.5b and c, Supplementary Figures 4.8 and 4.9). While SW_T-S and Sea ice_T-S metabolite contributions to POC and PN were similar to seawater, both the incubation and field meltwater metabolite pools made up a smaller %POC and %PN than other incubation or field samples (Figure 4.5b and c). The 20 most abundant metabolites accounted for about 70% of the total quantified metabolite pool in all samples (Figure 4.5a), with compatible solutes (glucosylglycerol, proline, glycine betaine [GBT], dimethylsulfoniopropionate [DMSP], etc.) and free amino acids (glutamic acid, glutamine, alanine, etc.) among the most abundant, similar to previous work (31,42,44). There were clear differences in metabolite composition between the environments sampled and between incubation treatments (Figure 4.5a). For example, seawater samples had high contributions (on a mole fraction carbon basis) from glucosylglycerol, proline, glutamic acid, glutamine, and alanine, while sea-ice and meltwater samples had high contributions from arginine and from gonyol and N-acetyl serine, respectively (Figure 4.5a and Supplementary Figure 4.10). In total, 95 of 134 metabolites contributed significantly to the separation of samples in NMDS ordination space (statistics available in Supplementary Table 4.15).

4.4.7 *Metabolite temperature and salinity sensitivities*

Normalizing to POC (nmol metabolite C µmol C^{-1}), the concentration of 45 (34%) metabolites differed significantly across temperature and salinity treatments (Figure 4.6a; Supplementary Table 4.16). Hierarchical clustering (Figure 4.6a and Supplementary Figure 4.11) indicated that half of those metabolites (23) increased under cold and salty conditions (Sea ice_T-S) and

decreased under warmer and fresher conditions (Meltwater_T-S) compared to seawater controls (SW_T-S). Many of these metabolites are known osmolytes that can accumulate to high intracellular concentrations (proline, DMSP, GBT). Proline was the most abundant metabolite quantified in our experiment (up to 1.3% of the total POC pool or 29% of the total metabolite C pool in Sea ice_T-S) and responded strongly to temperature and salinity change: proline was approximately 3 times higher in Sea ice_T-S (p = 0.00042), and 20 times lower in Meltwater_T-S (p = 0.011), compared to SW_T-S (Figure 4.6b). DMSP and GBT were less concentrated than proline (up to 0.3% and 0.1% of POC, respectively) but responded similarly to temperature and salinity change (Figure 4.6c and d).

Many other compatible solutes were present at much lower concentrations (0.00005% to 0.1% of POC) but clustered with proline, DMSP, and GBT, and responded similarly to temperature and salinity change. These include homarine, hypotaurine, taurine, homoserine, dimethylsulfonioacetate (DMS-Ac), ectoine, proline betaine, and betonicine (Figure 4.6a; Supplementary Table 4.11). A few compatible solutes (isethionic acid, gonyol, DHPS) did not show a significant response to temperature and salinity (Supplementary Figure 4.12). Only three metabolites were uniquely enriched under Meltwater_T-S conditions: cysteic acid, acetyl-L-carnitine, and (iso)butyryl-L-carnitine (Figure 4.6a, e and f). Propionyl-L-carnitine followed the same pattern, though the response was not statistically significant (Figure 4.6g and Supplementary Figure 4.12).

4.5 DISCUSSION

In this study, the microbial communities of three polar habitats (meltwater, seawater, and sea ice) with distinct physicochemical properties showed unique community structures and taxonomic compositions (Figures 4.2–4.4 and Supplementary Figures 4.2–4.3). This finding agrees with

previous observations (14,17), with warming spring sea ice associated with mixed pennate diatoms (here, largely *Fragilariopsis*) and flagellates (here, mainly *Pentapharsodinium*). Centric diatom taxa (*Rhizosolenia* and *Corethron*) became dominant in seawater and all incubation treatments, as commonly observed during phytoplankton blooms in WAP seawater (54–56). Community structure differed slightly between *in situ* seawater and our incubations (Figure 4.4a and b), but both had similar dominant algal and bacterial taxa (*Rhizosolenia* and *Polaribacter*, respectively; Figure 4.3), suggesting that our incubations remained representative of the seawater community. Numerically, copiotrophic bacteria (*Polaribacter*) overtook oligotrophic taxa (*Candidatus* Pelagibacter [SAR11] and *Candidatus* Thioglobus [SUP05]) during the onset of the phytoplankton bloom *in situ* (Figure 4.3b), as shown previously along the WAP (57) and in the open Southern Ocean (58). This trend, likely due to faster growth rates of copiotrophs with high availability of labile dissolved organic matter (DOM) (59), was amplified in our closed bottle incubations where DOC was approximately 15 times more concentrated than seawater levels (Supplementary Table 4.4 and Supplementary Figure 4.1e).

Microbial community composition is often sensitive to temperature and salinity in sea ice (17) and seawater (60). Temperature and salinity did not drive community restructuring during our 10-day incubations (Figures 4.2–4.4), possibly due to the length of the experiment or the stability of control variables that often vary alongside temperature and salinity in the environment (light, nutrients, habitable pore space). Previous studies on polar seawater also suggest that the influence of temperature and salinity on community structure is highly dependent on the starting community composition (60–62). Thus, changes in the timing of sea-ice formation and melt could lead to differences in the starting seawater community that will experience temperature and salinity shifts and may alter the resultant microbial community composition.

Congruency between eukaryotic and prokaryotic community structure across all of our samples (Figure 4.4c) indicates a consistent coupling between these domains. Algal production and bacterial heterotrophy are tightly coupled in other marine environments (63–65), and specific eukaryotic and prokaryotic taxa have been observed to co-occur in Antarctic sea ice (17,66) and seawater (67). Many positive correlations between eukaryotic and prokaryotic ASVs identified here (Supplementary Figure 4.4) are similar to those observed in an Arctic culture study (68) (e.g. a *Chaetoceros* diatom with the flavobacteria *Polaribacter* and a *Fragilariopsis* diatom with the alteromonad *Paraglaciecola)*. The specificity of co-occurrences (e.g., *Fragilariopsis sublineata* did not correlate positively with another alteromonad genus, *Glaciecola*) could reflect taxa-specific use of algal exudates by heterotrophic bacteria (68–73); it could also reflect shared environmental optima rather than direct metabolite exchanges or symbioses. Detecting these inter-domain co-occurrences provides a starting point to target algal-bacterial pairs for future studies of microbial interdependencies in polar oceans.

Particulate community metabolomes were distinct across WAP meltwater, seawater, and sea ice (Figures 4.4d and 4.5), following the pattern of community structure (Supplementary Figure 4.5). These metabolome distinctions were likely driven by a combination of habitat-unique taxonomic composition and physicochemical conditions (salinity, temperature, light, etc.). This explanation is consistent with previous seawater and culture studies, where metabolomes reflected community composition or individual taxa identity (31,44,74) but were also shaped by physiological responses to environmental conditions (30,75). For example, the dinoflagellate compatible solute gonyol (44,76) was proportionally enriched in our dinoflagellate-rich sea-ice and meltwater samples (Figure 4.5 and Supplementary 4.10) despite habitat differences in physicochemical factors (Table 4.1). In contrast, despite only minor changes in microbial

composition throughout our incubation, community metabolomes differed significantly between treatments (Figures 4.4d, 4.5, and 4.6), suggesting that the seawater taxa present had the metabolic flexibility to adapt to new temperatures and salinities and maintain growth. In this context, our metabolome results suggest that changes in temperature and salinity could significantly alter polar ocean carbon cycling and microbial interactions mediated by metabolites, even in taxonomically stable communities. The summed concentrations of metabolites in WAP surface seawater measured here (315–1325 nM C) were higher than those measured in surface marine particles across a North Pacific Ocean transect (68–234 nM C; (44)), but the metabolite contributions to total POC and PN were largely similar, suggesting that the differences could be attributable to the higher biomass levels in our WAP samples.

Metabolite profiles from the seawater and meltwater incubation treatments were largely similar to their *in situ* counterparts (Figure 4.4d). The Sea ice_T-S incubation did not group with the sea-ice samples, likely because the incubation conditions resemble wintertime sea ice (higher salinity and lower temperature than seawater), while the salinity and temperature of warming spring sea ice we sampled were likely closer to seawater or approaching meltwater. This colder and saltier treatment (Sea ice_T-S) was strongly distinguished by an increased contribution of proline (Supplementary Figure 4.10), a known compatible solute in polar microbe cultures (21,28–30). Proline was the most abundant metabolite quantified in our sample set, with seawater concentrations (0.5–1.1 nmol C µmol C^{-1}) similar to those measured in Arctic sea ice (0.5–1.5 nmol C µmol C^{-1}; (30)). Proline concentration in POC was elevated 3-fold in the Sea ice_T-S (Figure 4.6), a similar magnitude as in culture studies of two polar diatoms: *Fragilariopsis cylindrus* (28) and *Nitzschia lecointei* (30). Determining the exact source of this proline (or any metabolite) within POC, which includes total community biomass and detritus, is not possible

given the methods of this study, but an increase in metabolite concentration in particulate matter reflects that sources of the metabolite (biosynthesis, uptake from DOM, etc.) are greater than sinks (catabolism, release as DOM, etc.).

Many other metabolites also increased in concentration under cold and salty conditions and decreased in warmer and fresher conditions (Figure 4.6), supporting their potential roles in cryo- and osmoprotection (25,77). Some of these compounds are likely eukaryotic osmolytes (DMSP; (78–80)), but others are often associated with bacterial taxa (ectoine; (81–83)), reflecting a widespread community response to temperature and salinity change. Along with proline, three of these compounds are abundant in polar diatom cultures and show a similar response to cold and saline conditions: DMSP (30,32), GBT (30,33), and homarine (29,31). The majority, however, have never been quantified or confirmed to be temperature- and salinity-sensitive in culture or in mixed polar marine microbial communities. Thus, the present study has uncovered numerous compounds that deserve more focus as potential compatible solutes (homoserine, ectoine, DMS-Ac, N(e)-acetyl-lysine, etc.; Figure 4.6a) in polar contexts, where existing seasonal and future climate-altered shifts in temperature and salinity may impact the standing stocks and cycling of these labile compounds.

Seawater freshening left detectable imprints on organic matter across our samples, with the metabolomes of melt-influenced communities (Meltwater_T-S, meltwater, sea ice) more similar to each other than to higher salinity samples (seawater, SW_T-S, Sea ice_T-S; Supplementary Figure 4.6). Three acylcarnitines—acetyl-L-carnitine, (iso)butyryl-L-carnitine, and propionylcarnitine—accumulated under warm and fresh conditions in our incubation (Figure 4.6e–g) and contributed to the separation of field meltwater samples in multivariate space (Supplementary Figure 4.10). Acylcarnitines participate in the transport of fatty acids across

mitochondrial membranes for β-oxidation (84), and their accumulation may indicate changes in storage lipid pools, such as the degradation of fatty acids (85). This possibility aligns with our observation of decreased free concentrations of three essential polyunsaturated fatty acids (PUFAs; arachidonic acid, eicosapentaenoic acid, and docosahexaenoic acid) in low-salinity samples (Supplementary Figure 4.13) and previous observations of PUFA regulation by low salinity in diatoms (86,87) and Antarctic phytoplankton (88). Seawater freshening could thus have important consequences for Antarctic food webs, as the PUFAs produced widely by autotrophs are essential in animal diets (89). Fatty acid reorganization is also important for maintenance of membrane fluidity in polar microalgae under varying temperature (90) and potentially salinity (91), so this result may also be indicative of membrane restructuring in response to freshening and warming. Alternatively, acylcarnitines may play a role in diatom osmoadaptation or form as a secondary response to changes in amino acid synthesis (92,93), but these possibilities have yet to be explored in polar microbes.

Freshening also drove reduced total metabolite concentrations, relative to POC and PN, and elevated C:N ratios (Figures 4.1 and 4.5). This low-salinity signature was observed in both our incubation Meltwater_T-S (21 ppt) and field meltwater (25 ppt) despite differences in community composition, temperature, and nutrient concentrations (Figures 4.3, 4.4a, and 4.4b; Supplementary Table 4.4). Nitrogen limitation or carbon-rich EPS production does not appear to contribute to the higher C:N ratios at lower salinities (Supplementary Table 4.4 and Supplementary Figure 4.1c, respectively). This pattern could be due in part to the release of abundant N-rich compatible solutes under hypoosmotic conditions, as shown for GBT in sea-ice algae cultures (33). However, we estimate that the difference in metabolite concentrations between our freshened and ambient salinity treatments could only drive an approximate 1% change in C:N (6.16 versus 6.21 C:N;

calculation in Supplementary Table 4.17), much smaller than the difference measured here (23%; Figure 4.1c). Differences in C:N were likely driven instead by shifts in abundant macromolecular pools (lipids, carbohydrates, protein) that make up approximately 80% of POC in surface seawater (34).

Although our data suggest that fluctuations in particulate metabolite concentrations are unlikely to alter bulk stoichiometry, they may rapidly alter the composition of labile DOM during increasingly common freshening events. Many metabolites can be respired by the organisms that produce them (42), but others can enter the surrounding dissolved pool via lysis, passive exudation, or active excretion, which has been observed on subsecond timescales in a polar bacterium during freshening (94). Released N-rich compatible solutes, for example, can be taken up by other microbes and maintained for osmoregulation (33,95) or catabolized (26,39). Microbial metabolism of compatible solutes can lead to the production of marine aerosols, such as monomethylamine or dimethylamine production from GBT via trimethylamine and trimethylamine-N-oxide (96,97). Additionally, sulfur-containing compatible solutes (gonyol, DMS-Ac) can inhibit the production of dimethyl sulfide, the primary natural sulfate aerosol precursor, from DMSP (98), suggesting that their release during freshening could alter dimethyl sulfide emissions in polar regions and thus climate regulation (99). Specific molecular properties of marine DOM (molecular weight, nitrogen content, etc.) likely influence the composition and activity of the microbial community (65,100), such that environmentally driven changes in DOM composition may alter organic matter cycling, organism interactions, and climate-active marine aerosol production along the WAP.

4.6 Conclusions

In the present study, we show that different polar marine habitats harbor unique microbial communities distinct in both taxonomy and metabolite composition. Temperature and salinity

change drove strong metabolome changes in a coastal WAP seawater community even in the absence of strong taxonomic change. Warming and freshening drove a decrease in the concentration of metabolites—including compatible solutes—in particulate matter, which may have entered the labile DOM pool. As model predictions in the WAP suggest earlier ice breakup and longer open water periods with warmer and fresher conditions, a subsequent restructuring of the microbial chemical inventory seems possible, likely affecting the fate of organic matter and thus the balance between remineralization and sequestration of atmospheric CO_2.

4.7 Data Accessibility Statement

Supporting datasets are provided in the Supplementary Information (Datasets S1–S18).

4.8 Acknowledgements

This work was supported by grants from the National Science Foundation (OPP 1744645 to J.N.Y. and J.W.D.; 1846837 to J.B.), the Simons Foundation (561645 to J.N.Y.; 385428 and 329108 to A.E.I.), and the Alfred P. Sloan Foundation (Early-career Fellowship to J.N.Y.). We would like to thank Ben Van Mooy for the opportunity to sample sea ice; Rebecca Trinh, Jack Conroy, and Shawnee Traylor-Biglio for help with sample collection during the 2018 field season at Palmer Station; Shelly Carpenter for performing EPS measurements; Aaron Morello and the UW Marine Chemistry Lab for assistance with CHN, nutrient, DOC, and chlorophyll analysis; Katherine Heal and Angie Boysen for data processing advice; Will Kumler for statistics advice; and the staff of Palmer Station for their assistance.

References

1. Meredith MP, King JC. Rapid climate change in the ocean west of the Antarctic Peninsula during the second half of the 20th century. Geophys Res Lett. 2005;32(19):1–5.

2. Arrigo KR, van Dijken G, Pabi S. Impact of a shrinking Arctic ice cover on marine primary production. Geophys Res Lett. 2008;35(19):1–6.

3. Arrigo KR, Perovich DK, Pickart RS, Brown ZW, van Dijken GL, Lowry KE, et al. Phytoplankton blooms beneath the sea ice in the Chukchi sea. Deep Res Part II Top Stud Oceanogr. 2014;105:1–16.

4. Cape MR, Vernet M, Pettit EC, Wellner J, Truffer M, Akie G, et al. Circumpolar deep water impacts glacial meltwater export and coastal biogeochemical cycling along the west Antarctic Peninsula. Front Mar Sci. 2019;6(Mar):1–23.

5. Swart NC, Gille ST, Fyfe JC, Gillett NP. Recent Southern Ocean warming and freshening driven by greenhouse gas emissions and ozone depletion. Nat Geosci. 2018;11(11):836–41.

6. Schmidtko S, Heywood KJ, Thompson AF, Aoki S. Multidecadal warming of Antarctic waters. Science. 2014;346(6214):1227–31.

7. Stammerjohn S, Massom R, Rind D, Martinson D. Regions of rapid sea ice change: An inter-hemispheric seasonal comparison. Geophys Res Lett. 2012;39(6):1–8.

8. Stammerjohn SE, Martinson DG, Smith RC, Iannuzzi RA. Sea ice in the western Antarctic Peninsula region: Spatio-temporal variability from ecological and climate change perspectives. Deep Res Part II Top Stud Oceanogr. 2008;55(18–19):2041–58.

9. Harangozo SA. Atmospheric circulation impacts on winter maximum sea ice extent in the west Antarctic Peninsula region (1979–2001). Geophys Res Lett. 2006;33(2):2001–4.

10. Vaughan DG, Marshall GJ, Connolley WM, Parkinson C, Mulvaney R, Hodgson DA, et al. Recent rapid regional climate warming on the Antarctic Peninsula. Clim Change. 2003;60:243–74.

11. Bronselaer B, Winton M, Griffies SM, Hurlin WJ, Rodgers KB, Sergienko O V, et al. Change in future climate due to Antarctic meltwater. Nature. 2018;564(7734):53–8.

12. Boetius A, Anesio AM, Deming JW, Mikucki JA, Rapp JZ. Microbial ecology of the cryosphere: sea ice and glacial habitats. Nat Publ Gr. 2015;13(11):677–90.

13. Bowman JS, Rasmussen S, Blom N, Deming JW, Rysgaard S, Sicheritz-Ponten T. Microbial community structure of Arctic multiyear sea ice and surface seawater by 454 sequencing of the 16S RNA gene. ISME J. 2012;6(1):11–20.

14. van Leeuwe MA, Tedesco L, Arrigo KR, Assmy P, Campbell K, Meiners KM, et al. Microalgal community structure and primary production in Arctic and Antarctic sea ice: A synthesis. Elem Sci Anth. 2018;6.

15. McMinn A, Pankowskii A, Ashworth C, Bhagooli R, Ralph P, Ryan K. In situ net primary productivity and photosynthesis of Antarctic sea ice algal, phytoplankton and benthic algal communities. Mar Biol. 2010;157(6):1345–56.

16. Kohlbach D, Graeve M, Lange BA, David C, Schaafsma FL, van Franeker JA, et al. Dependency of Antarctic zooplankton species on ice algae-produced carbon suggests a sea ice-driven pelagic ecosystem during winter. Glob Chang Biol. 2018;24(10):4667–81.

17. Torstensson A, Dinasquet J, Chierici M, Fransson A, Riemann L, Wulff A. Physicochemical control of bacterial and protist community composition and diversity in Antarctic sea ice. Environ Microbiol. 2015;17(10):3869–81.

18. Collins ER, Rocap G, Deming JW. Persistence of bacterial and archaeal communities in sea ice through an Arctic winter. Environ Microbiol. 2010;12(7):1828–41.

19. Dieckmann GS, Thomas DN. Antarctic sea ice – a habitat for extremophiles. Science. 2002;295(5555):641–4.

20. Ewert M, Deming J. Sea ice microorganisms: Environmental constraints and extracellular responses. Biology (Basel). 2013;2(2):603–28.

21. Ewert M, Deming JW. Bacterial responses to fluctuations and extremes in temperature and brine salinity at the surface of Arctic winter sea ice. FEMS Microbiol Ecol. 2014;89(2):476–89.

22. Cox GFN, Weeks WF. Equations for determining the gas and brine volumes in sea-ice sample. J Glaciol. 1983;29(102):306–16.

23. Deming JW, Young JN. The role of exopolysaccharides in microbial adaptation to cold habitats. In: Margesin R, editor. Psychrophiles: from biodiversity to biotechnology. 2nd ed. Berlin Heidelberg, Germany: Springer-Verlag; 2017. p. 259–284.

24. Young JN, Schmidt K. It's what's inside that matters: Physiological adaptations of high-latitude marine microalgae to environmental change. New Phytologist. 2020;227:1307–1318.

25. Yancey PH, Clark ME, Hand SC, Bowlus RD, Somero GN. Living with water stress: Evolution of osmolyte systems 1982;217(4566):1214–22.

26. Welsh DT. Ecological significance of compatible solute accumulation by micro-organisms: from single cells to global climate. FEMS Microbiol Rev. 2000;24(3):263–90.

27. Lyon B, Mock T. Polar microalgae: New approaches towards understanding adaptations to an extreme and changing environment. Biology (Basel). 2014;3(1):56–80.

28. Krell A, Funck D, Plettner I, John U, Dieckmann G. Regulation of proline metabolism under salt stress in the psychrophilic diatom *Fragilariopsis cylindrus* (Bacillariophyceae). J Phycol. 2007;43(4):753–62.

29. Boroujerdi AFB, Lee PA, DiTullio GR, Janech MG, Vied SB, Bearden DW. Identification of isethionic acid and other small molecule metabolites of *Fragilariopsis cylindrus* with nuclear magnetic resonance. Anal Bioanal Chem. 2012;404(3):777–84.

30. Dawson HM, Heal KR, Boysen AK, Carlson LT, Ingalls AE, Young JN, et al. Potential of temperature- and salinity-driven shifts in diatom compatible solute concentrations to impact biogeochemical cycling within sea ice. Elem Sci Anth. 2020;8(25).

31. Dawson HM, Heal KR, Torstensson A, Carlson LT, Ingalls AE, Young JN. Large diversity in nitrogen- and sulfur-containing compatible solute profiles in polar and temperate diatoms. Integr Comp Biol. 2020;60(6):1401–13.

32. Lyon BR, Bennett-Mintz JM, Lee PA, Janech MG, Ditullio GR. Role of dimethylsulfoniopropionate as an osmoprotectant following gradual salinity shifts in the sea-ice diatom *Fragilariopsis cylindrus*. Environ Chem. 2016;13(2):181–94.

33. Torstensson A, Young JN, Carlson LT, Ingalls AE, Deming JW. Use of exogenous glycine betaine and its precursor choline as osmoprotectants in Antarctic sea-ice diatoms. J Phycol. 2019;70:1–13.

34. Lee C, Wakeham S, Arnosti C. Particulate organic matter in the sea: The composition conundrum. Ambio. 2004;33(8):565–75.

35. Yancey PH. Organic osmolytes as compatible, metabolic and counteracting cytoprotectants in high osmolarity and other stresses. J Exp Biol. 2005;208(15):2819–30.

36. McParland EL, Alexander H, Johnson WM. The osmolyte ties that bind: genomic insights into synthesis and breakdown of organic osmolytes in marine microbes. Front Mar Sci. 2021;8(Jul).

37. Moran MA, Kujawinski EB, Schroer WF, Amin SA, Bates NR, Bertrand EM, et al. Microbial metabolites in the marine carbon cycle. Nat Microbiol. 2022;7(4):508–23.

38. Johnson WM, Kido Soule MC, Kujawinski EB. Evidence for quorum sensing and differential metabolite production by a marine bacterium in response to DMSP. ISME J. 2016;10(9):2304–16.

39. Durham BP, Boysen AK, Carlson LT, Groussman RD, Heal KR, Cain KR, et al.

Sulfonate-based networks between eukaryotic phytoplankton and heterotrophic bacteria in the surface ocean. Nat Microbiol. 2019;4(10):1706–15.

40. Durham BP, Sharma S, Luo H, Smith CB, Amin SA, Bender SJ, et al. Cryptic carbon and sulfur cycling between surface ocean plankton. Proc Natl Acad Sci. 2015;112(2):453–7.

41. Amin SA, Hmelo LR, van Tol HM, Durham BP, Carlson LT, Heal KR, et al. Interaction and signalling between a cosmopolitan phytoplankton and associated bacteria. Nature. 2015;522(7554):98–101.

42. Boysen AK, Carlson LT, Durham BP, Groussman RD, Aylward FO, Ribalet F, et al. Particulate metabolites and transcripts reflect diel oscillations of microbial activity in the surface ocean. mSystems. 2021;6(3).

43. Johnson WM, Longnecker K, Kido Soule MC, Arnold WA, Bhatia MP, Hallam SJ, et al. Metabolite composition of sinking particles differs from surface suspended particles across a latitudinal transect in the South Atlantic. Limnol Oceanogr. 2020;65:111–127.

44. Heal KR, Durham BP, Boysen AK, Carlson LT, Qin W, Ribalet F, et al. Marine Community Metabolomes carry fingerprints of phytoplankton community composition. mSystems. 2021;6(3).

45. Moran MA. The global ocean microbiome. Science. 2015;350(6266).

46. Waters KJ, Smith RC. Palmer LTER : A sampling grid for the Palmer LTER program. Antarct J United States. 1992;27(5):236–9.

47. Guillard RRL. Culture of phytoplankton for feeding marine invertebrates. In: Smith WL, Chanley MH, editors. Culture of Marine Invertebrate Animals. Boston, MA: Springer; 1975. p. 29–60.

48. Boysen AK, Heal KR, Carlson LT, Ingalls AE. Best-matched internal standard normalization in liquid chromatography-mass spectrometry metabolomics applied to environmental samples. Anal Chem. 2018;90(2):1363–1369.

49. MacLean B, Tomazela DM, Shulman N, Chambers M, Finney GL, Frewen B, et al. Skyline: An open source document editor for creating and analyzing targeted proteomics experiments. Bioinformatics. 2010;26(7):966–8.

50. McMurdie PJ, Holmes S. Phyloseq: An R package for reproducible interactive analysis and graphics of microbiome census data. PLoS One. 2013;8(4).

51. Callahan BJ, Sankaran K, Fukuyama JA, McMurdie PJ, Holmes SP. Bioconductor workflow for microbiome data analysis: From raw reads to community analyses. F1000Research. 2016;5:1–50.

52. Benjamini Y, Hochberg Y. Controlling the false discovery rate: a practical and powerful approach to multiple testing. J R Stat Soc. 1995;57(1):289 –300.

53. Junge K, Courville Z, Carpenter S, Light B, Lieblappen R, Orellana MV, et al. Physical and optical characteristics of heavily melted "rotten"; Arctic sea ice. Cryosph Discuss. 2018;2009(Sep):1–30.

54. Annett AL, Carson DS, Crosta X, Clarke A, Ganeshram RS. Seasonal progression of diatom assemblages in surface waters of Ryder Bay, Antarctica. Polar Biol. 2010;33(1):13–29.

55. Schofield O, Saba G, Coleman K, Carvalho F, Couto N, Ducklow H, et al. Decadal variability in coastal phytoplankton community composition in a changing West Antarctic Peninsula. Deep Res Part I Oceanogr Res Pap. 2017;124(Nov):42–54.

56. Prezelin BB, Hofmann EE, Mengelt C, Klinck JM. The linkage between Upper Circumpolar Deep Water (UCDW) and phytoplankton assemblages on the west Antarctic Peninsula continental shelf. J Mar Res. 2000;58(2):165–202.

57. Bowman JS, Amaral-Zettler LA, Rich JJ, Luria CM, Ducklow HW. Bacterial community segmentation facilitates the prediction of ecosystem function along the coast of the western Antarctic Peninsula. ISME J. 2017;11(6):1460–71.

58. Liu Y, Blain S, Crispi O, Rembauville M, Obernosterer I. Seasonal dynamics of prokaryotes and their associations with diatoms in the Southern Ocean as revealed by an autonomous sampler. Environ Microbiol. 2020;22(9):3968–84.

59. Buchan A, LeCleir GR, Gulvik CA, González JM. Master recyclers: features and functions of bacteria associated with phytoplankton blooms. Nat Rev Microbiol. 2014;12(10):686–98.

60. Antoni JS, Almandoz GO, Ferrario ME, Hernando MP, Varela DE, Rozema PD, et al. Response of a natural Antarctic phytoplankton assemblage to changes in temperature and salinity. J Exp Mar Bio Ecol. 2020;532(Aug):151444.

61. Hernando M, Varela DE, Malanga G, Almandoz GO, Schloss IR. Effects of climate-induced changes in temperature and salinity on phytoplankton physiology and stress responses in coastal Antarctica. J Exp Mar Bio Ecol. 2020;530–531(May):151400.

62. Piquet AMT, Bolhuis H, Meredith MP, Buma AGJ. Shifts in coastal Antarctic marine microbial communities during and after melt water-related surface stratification. FEMS Microbiol Ecol. 2011;76(3):413–27.

63. Azam F, Malfatti F. Microbial structuring of marine ecosystems. Nat Rev Microbiol. 2007;5(10):782–91.

64. Zhou J, Richlen ML, Sehein TR, Kulis DM, Anderson DM, Cai Z. Microbial community structure and associations during a marine dinoflagellate bloom. Front Microbiol. 2018;9(Jun):1–21.

65. Kieft B, Li Z, Bryson S, Hettich RL, Pan C, Mayali X, et al. Phytoplankton exudates and lysates support distinct microbial consortia with specialized metabolic and ecophysiological traits. Proc Natl Acad Sci U S A. 2021;118(41):1–12.

66. Kaartokallio H, Tuomainen J, Kuosa H, Kuparinen J, Martikainen PJ, Servomaa K. Succession of sea-ice bacterial communities in the Baltic Sea fast ice. Polar Biol. 2008;31(7):783–93.

67. Delmont TO, Hammar KM, Ducklow HW, Yager PL, Post AF. *Phaeocystis antarctica* blooms strongly influence bacterial community structures in the Amundsen Sea polynya. Front Microbiol. 2014;5(Dec):1–13.

68. Tisserand L, Dadaglio L, Intertaglia L, Catala P, Panagiotopoulos C, Obernosterer I, et al. Use of organic exudates from two polar diatoms by bacterial isolates from the Arctic Ocean: Diatom exudates and Arctic bacteria. Philos Trans R Soc A Math Phys Eng Sci. 2020;378(2181).

69. Tada Y, Nakaya R, Goto S, Yamashita Y, Suzuki K. Distinct bacterial community and diversity shifts after phytoplankton-derived dissolved organic matter addition in a coastal environment. J Exp Mar Bio Ecol. 2017;495(Jun):119–28.

70. Bertrand EM, McCrow JP, Moustafa A, Zheng H, McQuaid JB, Delmont TO, et al. Phytoplankton-bacterial interactions mediate micronutrient colimitation at the coastal Antarctic sea ice edge. Proc Natl Acad Sci USA. 2015;112(32):9938–43.

71. Amin SA, Parker MS, Armbrust E V. Interactions between diatoms and bacteria. Microbiol Mol Biol Rev. 2012;76(3):667–84.

72. Ferrer-González FX, Widner B, Holderman NR, Glushka J, Arthur S, Kujawinski EB, et al. Resource partitioning of phytoplankton metabolites that support bacterial heterotrophy. ISME J. 2020;15:762–773.

73. Dadaglio L, Dinasquet J, Obernosterer I, Joux F. Differential responses of bacteria to diatom-derived dissolved organic matter in the Arctic Ocean. Aquat Microb Ecol. 2019;82(1):59–72.

74. Durham BP, Boysen AK, Heal KR, Carlson LT, Boccamazzo R, Deodato CR, et al. Chemotaxonomic patterns in intracellular metabolites of marine microbial plankton. Front Mar Sci. 2022;(Sep):1–17.

75. Heal KR, Kellogg NA, Carlson LT, Lionheart RM, Ingalls AE. Metabolic consequences of cobalamin scarcity in the diatom *Thalassiosira pseudonana* as revealed through

metabolomics. Protist. 2019;170(3):328–48.

76. Gebser B, Pohnert G. Synchronized regulation of different zwitterionic metabolites in the osmoadaption of phytoplankton. Mar Drugs. 2013;11(6):2168–82.

77. Brown AD. Microbial water stress. Bacteriol Rev. 1976;40(4):803–46.

78. Keller MD. Dimethyl sulfide production and marine phytoplankton: the importance of species composition and cell size. Biol Oceanogr. 1988;6(5–6):375–82.

79. McParland EL, Wright A, Art K, He M, Levine NM. Evidence for contrasting roles of dimethylsulfoniopropionate production in *Emiliania huxleyi* and *Thalassiosira oceanica*. New Phytol. 2020;226(2):396–409.

80. Karsten U, Kück K, Vogt C, Kirst GO. Dimethylsulfoniopropionate production in phototrophic organisms and its physiological functions as a cryoprotectant. In: Kiene RP, Visscher PT, Keller MD, Kirst Gunter O, editors, Biological and environmental chemistry of DMSP and related sulfonium compounds. Boston, MA: Springer US. p. 143–153.

81. Vargas C, Jebbar M, Carrasco R, Blanco C, Calderón MI, Iglesias-Guerra F, et al. Ectoines as compatible solutes and carbon and energy sources for the halophilic bacterium *Chromohalobacter salexigens*. J Appl Microbiol. 2006;100(1):98–107.

82. Kuhlmann AU, Hoffmann T, Bursy J, Jebbar M, Bremer E. Ectoine and hydroxyectoine as protectants against osmotic and cold stress: Uptake through the SigB-controlled betaine-choline-carnitine transporter-type carrier EctT from *Virgibacillus pantothenticus*. J Bacteriol. 2011;193(18):4699–708.

83. Fenizia S, Thume K, Wirgenings M, Pohnert G. Ectoine from bacterial and algal origin is a compatible solute in microalgae. Mar Drugs. 2020;18(1):1–13.

84. Pan Y, Yang J, Gong Y, Li X, Hu H. 3-Hydroxyisobutyryl-coa hydrolase involved in isoleucine catabolism regulates triacylglycerol accumulation in *Phaeodactylum tricornutum*. Philos Trans R Soc B Biol Sci. 2017;372(1728).

85. Boysen A. Marine microbial metabolomics: a journey through time, space, and metabolism [dissertation]. University of Washington; 2020.

86. Chen GQ, Jiang Y, Chen F. Salt-induced alterations in lipid composition of diatom *Nitzschia laevis* (Bacillariophyceae) under heterotrophic culture condition. J Phycol. 2008;44(5):1309–14.

87. Torstensson A, Jiménez C, Nilsson AK, Wulff A. Elevated temperature and decreased salinity both affect the biochemical composition of the Antarctic sea-ice diatom *Nitzschia lecointei*, but not increased pCO_2. Polar Biol. 2019;42(11):2149–64.

88. Hernando M, Schloss IR, Almandoz GO, Malanga G, Varela DE, De Troch M. Combined effects of temperature and salinity on fatty acid content and lipid damage in Antarctic phytoplankton. J Exp Mar Bio Ecol. 2018;503(Nov):120–8.

89. Brett MT, Müller-Navarra DC. The role of highly unsaturated fatty acids in aquatic foodweb processes. Freshw Biol. 1997;38(3):483–99.

90. Teoh ML, Phang SM, Chu WL. Response of Antarctic, temperate, and tropical microalgae to temperature stress. J Appl Phycol. 2013;25(1):285–97.

91. An M, Mou S, Zhang X, Zheng Z, Ye N, Wang D, et al. Expression of fatty acid desaturase genes and fatty acid accumulation in *Chlamydomonas* sp. ICE-L under salt stress. Bioresour Technol. 2013;149:77–83.

92. Nikitashina V, Stettin D, Pohnert G. Metabolic adaptation of diatoms to hypersalinity. Phytochemistry. 2022;201:113267.

93. Peluso G, Barbarisi A, Savica V, Reda E, Nicolai R, Benatti P, et al. Carnitine: An osmolyte that plays a metabolic role. J Cell Biochem. 2000;80(1):1–10.

94. Firth E, Carpenter SD, Sørensen HL, Collins RE, Deming JW. Bacterial use of choline to tolerate salinity shifts in sea-ice brines. Elem Sci Anth. 2016;4:000120.

95. Kiene RP, Hoffmann Williams LP. Glycine betaine uptake, retention, and degradation by microorganisms in seawater. Limnol Oceanogr. 1998;43(7):1592–603.

96. Boysen AK, Durham BP, Kumler W, Key RS, Heal KR, Carlson LT, et al. Glycine betaine uptake and metabolism in marine microbial communities. Environ Microbiol. 2022;24(5):2380–403.

97. Chen Y, Patel NA, Crombie A, Scrivens JH, Murrell JC. Bacterial flavin-containing monooxygenase is trimethylamine monooxygenase. Proc Natl Acad Sci USA. 2011;108(43):17791-17796.

98. Gebser B, Thume K, Schiller F, Steinke M, Pohnert G. Phytoplankton-derived zwitterionic gonyol and dimethylsulfonioacetate interfere with microbial dimethylsulfoniopropionate sulfur cycling. Microbiol Open. 2020;9(5):1–14.

99. Malin G, Turner SM, Liss PS. Sulfur : The plankton/climate connection. J Phycol. 1992;28(5):590–7.

100. Moran MA, Kujawinski EB, Stubbins A, Fatland R, Aluwihare LI, Buchan A, et al. Deciphering ocean carbon in a changing world. Proc Natl Acad Sci USA. 2016;113(12):3143–51.

4.9 TABLES AND FIGURES

Table 4.1. Summary of samples collected and analyzed in this study.

Date	Sample type	Sample name	Latitude	Longitude	*n*	T (˚C)	S (ppt)	PAR (mmol $m^{-2}s^{-1}$)
2018-11-05	Sea-ice meltwater	Meltwater	–64.78	–64.05	3	–0.7	25	320
2018-11-08	Seawater	SW_08	–64.78	–64.07	3	–0.9	35.7	305
2018-11-12	Seawater	SW_12	–64.78	–64.07	3	–0.7	35.2	375
2018-11-15	Seawater	SW_15	–64.78	–64.07	3	–0.3	35.2	1100
2018-11-17	Seawater	SW_17	–64.78	–64.07	3	–0.1	35.2	850
2018-11-19	Seawater	SW_19	–64.78	–64.07	3	0	35.2	700
2018-11-19	Sea ice	Sea ice _1	n.d.	n.d.	3	n.d.	12*	n.d.
2018-11-14	Sea ice	Sea ice _2	n.d.	n.d.	1	n.d.	15*	n.d.
2018-11-20	Sea ice	Sea ice _3	n.d.	n.d.	1	n.d.	20*	n.d.
2018-11-20	Incubation treatment Meltwater	Meltwater_T-S	n.a.	n.a.	3	3	21	100
2018-11-20	Incubation treatment Seawater	SW_T-S	n.a.	n.a.	3	0	35	100
2018-11-21	Incubation treatment Sea ice	Sea ice_T-S	n.a.	n.a.	3	–3	52	100

n.d., not determined

n.a., not applicable

*Salinity measured following ice-core melt into filtered seawater.

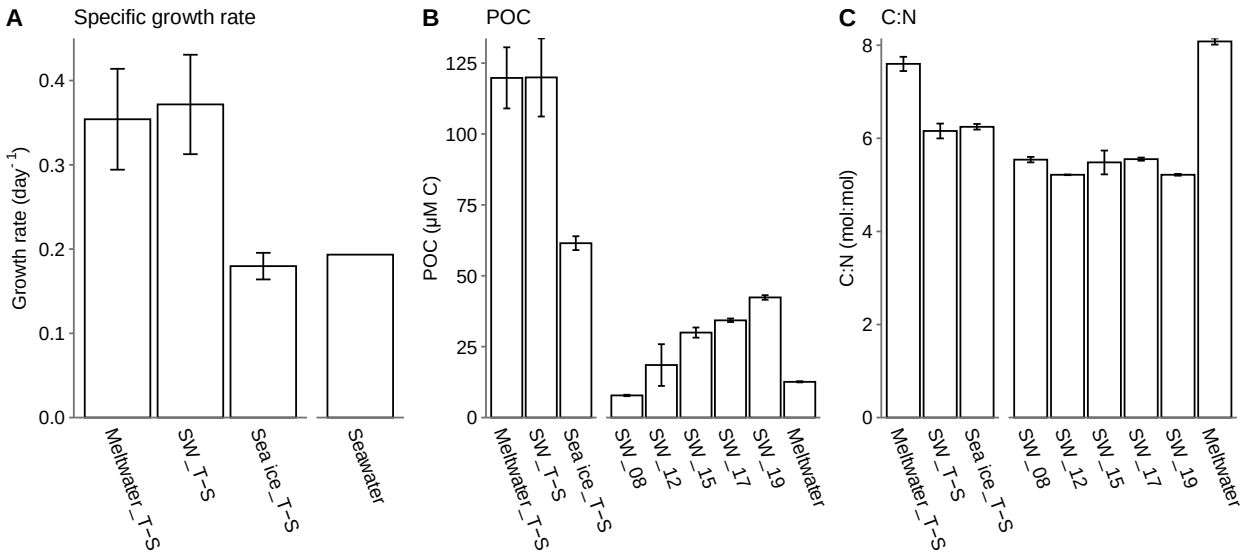

Figure 4.1. General parameters for incubation and field samples. A) Specific growth rate (day^{-1}) in incubated samples based on exponential change in Chl *a* fluorescence (during days 5–9 for Meltwater_T-S and Seawater_T-S, and days 6–10 for Sea ice_T-S) and in POC (days 6–10) for the seawater field samples; B) concentration of particulate organic carbon (POC in µM C); and C) molar ratio of C:N. Error bars represent standard deviation of the mean (n = 3). For all plots, x-axis break separates incubation treatment samples on the left and field samples on the right. Growth curves used to generate specific growth rate are provided in Supplementary Figures 4.1a and b; full data are available in Supplementary Table 4.4. Note that we do not have POC or C:N measurements to pair with sea-ice field samples.

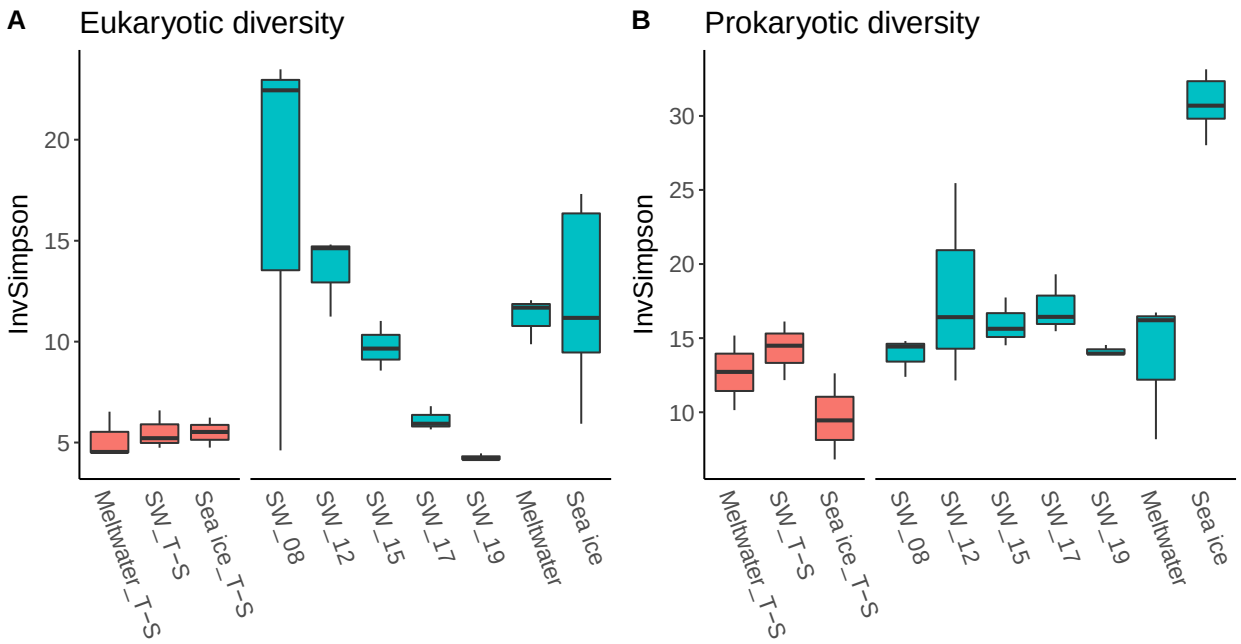

Figure 4.2. Alpha diversity in incubation and field samples. Inverse Simpson (InvSimpson) indices of alpha diversity for A) the eukaryotic community and B) the prokaryotic community in both incubation (pink) and field (aqua) samples. In the box plots, the total data range, median, and the 25–75% quartile range (box) are shown. For all plots, x-axis break separates incubation treatment samples on the left and field samples on the right.

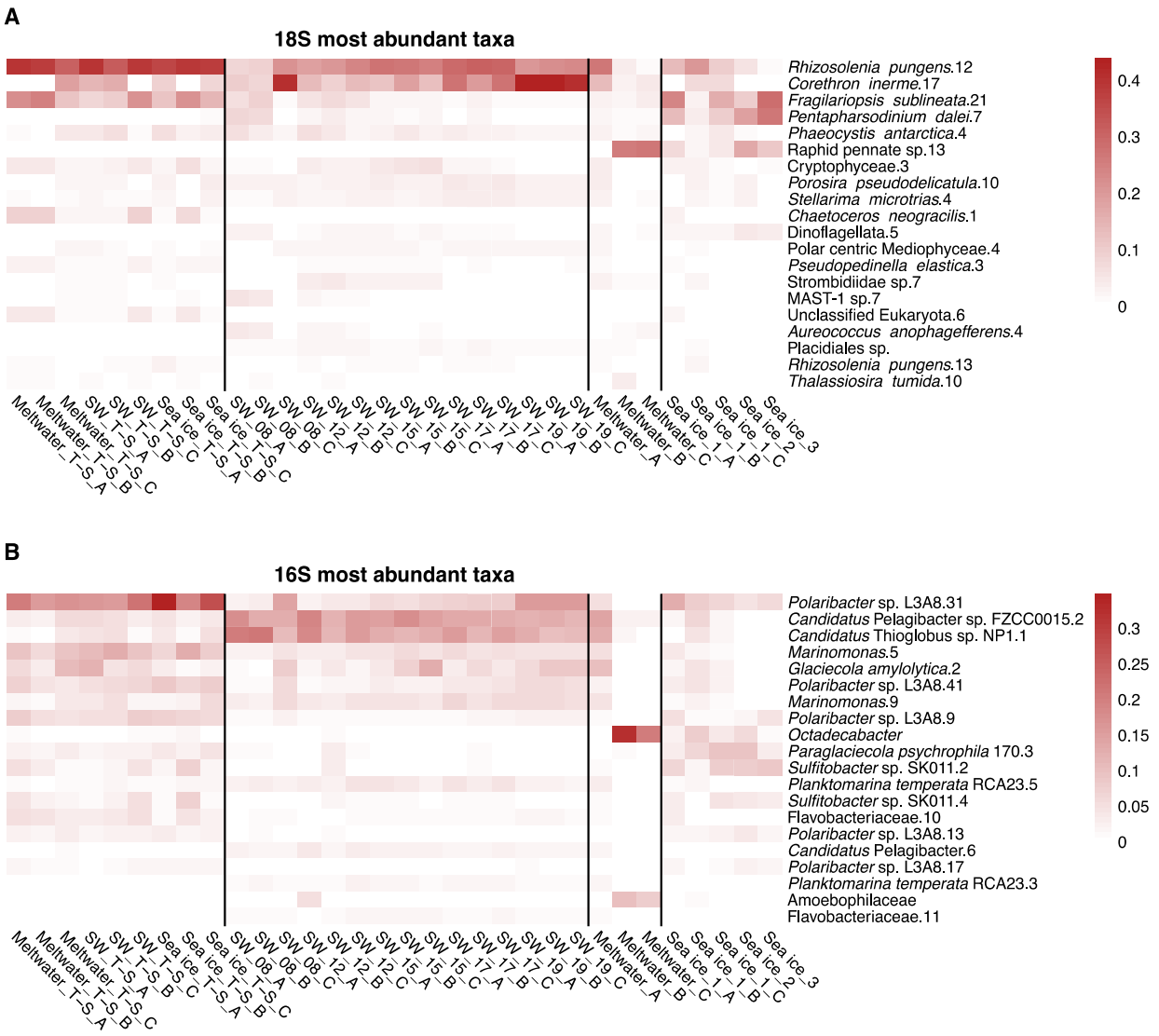

Figure 4.3. Community composition of incubation and field samples. Color-scaled relative abundance of the 20 most abundant A) eukaryotic (18S) closest completed genomes (CCGs) and closest estimated genomes (CEGs) and B) prokaryotic (16S) CCGs and CEGs. Vertical lines separate incubation samples for all sample types (left) from field samples by sample type; sample designations A, B and C indicate triplicate samples. Full data available in Supplementary Tables 4.5 and 4.6.

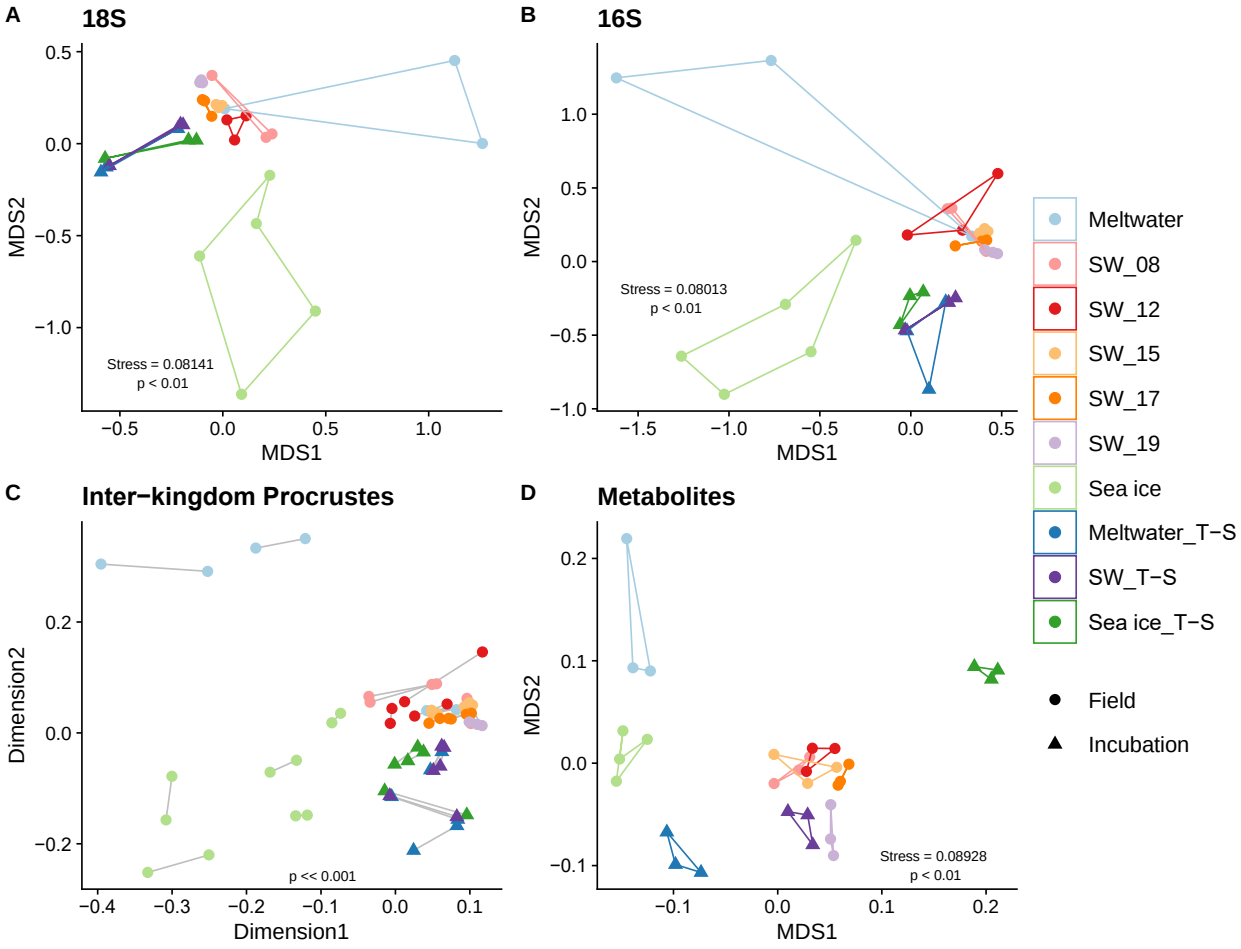

Figure 4.4. Multidimensional structure of community and metabolite composition in incubation and field samples. Non-metric dimensional scaling (NMDS) ordination, using Bray-Curtis dissimilarities, comparing A) the eukaryotic (18S) composition and B) the prokaryotic (16S) composition of each sample. C) Procrustes analysis, where points represent individual samples, line connections between points represent eukaryotic and prokaryotic community composition from the same sample, and longer lines indicate greater within-sample dissimilarity between eukaryotic and prokaryotic community structure. D) NMDS ordination, using Euclidean distance, comparing the metabolite composition of each sample. Metabolite concentrations are scaled to

mole fraction of carbon. Colors indicate sample type. Full data for 18S, 16S, and metabolites are provided in Supplementary Tables 4.5, 4.6, and 4.11, respectively.

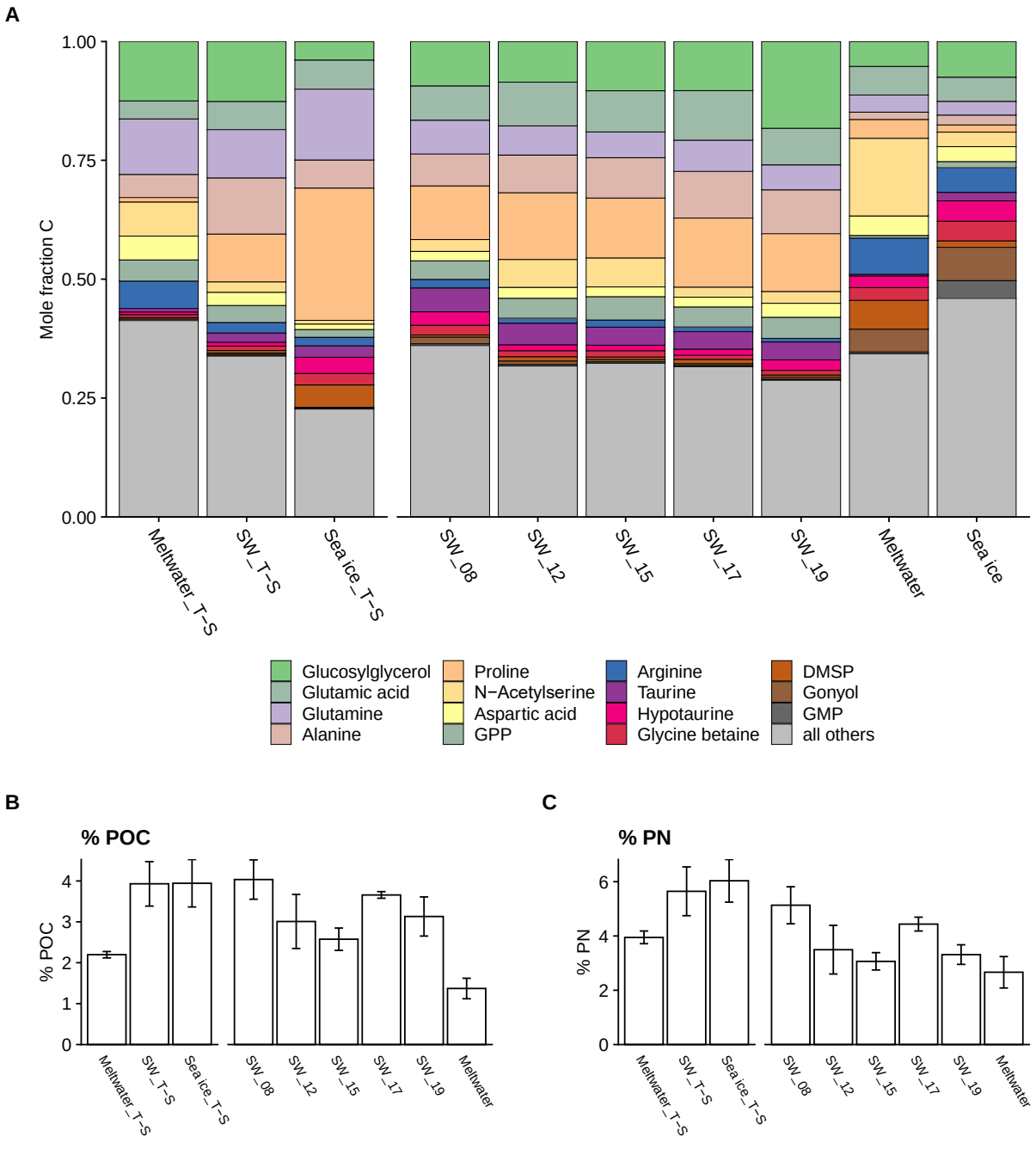

Figure 4.5. Metabolite composition of particulate matter in incubation and field samples. A) Metabolite abundance presented as mole fraction of carbon of total identified metabolites across the incubation and field samples. Average of triplicates are shown, except for sea-ice core where $n = 4$. The most abundant 15 molecules for each sample are color-coded, with "all others" (gray) containing the sum of the remaining quantified metabolites (119). Total quantified metabolite concentration as the percentage of B) particulate organic carbon (POC) and C) particulate nitrogen (PN), where error bars represent standard deviation of the mean ($n = 3$). For all plots, x-axis break separates incubation treatment samples on the left and field samples on the right. Full data available in Supplementary Table 4.11; individual metabolite contributions as %POC and %PN, available in Supplementary Figures 4.8 and 4.9, respectively. Note that we do not have POC or PN to pair with sea-ice field samples.

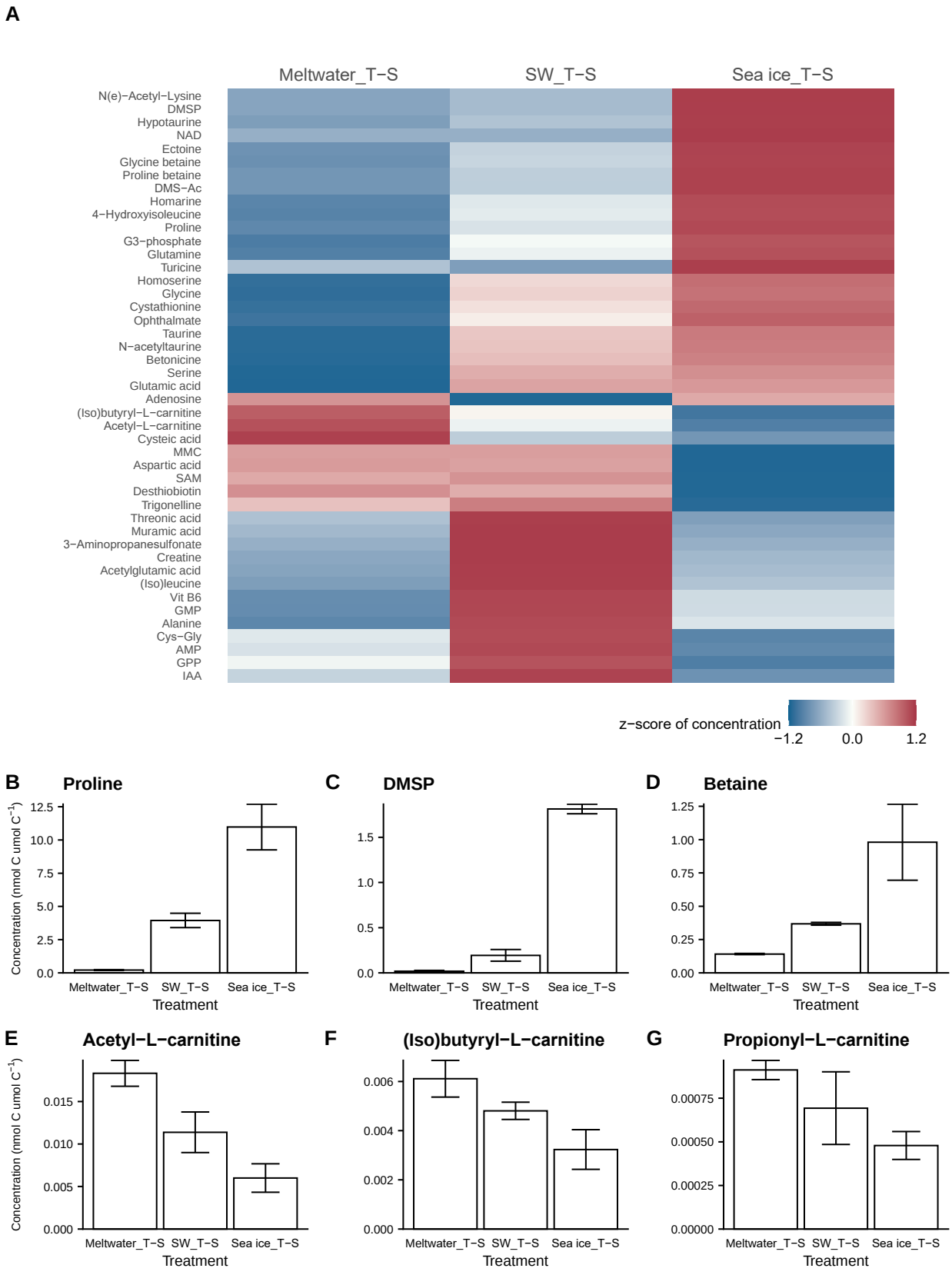
A
Meltwater_T−S
SW_T−S
Sea ice_T−S
N(e)−Acetyl−Lysine
DMSP
Hypotaurine
NAD
Ectoine
Glycine betaine
Proline betaine
DMS−Ac
Homarine
4−Hydroxyisoleucine
Proline
G3−phosphate
Glutamine
Turicine
Homoserine
Glycine
Cystathionine
Ophthalmate
Taurine
N−acetyltaurine
Betonicine
Serine
Glutamic acid
Adenosine
(Iso)butyryl−L−carnitine
Acetyl−L−carnitine
Cysteic acid
MMC
Aspartic acid
SAM
Desthiobiotin
Trigonelline
Threonic acid
Muramic acid
3−Aminopropanesulfonate
Creatine
Acetylglutamic acid
(Iso)leucine
Vit B6
GMP
Alanine
Cys−Gly
AMP
GPP
IAA
z−score of concentration
−1.2
0.0
1.2
B
Proline
C
DMSP
D
Betaine
Concentration (nmol C umol C−1)
Meltwater_T−S
SW_T−S
Sea ice_T−S
Treatment
E
Acetyl−L−carnitine
F
(Iso)butyryl−L−carnitine
G
Propionyl−L−carnitine

Figure 4.6. Particulate metabolite responses to temperature and salinity change during the incubation experiments. A) Heat map color-coded by z-score standardized concentrations of metabolites (nmol metabolite C μmol C^{-1}), arranged by average linkage hierarchical clustering of Euclidean distance (dendrogram of clustering available in Supplementary Figure 4.11), for the three different treatments. Compounds listed were each significantly different ($p < 0.05$) with treatment, as determined by false discovery rate-corrected *p*-values from one-way ANOVAs (detailed in Supplementary Table 4.16); compounds not significantly different ($p > 0.05$) are available in Supplementary Figure 4.12B–G) Concentration (nmol metabolite C μmol C^{-1}) of compatible solutes in the incubations, grouped by treatment, for B) proline, C) DMSP, and D) GBT, and of acylcarnitines for E) acetyl-L-carnitine, F) Isobutyryl-L-carnitine, and G) Propionyl-L-carnitine. Error bars represent standard deviation of the mean ($n = 3$).

4.10 SUPPLEMENTARY METHODS

4.10.1 *Temperature and salinity incubation experiment set up and monitoring*

On 12 November 2018, we collected additional seawater (sample SW_12; Table 4.1) for incubation experiments that simulated temperature(T)-salinity(S) conditions of sea-ice melt (3˚C and 21 ppt, designated Meltwater_T-S), ambient seawater (0˚C and 35 ppt, SW_T-S), and sea ice (–3˚C and 52 ppt, Sea ice_T-S). Triplicate 10-L polycarbonate carboys were used for each treatment. All samples were enriched with f/2 nutrients with silica (1) and incubated for approximately 10 days at 100 μmol photons m^{-2} s^{-1} light on a 20:4 h light:dark cycle. All the carboys remained unfrozen throughout the experiment. Salinity was adjusted by dilution with MilliQ water or addition of artificial sea salts (top 6 salts by molar concentration from Enriched Seawater, Artificial Water (2)). All treatments contained the same volume of seawater inoculum (4.5 L) and reached the same total volume (9 L). Temperature was controlled using custom-built aquaria and monitored using Onset HOBO pendant data loggers. Incubations were subsampled daily for growth and harvested during exponential growth on day 8 for Meltwater_T-S and SW_T-S and day 9 for Sea ice_T-S for metabolomics, DNA sequencing, chlorophyll *a* (Chl *a*), particulate organic carbon and nitrogen (POC, PN), dissolved organic carbon (DOC), particulate and dissolved extracellular polysaccharides (pEPS, dEPS), and major nutrients (NO_3^-, NO_2^-, NH_4, SiO_4, PO_4^{3-}). Growth of photosynthetic organisms was monitored by daily changes in relative fluorescence units (RFU) using a Turner fluorometer.

4.10.2 *Sample filtration and processing*

Samples for particulate metabolomics were collected as described in Boysen et al. (2018). Briefly, samples were collected into polycarbonate containers, filtered onto 47 mm 0.2

μm polytetrafluoroethylene Omnipore Membrane filters using peristaltic pumping, stored in combusted aluminum foil, flash-frozen in liquid N_2, and kept at –80°C until extraction. Methodological blanks were collected by passing filtrate over a second 0.2 μm polytetrafluoroethylene filter to account for any dissolved or salt matrix contaminants, as in Heal et al. (2020). Samples for DNA sequencing were filtered onto 47 mm 0.2 μm Pall Supor polyethersulfone membranes and were then stored in their original sterile packaging, and frozen at –80°C until extraction.

Samples for POC, PN, DOC, Chl *a*, and major nutrients were collected and processed according to protocols of Marine Chemistry Laboratory at the University of Washington. Samples for POC and PN were filtered through combusted (450°C, 4 h) 25 mm glass fiber filters (GF/F, pore size 0.7 μm pre-combustion) and frozen at –80°C until analysis. Following fuming with HCl to remove inorganic carbon, CHN was measured on a CEC440 Elemental Analyzer (Leeman Labs) in the Marine Chemistry Laboratory (MCL) at the University of Washington. DOC was measured on 0.2 μm filtrate on a TOC-VCSH DOC analyzer (Shimadzu) in the MCL. pEPS and dEPS were measured in glucose-equivalents using the phenol-sulfuric acid method and converted to carbon-equivalents following Krembs et al. (2011). Samples for EPS were filtered through 0.4 μm polycarbonate filters; the filter and filtrate (< 0.4 μm) were used for pEPS and dEPS, respectively. Nutrients were analyzed in the MCL using a Technicon AutoAnalyzer II (6). Samples for Chl *a* were collected onto 25 mm glass fiber filters (GF/F, pore size 0.7 μm pre-combustion) and measured according to Welschmeyer (1994). Temperature, salinity, and photosynthetically active radiation (PAR) were measured using a digital thermometer, refractometer, and Walz US-SQS spherical quantum sensor -ULM-500 light meter, respectively.

4.10.3 *Metabolite sample extractions and analysis*

Metabolites were extracted from sample filters as detailed in Boysen et al. (2018). Briefly, metabolites were extracted using a modified Bligh-Dyer extraction in 1:1:2 methanol:water:dichloromethane, resulting in a polar aqueous (methanol and water soluble) and a non-polar organic (dichloromethane soluble) extract. Metabolites in the polar aqueous fraction were analyzed in this study, in addition to three fatty acids in the organic extract, as detailed below. A suite of internal standards (Supplementary Table 4.3) were added before and after extraction as in Boysen et al. (2018) to use in downstream data normalization. Sample extracts were dried under clean N2 and reconstituted in 400 µL of Optima LC/MS grade water. Note that for the sample Sea ice_3 metabolite data is not shown throughout.

Metabolites from the polar aqueous extract were separated via liquid chromatography as in Boysen et al. (2018) with a Waters Acquity I-Class UPLC equipped with either a reversed phase (RP) or hydrophilic interaction liquid chromatography (HILIC) column, as detailed below. Both liquid chromatography configurations were coupled to a Thermo Q-Exactive (QE) mass spectrometer and data was acquired in full scan mode for compound quantification as modified from Boysen et al. (2018), as detailed below. Metabolites from the non-polar organic extract were similarly separated via liquid chromatography (Waters Acquity UPLC CSH C18 column) and analyzed on a coupled Thermo Q-Exactive (QE) mass spectrometer, as detailed below (referred to as “lipid analysis”).

4.10.4 *HILIC analysis liquid chromatography method*

For HILIC, a SeQuant ZIC-pHILIC column (5 um particle size, 2.1 mm x 150 mm, from Millipore) was used with 10mM ammonium carbonate in 85:15 water to acetonitrile (Solvent A) and 10mM ammonium carbonate in 85:15 acetonitrile to water (Solvent B) at a flow rate of 0.15 mL/min. The

column was held at 100% B for 2 minutes, ramped to 64% A over 18 minutes, ramped up to 100% A over 1 minute, held at 100% A for 7 minutes, and equilibrated at 100% B for 22 minutes (total time is 50 minutes). The column was maintained at 30˚C.

4.10.5 *Reversed-Phase analysis liquid chromatography method*

For reversed-phase, a Waters Acquity UPLC HSS Cyano column (1.8 um particle size, 2.1 mm x 100 mm) equipped with a Acquity UPLC HSS Cyano guard column (1.8 um particle size, 2.1 mm x 5 mm) was used with 0.1% formic acid in water (Solvent A) and 0.1% formic acid in acetonitrile (Solvent B) at a flow rate of 0.4 mL/min. The column was held at 5% B for 2 minutes, ramped to 100% B over 18 minutes, held at 100% B for 2 minutes, and equilibrated at 5% B for 5 minutes (total run time is 25 minutes). The column was maintained at 35˚C.

4.10.6 *Lipid analysis liquid chromatography method*

For lipid analysis, a Waters Acquity UPLC CSH C18 column (1.7 um particle size, 2.1 mm x 150 mm) was used with 10mM ammonium formate in 60:40 acetonitrile to water and 0.1% formic acid (Solvent A) and 10mM ammonium formate in 90:10 isopropyl alcohol to acetonitrile and 0.1% formic acid (Solvent B) at a flow rate of 0.45 mL/min. Initial conditions were 90% A and 10% B. The column was ramped to 80% B over 33 minutes, ramped up to 90% B over 12 minutes, held at 90% B for 1 minute, and equilibrated to 90%A and 10% B for 6 minutes (total time is 52 minutes). The column was maintained at 65°C.

4.10.7 *QE (Orbitrap) mass spectrometry method*

Metabolites were measured using both hydrophilic interaction liquid chromatography (HILIC) and reverse phase chromatography (RP) on a Waters Acquity UPLC system coupled to a Thermo

Qexactive HF (QE-HF) high-resolution mass spectrometer equipped with heated electrospray ionization (H-ESI).

The mass spectrometer was calibrated weekly in positive and negative mode using solutions provided by the manufacturer. For HILIC, a full scan method employing positive and negative switching was used with a scan range of 60 to 900 m/z and a resolution of 60,000. The capillary temperature was 320˚C, the H-ESI spray voltage was 3.5 kV, and the auxiliary gas heater temperature was 90˚C. The S-lens RF level was 65. Sheath gas, auxiliary gas, and sweep gas flow rates were maintained at 16, 3, and 1, respectively. For the quality control pooled samples, high-resolution MS scans were collected and separate injections were done for positive and negative ion modes.

For reverse phase, a full scan method was used with a scan range of 90 to 900 m/z and a resolution of 120,000 in positive mode. The capillary temperature was 320˚C, the H-ESI spray voltage was 3.8 kV, and the auxiliary gas heater temperature was 90˚C. The S-lens RF level was 65. Sheath gas, auxiliary gas, and sweep gas flow rates were maintained at 40, 10, and 1, respectively. For the quality control pooled samples, high-resolution MS scans were collected.

For lipid analysis, a full scan method was used with a scan range of 150 to 2000 m/z and a resolution of 120,000 in positive mode and negative mode (separate injections). The capillary temperature was 320°C, the H-ESI spray voltage was 3.8 kV, and the auxiliary gas heater temperature was 150°C. The S-lens RF level was 65. Sheath gas, auxiliary gas, and sweep gas flow rates were maintained at 40, 10, and 1, respectively. For the quality control pooled samples, high-resolution MS scans were collected with separate injections for positive and negative ion modes. Only data for three fatty acids (arachidonic acid, eicosapentaenoic acid, and docosahexaenoic acid) from the negative mode are presented in this study.

4.10.8 *Metabolomic data processing*

Metabolite peaks obtained from mass spectrometry were integrated using Skyline for small molecules (8). Full and abbreviated compound names are listed in Supplementary Table 4.1, with abbreviated names used in figures throughout. Leucine and isoleucine, as well as butyryl-l-carnitine and isobutyryl-l-carnitine, did not separate chromatographically, so were integrated as a combined signal, referred to here as (iso)leucine and (iso)butyryl-l-carnitine, respectively. Integrated peak areas were subject to quality control, where peaks that did not meet minimum criteria (Supplementary Table 4.2) were excluded from further analysis to ensure correct compound identification and peak quality. Only compounds detected in at least three samples and at least 2 of 3 sample replicates (excluding sea-ice samples where samples were not collected in triplicate for Sea ice_2 and Sea ice_3) were included in further analysis. As in Heal et al. (2019), for compounds that were detected or passed through quality control in only a subset of replicates, the remaining replicates were assigned a value representing an upper estimate of how large a peak could be and still remain below the detection limit (3 x peak area in blank + 100). Peak areas were then normalized using best-matched internal standard normalization to reduce variability due to changes in instrument response throughout the run (Boysen et al., 2018). As in Heal et al. (2019), a 20% improvement to the relative standard deviation of each compound in a pooled sample was used as criteria to apply normalization; compounds with a raw RSD of <10% across the raw pooled areas were not normalized. Three polyunsaturated fatty acids (arachidonic acid, eicosapentaenoic acid, and docosahexaenoic acid) that were quantified from the organic extract were not subject to best-matched internal standard normalization since concentrations were calculated directly from raw peak areas, as detailed below.

4.10.9 *Metabolite concentration calculations*

Absolute concentrations of compounds were calculated or estimated from peak areas using commercially available standards run in the same batch as our samples, similar to previous work (Dawson et al., 2020b; Boysen et al., 2020; Heal et al., 2020). In short, for metabolites where isotopically labeled standards were added to the samples as part of the internal standard suite ("Matched compound" in Supplementary Table 4.3), concentrations were calculated directly (labeled "isotopologue" in quantification method of Supplementary Table 4.1). For compounds without isotopologues, approximate concentrations were estimated by correcting for ionization efficiency and ion suppression using authentic standards mixed into water and a representative matrix by calculation of response factor (RF) and RF ratio as in previous work (Dawson et al., 2020b; Boysen et al., 2020; Heal et al., 2020), labeled "direct RF and RFratio" in quantification methods of Supplementary Table 4.3. For glutathione, a literature value for RFratio (Boysen et al., 2018) was assumed, rather than using the calculated value which was negative, labeled "direct RF and RFratio assumed" in quantification methods of Supplementary Table 4.1 (which contains all quantification details). Dimethylsulfoniopropionate (DMSP) may volatilize during sample processing resulting in some loss (Spielmeyer and Pohnert, 2010), but good agreement across replicates suggests that potential losses were similar across samples and that estimated concentrations presented here can be taken as a minimum value. The free concentrations of three polyunsaturated fatty acids (arachidonic acid, eicosapentaenoic acid, and docosahexaenoic acid) were calculated directly using isotopically labeled standards (Supplementary Table 4.3) added to the samples ("isotopologue", as above). Fatty acid data was used only to contextualize the results on certain metabolites from the aqueous extract, and are not included in analyses of "all metabolites".

4.10.10 *DNA extraction, sequencing, and processing*

DNA extraction, sequencing, and sequence analysis were performed following Erazo and Bowman (2021). Briefly, DNA was extracted using the Qiagen DNeasy Power Water Kit following the manufacturer protocol with an additional heating step to aid lysis. Extracted DNA concentration was measured using the Qubit HS DNA quantification kit (Invitrogen) and quality-checked by gel electrophoresis and PCR amplification of the V3-V4 region of the 16S rRNA gene using primers 515F and 806R (14) for Bacteria and Archaea and the V9 region of the 18S rRNA gene using primers 1380F and 1510R (15). High quality DNA was submitted for sequencing to the Argonne National Laboratory sequencing center for amplification and library preparation with the same primer set, followed by 2 x 151 paired-end sequencing on the Illumina Miseq platform. Reads generated from Illumina MiSeq were then demultiplexed using the 'iu-demultiplex' command in Illumina utils (16) quality-controlled, denoised, and merged using the dada2 package (Callahan et al., 2016a) in R. Reads were then analyzed using the paprica pipeline (Bowman and Ducklow, 2015; https://github.com/bowmanjeffs/paprica) to obtain community structure for all unique amplicon sequence variants (ASVs) by placing reads on a phylogenetic tree created from the complete 16S +23S rRNA or 18S rRNA genes from all completed genomes in the NCBI RefSeq database (19). ASVs are named according to their lowest consensus taxonomic ranking for phylogenetic placements to terminal edges (closest completed genomes, CCGs) or according to their closest relative on the phylogenetic reference tree for placements to non-terminal edges (closest estimated genomes, CEGs). Distinct ASVs assigned the taxonomic name are differentiated throughout by a number following the name (e.g. *Rhizosolenia pungens*.12 versus *Rhizosolenia pungens*.13). The paprica pipeline relies on Infernal for read alignment (20), EPA-ng for read

placement (21), Gappa (22), and the PR2 (23) and RefSeq (19) databases. Reads in the 16S rRNA dataset assigned to chloroplasts were discarded.

4.10.11 *Statistical approaches*

Differences in community structure, both prokaryotic and eukaryotic, and metabolite composition were evaluated for each dataset separately using non-metric dimensional scaling (NMDS) (24). NMDS analyses on community structure were based on a Bray-Curtis dissimilarity matrix by Hellinger-transformed ASV data. NMDS using a Euclidean distance matrix, based on the proportional contribution of each metabolite to the quantified metabolite carbon pool (mole fraction of carbon), was used to compare samples based on targeted metabolite profiles. This approach accommodates our low sample numbers, high variable numbers, and the non-normal distribution of metabolomics data to avoid overfitting (25). Dimensionality of each NMDS was assessed with a scree plot, and probability was calculated with a Monte Carlo permutation test. Analysis of similarity (ANOSIM) (26) was used to evaluate significant differences with respect to field sample types and incubation treatments. ANOSIMS were performed with 999 permutations for nonsignificant results ($p > 0.05$) and 19999 permutations for significant results ($p < 0.05$) to obtain exact *p*-values, where possible. Data transformation, standardization, NMDS, and ANOSIMS statistics were done in R using the vegan (v2.5.7) package (Oksasen et al. 2020). Metabolite contributions to the sample ordination were quantified using the envfit function from the R vegan package (Oksasen et al. 2020) with 1000 permutations to assess their correlation with the ordination (R^2) and significance, and *p*-values corrected for false discovery rate (27).

Overall degree of congruency between our prokaryotic and eukaryotic community structures was tested using a Procrustean superimposition approach (28). The Procrustes function in the R package vegan (Oksasen et al. 2020) was applied to the NMDS scores generated for each

dataset. A PROcrustean Randomization TEST (PROTEST; (29)) with 19999 permutations was then used to assess the statistical significance of the Procrustean fit using the vegan package (Oksasen et al. 2020). Unique ASV correlations were performed using the Spearman's rank correlation coefficient using the psych (v.2.1.9) package in R (Revelle 2021) with *p*-values corrected for false discovery rate (27). Relative abundance data was first centered log-ratio (CLR) transformed (30) prior to correlation analyses to ensure compositional robustness in R. Correlation results were visualized as a network using the igraph package in R (31).

Individual metabolite concentrations as molar carbon concentration relative to POC concentration (nmol C µmol C^{-1}) were compared between incubation treatments using one-way analysis of variance (ANOVA) in R, with *p*-values corrected for false discovery rate (27). Metabolites with significantly different concentrations across treatments were then clustered based on Euclidean distances and average-linkage clustering using the dist and hclust functions from the stats R package. One-way ANOVAs were also used to assess statistical differences in ancillary measurements (diversity, etc.) between samples. Post-hoc Tukey's HSD (honestly significant difference) tests were used to explore specific significant relationships between all treatments when a significant overall effect of treatment was observed. For all statistical analyses, a probability level of ≤ 0.05 was used to determine statistical significance.

References

1. Guillard RRL. Culture of phytoplankton for feeding marine invertebrates. In: Smith WL, Chanley MH, editors. Culture of Marine Invertebrate Animals. Boston, MA: Springer; 1975. p. 29–60.

2. Harrison PJ, Waters RE, Taylor FJR. A broad spectrum artificial seawater medium for coastal and open ocean phytoplankton. J Phycol. 1980;16(1):28–35.

3. Boysen AK, Heal KR, Carlson LT, Ingalls AE. Best-matched internal standard normalization in liquid chromatography-mass spectrometry metabolomics applied to environmental samples. Anal Chem. 2018;90(2):1363–1369.

4. Heal KR, Durham BP, Boysen AK, Carlson LT, Qin W, Ribalet F, et al. Metabolomes carry fingerprints of phytoplankton community composition. mSystems. 2021;6(3).

5. Krembs C, Eicken H, Deming JW. Exopolymer alteration of physical properties of sea ice and implications for ice habitability and biogeochemistry in a warmer Arctic. Proc Natl Acad Sci USA. 2011;108(9):3653–8.

6. Knap A., Michaels A., Close A., Ducklow H., Dickson A. Protocols for the Joint Global Ocean Flux Study (JGOFS) Core Measurements. UNESCO. 1996.

7. Welschmeyer NA. Fluorometric analysis of chlorophyll a in the presence of chlorophyll b and pheopigments. Limnol Oceanogr. 1994;39(8):1985–92.

8. MacLean B, Tomazela DM, Shulman N, Chambers M, Finney GL, Frewen B, et al. Skyline: An open source document editor for creating and analyzing targeted proteomics experiments. Bioinformatics. 2010;26(7):966–8.

9. Heal KR, Kellogg NA, Carlson LT, Lionheart RM, Ingalls AE. Metabolic consequences of cobalamin scarcity in the diatom *Thalassiosira pseudonana* as revealed through metabolomics. Protist. 2019;170(3):328–48.

10. Boysen AK, Carlson LT, Durham BP, Groussman RD, Aylward FO, Ribalet F, et al. Particulate metabolites and transcripts reflect diel oscillations of microbial activity in the surface ocean. mSystems. 2021;6(3).

11. Dawson HM, Heal KR, Torstensson A, Carlson LT, Ingalls AE, Young JN. Large diversity in nitrogen- and sulfur-containing compatible solute profiles in polar and temperate diatoms. Integr Comp Biol. 2020;60(6):1401–13.

12. Dawson HM, Heal KR, Boysen AK, Carlson LT, Ingalls AE, Young JN, et al. Potential of temperature- and salinity-driven shifts in diatom compatible solute concentrations to impact biogeochemical cycling within sea ice. Elem Sci Anth. 2020;8(25).

13. Erazo NG, Bowman JS. Sensitivity of the mangrove-estuarine microbial community to aquaculture effluent. iScience. 2021;24(3):102204.

14. Walters W, Hyde ER, Berg-lyons D, Ackermann G, Humphrey G, Parada A, et al. Transcribed spacer marker gene primers for microbial community surveys. mSystems. 2015;1(1):e0009-15.

15. Amaral-Zettler LA, McCliment EA, Ducklow HW, Huse SM. A method for studying protistan diversity using massively parallel sequencing of V9 hypervariable regions of small-subunit ribosomal RNA Genes. PLoS One. 2009;4(7):1–9.

16. Eren AM, Maignien L, Sul WJ, Murphy LG, Grim SL, Morrison HG, et al. Oligotyping: Differentiating between closely related microbial taxa using 16S rRNA gene data. Methods Ecol Evol. 2013;4(12):1111–9.

17. Callahan BJ, McMurdie PJ, Rosen MJ, Han AW, Johnson AJA, Holmes SP. DADA2: High-resolution sample inference from Illumina amplicon data. Nat Methods. 2016;13(7):581–3.

18. Bowman JS, Ducklow HW. Microbial communities can be described by metabolic structure: A general framework and application to a seasonally variable, depth-stratified microbial community from the coastal West Antarctic Peninsula. PLoS One. 2015;10(8):1–18.

19. Haft DH, DiCuccio M, Badretdin A, Brover V, Chetvernin V, O'Neill K, et al. RefSeq: An update on prokaryotic genome annotation and curation. Nucleic Acids Res. 2018;46(D1):D851–60.

20. Nawrocki EP, Eddy SR. Infernal 1.1: 100-fold faster RNA homology searches. Bioinformatics. 2013;29(22):2933–5.

21. Barbera P, Kozlov AM, Czech L, Morel B, Darriba D, Flouri T, et al. EPA-ng: Massively parallel evolutionary placement of genetic sequences. Syst Biol. 2019;68(2):365–9.

22. Czech L, Barbera P, Stamatakis A. Genesis and Gappa: Processing, analyzing and visualizing phylogenetic (placement) data. Bioinformatics. 2020;36(10):3263–5.

23. Guillou L, Bachar D, Audic S, Bass D, Berney C, Bittner L, et al. The protist ribosomal reference database (PR2): A catalog of unicellular eukaryote small sub-unit rRNA sequences with curated taxonomy. Nucleic Acids Res. 2013;41(D1):597–604.

24. Kruskal J, Wish M. Multidimensional Scaling. Thousand Oaks, California; 1978.

25. Saccenti E, Hoefsloot HCJ, Smilde AK, Westerhuis JA, Hendriks MMWB. Reflections on univariate and multivariate analysis of metabolomics data. Metabolomics. 2014;10(3):361–74.

26. Clarke KR. Non-parametric multivariate analyses of changes in community structure. Aust J Ecol. 1993;18(1):117–43.

27. Benjamini Y, Hochberg Y. Controlling the false discovery rate: a practical and powerful approach to multiple testing. J R Stat Soc. 1995;57(1):289 –300.

28. Gower JC. Statistical methods of comparing different multivariate analyses of the same data. In: FR H, DG K, P T, editors. Mathematics in the archaeological and historical science. Edinburgh: Edinburgh University Press; 1971. p. 138–49.

29. Jackson DA. PROTEST: A PROcrustean Randomization TEST of community environment concordance. Écoscience. 1995;2(3):297–303.

30. Aitchison J, Society S, Methodological SB. The statistical analysis of compositional data The statistical analysis of compositional data. 1982;44(2):139–77.

31. Csardi G, Nepusz T. The igraph software package for complex network research. InterJournal. 2006;Complex Sy:1695.

32. Oksanen, F.J., et al. (2017) Vegan: Community Ecology Package. R package Version 2.5-7. https://CRAN.R-project.org/package=vegan.

33. Revelle W (2022). psych: Procedures for Psychological, Psychometric, and Personality Research. Northwestern University, Evanston, Illinois. R package version 2.1.9, https://CRAN.R-project.org/package=psych.

4.11 SUPPLEMENTARY TABLES AND FIGURES

Supplementary Table 4.1. Quantification method for each quantified metabolite in all samples. Full and abbreviated compound names are listed for each metabolite. Details of quantification methods are provided in methods. This table is provided as a separate file.

Supplementary Table 4.2. Quality control (QC) parameters used following peak integration and preceding B-MIS normalization for HILIC and RP data. Peaks were removed from the data set (marked NA) if they did not meet the listed limits for minimum area to qualify as a real peak (Areamin), maximum fraction media blank can be of a sample (BlankRatiomax), parts per million mass error flexibility (ppmflex), minimum signal/noise ratio (SNmin), and minimum number of replicates detected (Repmin). Peaks were also removed if the retention time within a sample was greater than the allowed RT flexibility (RTflex) around the range of retention time of the compound in our concurrently run mix of standards. Peaks were also removed if detected in fewer than the allowed minimum number of samples (Samplemin) or replicates (Repilcatemin). This table is provided as a separate file.

Supplementary Table 4.3. Isotopically-labeled internal standards used in B-MIS normalization and isotopologue quantification for all samples. The column, ion mode (z), injection concentration, and extracted *m*/*z* used for analysis for each standard. Whether each standard was used for B-MIS normalization or for quantification is noted. This table is provided as a separate file.

Supplementary Table 4.4. Chemical parameters from field and incubation samples. PC is particulate organic carbon (μM); PN is particulate nitrogen (μM); CN is carbon:nitrogen

(mol:mol); Chl is chl a (mg m^{-3}); DOC is dissolved organic carbon (µM); pEPS is particulate extracellular polysaccharides (µM carbon equivalents); dEPS is dissolved extracellular polysaccharides (µM carbon equivalents); PO4, SIO4, NO3, NO2, and NH4 are inorganic nutrients (µM). Mean and standard deviation are listed per measurement, denoted by the ending "_ave" and "_sd", respectively. Where standard deviation is na, n = 1. For DOC and dEPS "seawater" and "sea ice" samples, n = 2. For all others, n = 3. Note that we do not have ancillary chemical measurements paired with the sea-ice samples. This table is provided as a separate file.

Supplementary Table 4.5. Taxonomic assignment of ASVs within the 18S rRNA gene amplicon dataset. The mean relative abundance for the respective group of samples is shown, including closest taxonomic assignment. Warmer colors indicate higher abundances of respective ASVs. This table is provided as a separate file.

Supplementary Table 4.6. Taxonomic assignment of ASVs within the 16S rRNA gene amplicon dataset. The mean relative abundance for the respective group of samples is shown, including closest taxonomic assignment. Warmer colors indicate higher abundances of respective ASVs. This table is provided as a separate file.

Supplementary Table 4.7. Results from eukaryotic ANOSIM analysis. ANOSIM statistic(R), *p*-values, and number of permutations are given for differentiating eukaryotic community composition across samples based on the Bray-Curtis dissimilarity matrix by Hellinger-transformed unique sequence (ASV) data. This table is provided as a separate file.

Supplementary Table 4.8. Results from prokaryotic ANOSIM analysis. ANOSIM statistic(R), *p*-values, and number of permutations are given for differentiating prokaryotic community composition across samples based on the Bray-Curtis dissimilarity matrix by Hellinger-transformed unique sequence (ASV) data. This table is provided as a separate file.

Supplementary Table 4.9. Correlations between top 20 prokaryotic and eukaryotic taxa across all samples (incubation treatment and field samples). Spearman correlation coefficients (rho.clr) between prokaryotic and eukaryotic unique ASVs following centered log-ratio transformation. Significance of each correlation given by unadjusted (p.clr) and fdr-corrected (fdr.clr) *p*-value. This table is provided as a separate file.

Supplementary Table 4.10. Correlations between top 20 prokaryotic and eukaryotic taxa across field samples only. Spearman correlation coefficients (rho.clr) between prokaryotic and eukaryotic unique ASVs following centered log-ratio transformation. Significance of each correlation given by unadjusted (p.clr) and fdr-corrected (fdr.clr) *p*-value. This table is provided as a separate file.

Supplementary Table 4.11. Quantified metabolites from all samples. Full compound names are given for clarity as well as abbreviated compound names as reported in figures. *m*/*z* is mass to charge ratio observed; RT is retention time (in minutes); Column is the chromatography method used (HILIC or RP); z is charge state in which the mass feature was observed (1 is positive, –1 is negative); SampID is the sample identifier (elaborated in Table 1). Metabolites abundances are expressed as normalized peak areas per water volume filtered (area L^{-1}), metabolite carbon concentration per water volume filtered (nmol metabolite C L^{-1}), metabolite carbon concentration

per total particulate carbon (nmol metabolite C µmol C^{-1}), mole fraction of carbon of total identified metabolites, portion of particulate carbon (% POC), and as portion of particulate nitrogen (% PN). Note that we do not have exact dilution factor data to pair with the field sea-ice samples, so metabolite concentrations in terms of normalized area per L of water filtered and nmol metabolite C per L of water filtered are an underestimate (by approximately 2x) of concentrations in bulk sea ice. Note also that we do not have POC or PN to pair with sea-ice field samples, so metabolite concentrations in terms of nmol C per µmol C, %POC, and %PN are not provided. This table is provided as a separate file.

Supplementary Table 4.12. Results from metabolomic ANOSIM analysis. ANOSIM statistic(R), *p*-values, and number of permutations are given for differentiating metabolite composition across samples based on the Euclidean distance matrix of metabolite abundance data (mole fraction of carbon of total identified metabolites). This table is provided as a separate file.

Supplementary Table 4.13. Pairwise sample distances in metabolite space compared to community structure space. Pairwise sample distances in metabolite space (Euclidean distance) compared to sample distances in eukaryotic and prokaryotic space (Bray-Curtis dissimilarity) in field samples from sea ice, meltwater, and seawater. Incubation treatment samples are not included. This table is provided as a separate file.

Supplementary Table 4.14. Total quantifiable metabolites as a fraction of the particulate carbon and nitrogen pools. Note that we do not have bulk particulate carbon or nitrogen measurements paired with the sea-ice samples. This table is provided as a separate file.

Supplementary Table 4.15. Metabolite contributions to the NMDS sample ordination calculated using envfit(). MDS1 and MDS2 are direction cosines which are the coordinates in ordination space of the heads of unit length vectors in Supplementary Figure 4.6; R2 is the correlation value; p is *p*-value calculated using a permutation test, corrected for false discovery rate (*q*-value). This table is provided as a separate file.

Supplementary Table 4.16. Particulate metabolite responses to temperature and salinity change during the incubation experiment. *p*-values and *q*-values (fdr-corrected *p*-values) are provided for each compound based on one-way ANOVAs on concentrations of metabolites (nmol metabolite C μmol C^{-1}) across incubation treatments. Significance represents statistical significance, where $q < 0.05$ is TRUE and $q > 0.05$ is FALSE. This table is provided as a separate file.

Supplementary Table 4.17. Calculation of the potential impact of metabolite C and N loss due to freshening on C:N ratios. This table is provided as a separate file.

Supplementary Table 4.18. Select quantified free fatty acids from all samples. Full compound names are given for clarity as well as abbreviated compound names as reported in figures. *m*/*z* is mass to charge ratio observed; RT is retention time (in minutes); Column is the chromatography method used; z is charge state in which the mass feature was observed (1 is positive, –1 is negative); SampID is the sample identifier (elaborated in Table 4.1). Fatty acid abundances are expressed as metabolite concentration per total particulate carbon (nmol metabolite μmol C^{-1}).

Note that we do not have POC to pair with sea-ice field samples, so fatty acid concentrations are not provided for those samples. This table is provided as a separate file.

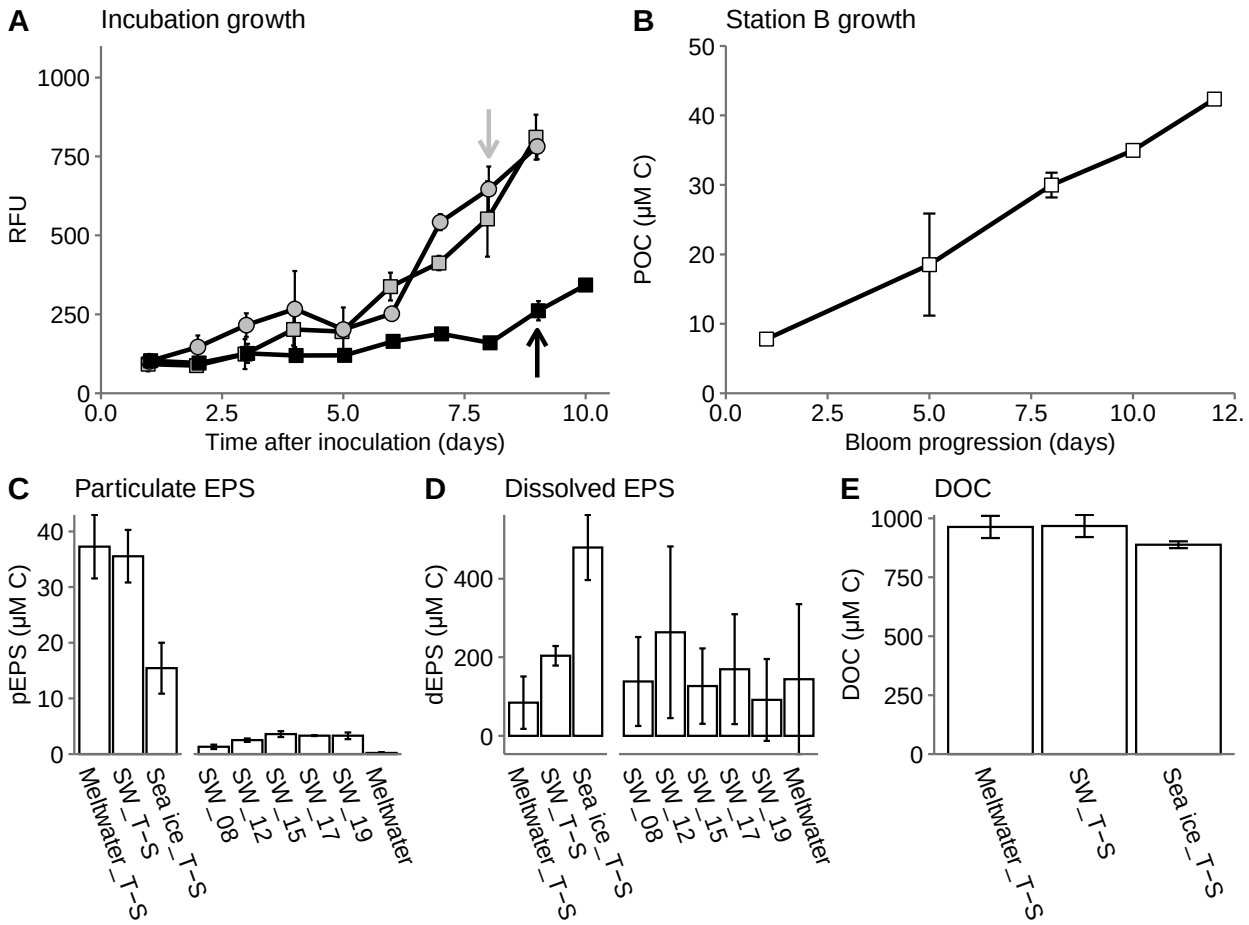

Supplementary Figure 4.1. Ancillary data from incubation and field samples. a) Growth curves of incubation treatments under the three experimental conditions, with symbols as in Figure 4.1a. Treatments grown at meltwater (grey circles) and seawater (grey squares) conditions were harvested at grey arrow and treatments grown at sea ice conditions were harvested at black arrow. RFU = relative fluorescence units, error bars are standard deviation (*n* = 3 for all time points). b) Growth curve of Station B seawater samples (SW_08 – SW_19). POC = particulate organic carbon, error bars are standard deviation (*n* = 3 for all time points). c) Concentration of particulate extracellular polysaccharides (pEPS) in incubation and field samples, shown in terms of µM carbon equivalents. Error bars are standard deviation (*n* = 3 for all). The x-axis break separates incubation treatment samples on the left and field samples on the right. d) Concentration of dissolved extracellular polysaccharides (dEPS) in incubation and field samples, shown in terms of

μM carbon equivalents. Error bars are standard deviation (n = 2 for SW_T-S, Sea ice_T-S, and Meltwater, n = 3 for rest). The x-axis break separates incubation treatment samples on the left and field samples on the right. e) Concentration of dissolved organic carbon (DOC) in incubation and field samples, shown in terms of μM carbon equivalents. Error bars are standard deviation of the mean (n = 3 for the meltwater treatment, n = 2 for the seawater and sea-ice treatments, and n = 1 for the seawater and meltwater field samples). Full data for panels c–e are available in Supplementary Table 4.4. Note that we do not have ancillary chemical measurements to pair with the sea-ice samples.

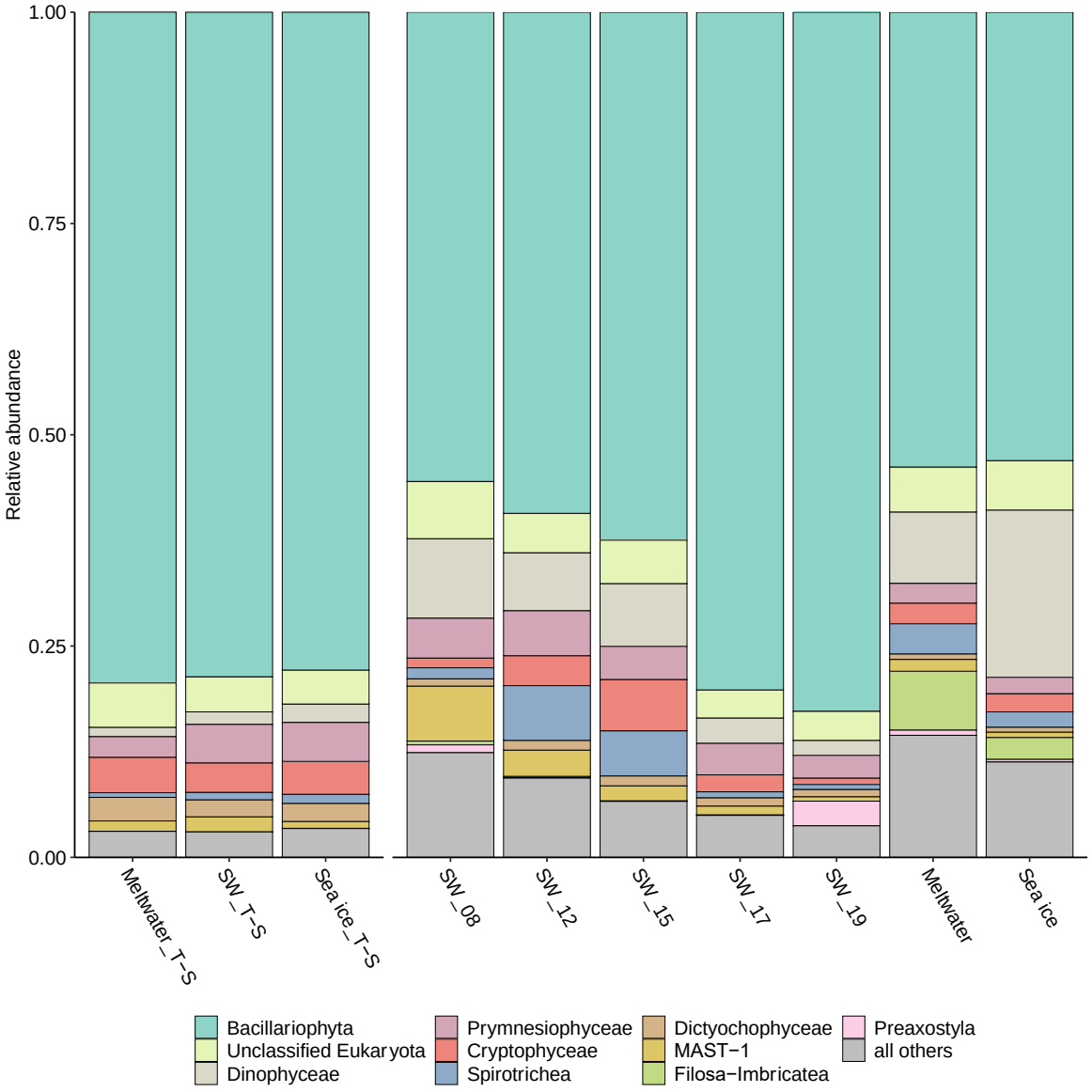

Supplementary Figure 4.2. Relative abundance of eukaryotic taxa in field and incubation samples at the class level. Average of triplicates is shown, except for sea-ice core where $n = 5$. The most abundant 10 classes across the sample set for each sample are shown, with "all others" containing the sum of the remaining classes. The x-axis break separates incubation treatment samples on the left and field samples on the right. Full data available in Supplementary Table 4.5.

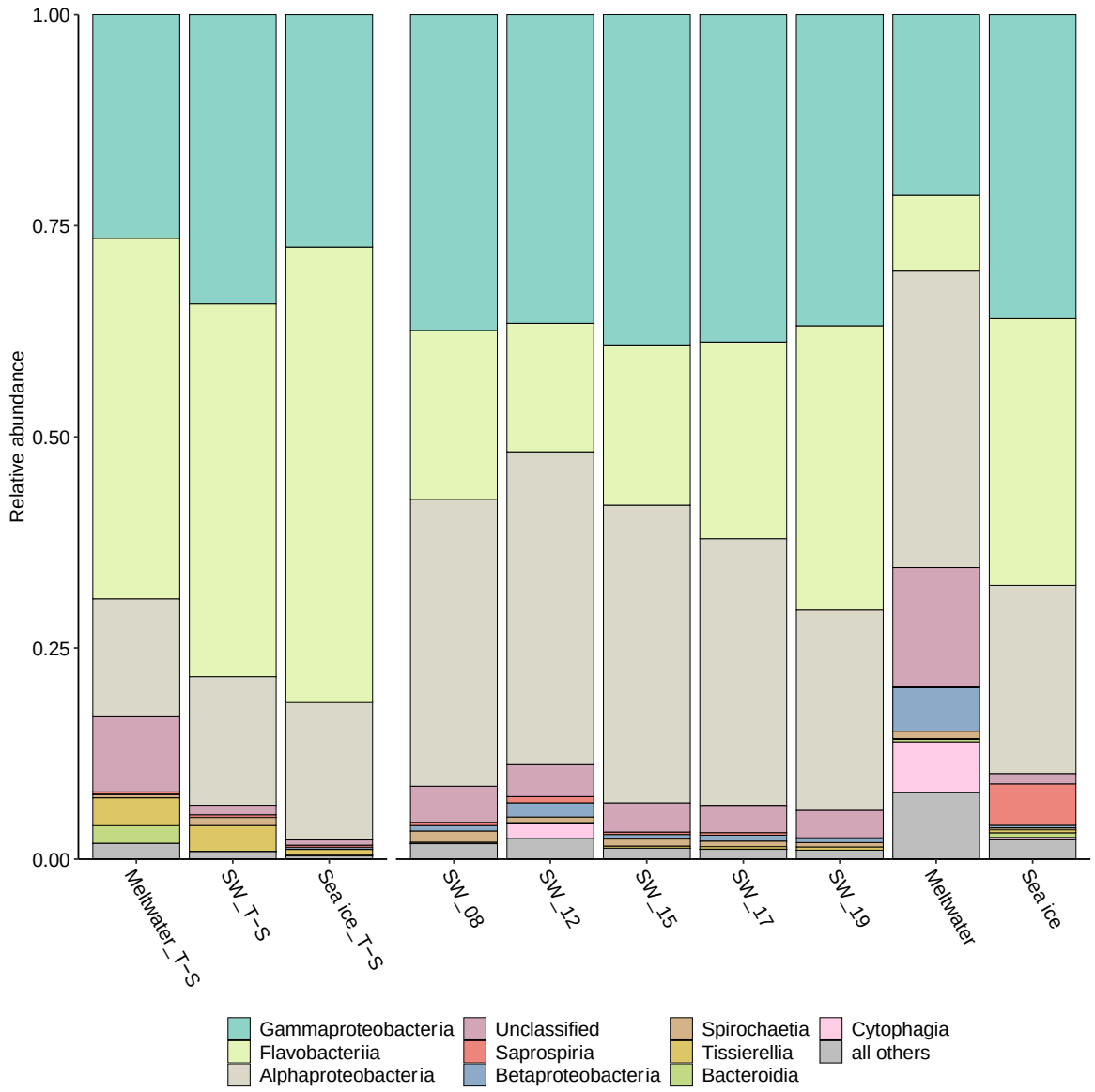

Supplementary Figure 4.3. Relative abundance of prokaryotic taxa in field and incubation samples at the class level. Average of triplicates is shown, except for sea-ice core where $n = 5$. The most abundant 10 classes across the sample set for each sample are shown, with "all others" containing the sum of the remaining classes. The x-axis break separates incubation treatment samples on the left and field samples on the right. Full data available in Supplementary Table 4.6.

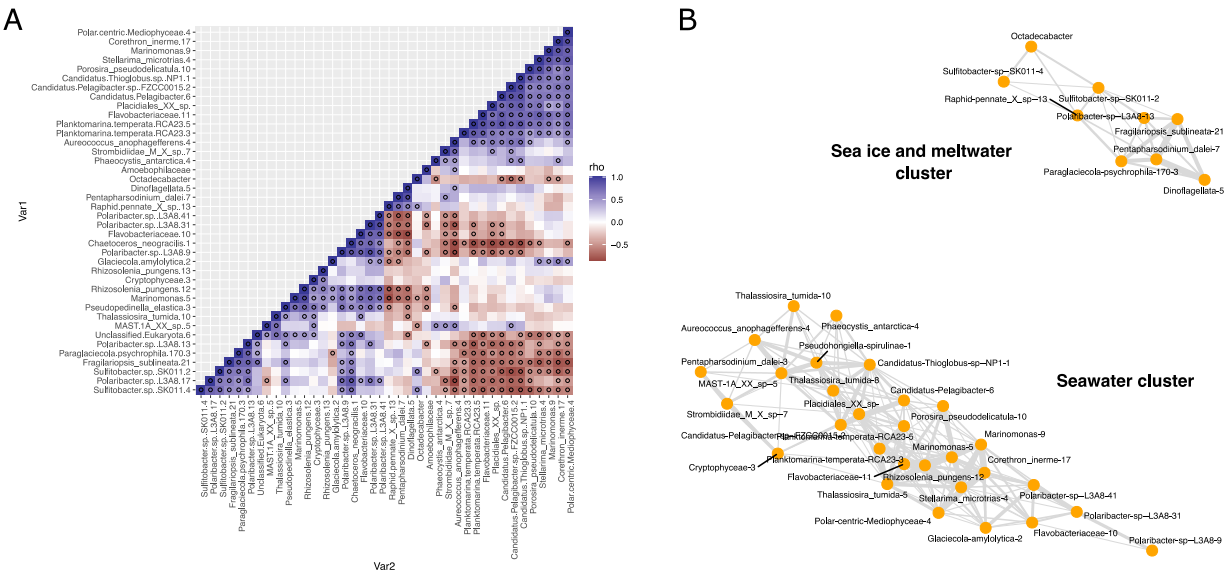

Supplementary Figure 4.4. Correlation patterns between most abundant eukaryotic and prokaryotic ASVs. a) Correlations for the top 20 prokaryotic and eukaryotic ASVs across entire sample set (incubation and field samples) based on the Spearman correlation of centered log-ratio-transformed data. Significant correlations (fdr-corrected *p*-value < 0.05) are denoted with black circles. b) Network visualization of significant ($p < 0.05$) positive correlations between ASVs across field samples only. Each ASV is depicted as a node (as labeled in Figure 4.3). The width of edges is proportional to the strength of the correlation (Spearman correlation coefficient). Correlation and significance data for all samples and for field samples only are available in Supplementary Tables 4.9 and 4.10, respectively.

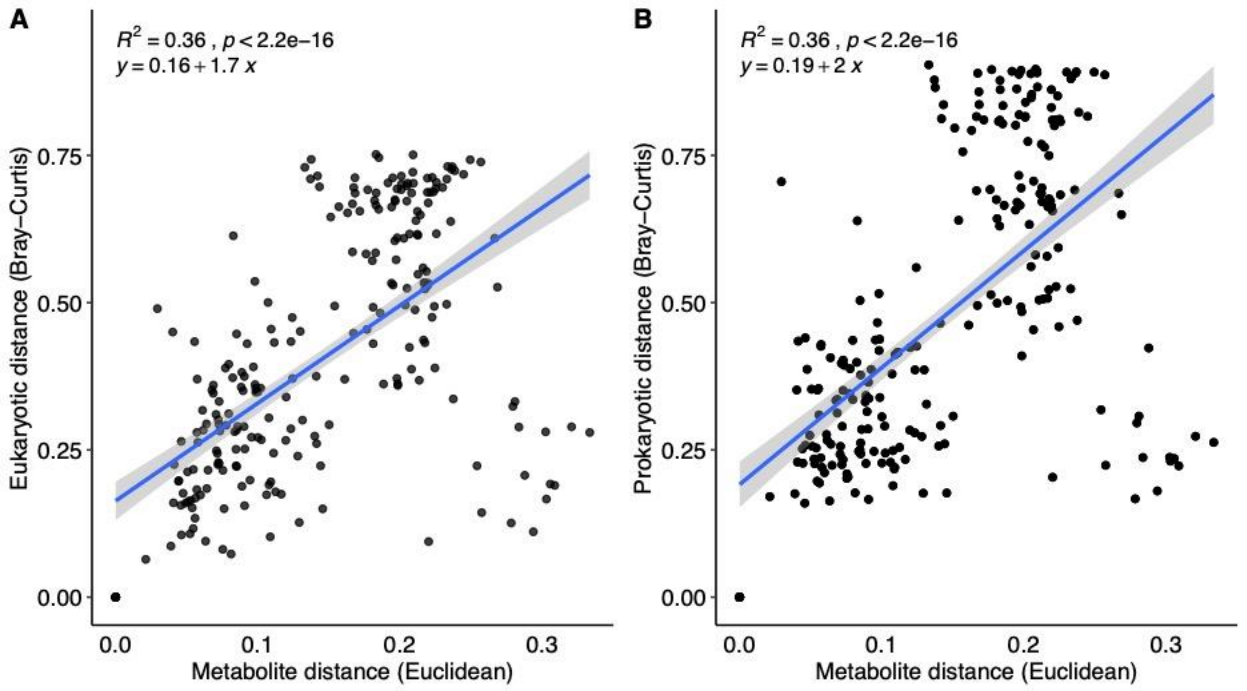

Supplementary Figure 4.5. Sample similarity in metabolite space compared to community structure space. Pairwise sample distances in metabolite space (Euclidean distance) compared to sample distances in eukaryotic (A) and prokaryotic (B) space (Bray-Curtis dissimilarity) in field samples from sea ice, meltwater, and seawater. Incubation treatment samples are not included. Linear regression statistics are provided on the plot. The shaded area represents a pointwise 95% confidence interval of the fitted values. Full data available in Supplementary Table 4.13.

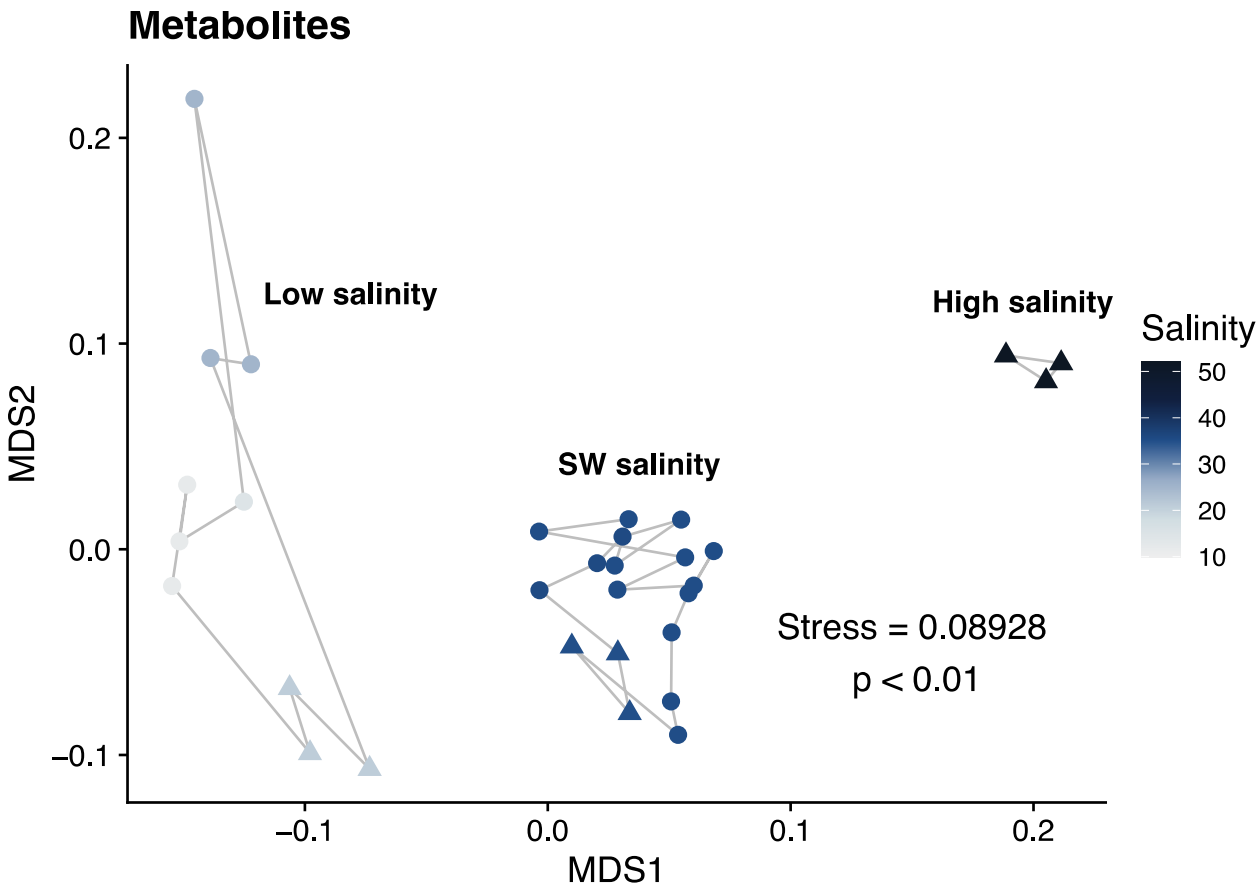

Supplementary Figure 4.6. Impact of salinity status on metabolite composition. NMDS ordination comparing the mole fraction of carbon metabolite composition of each sample (as shown in Figure 4.4d) with colors showing the measured sample salinity conditions in ppt. Samples with similar salinity status (from left to right as labeled on plot: Low salinity = Meltwater_T-S, Meltwater, and Sea ice; SW salinity = Seawater_T-S and all field seawater samples; and High salinity = Sea ice_T-S;) are shown connected, with incubation treatment samples in triangles and field samples in circles. Full salinity data can be found in Table 4.1. Full metabolomics data can be found in Supplementary Table 4.11.

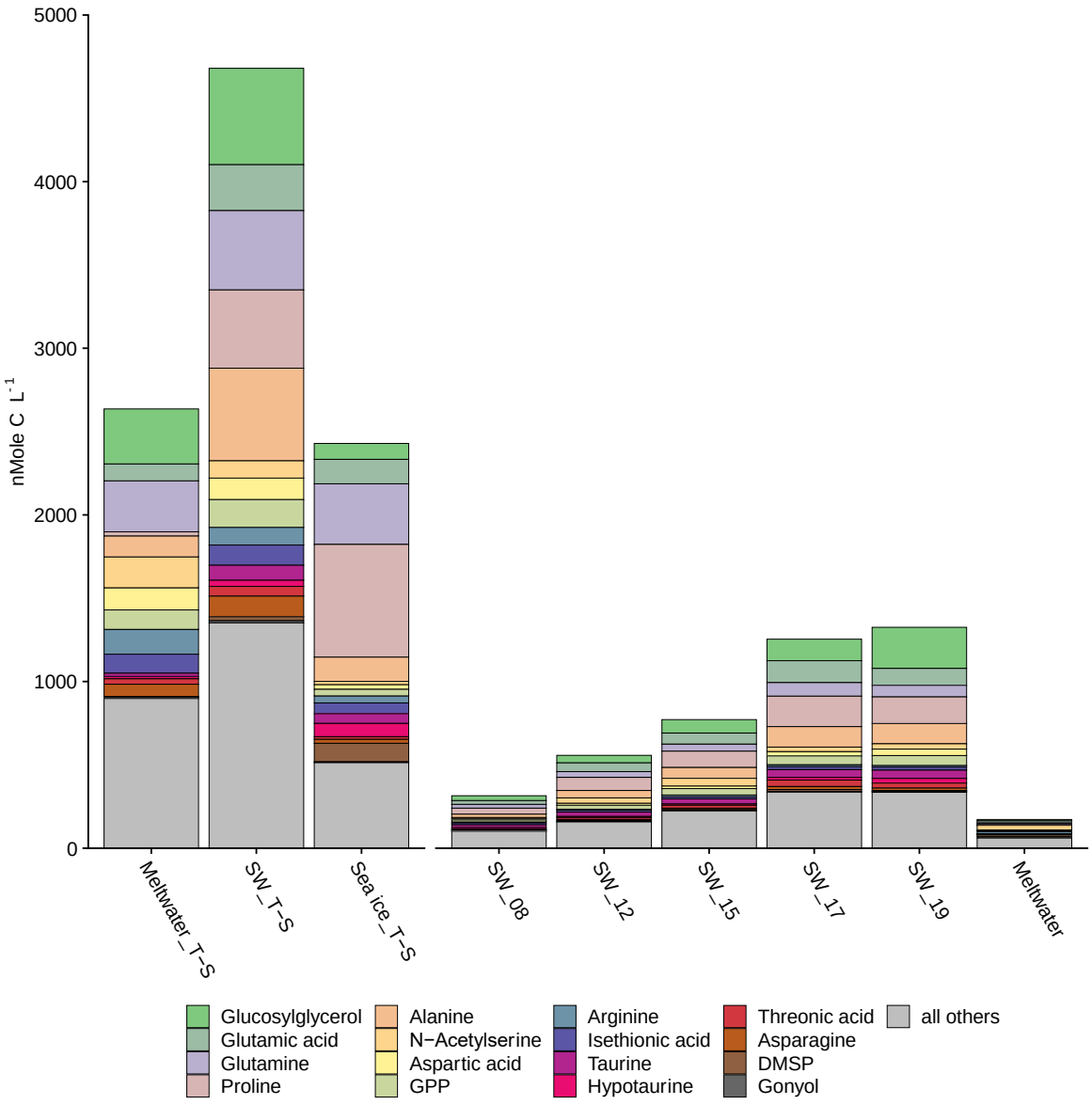

Supplementary Figure 4.7. Estimated particulate concentrations (nMole C L^{-1}) of metabolites across incubation and field samples. Average of triplicates is shown. The most abundant 16 molecules for each sample are shown, with "all others" containing the sum of the remaining quantified metabolites (118). Note that we do not have exact dilution factor data to pair with the sea-ice samples, so they are excluded from this figure. The x-axis break separates incubation

treatment samples on the left and field samples on the right. Full data available in Supplementary Table 4.11.

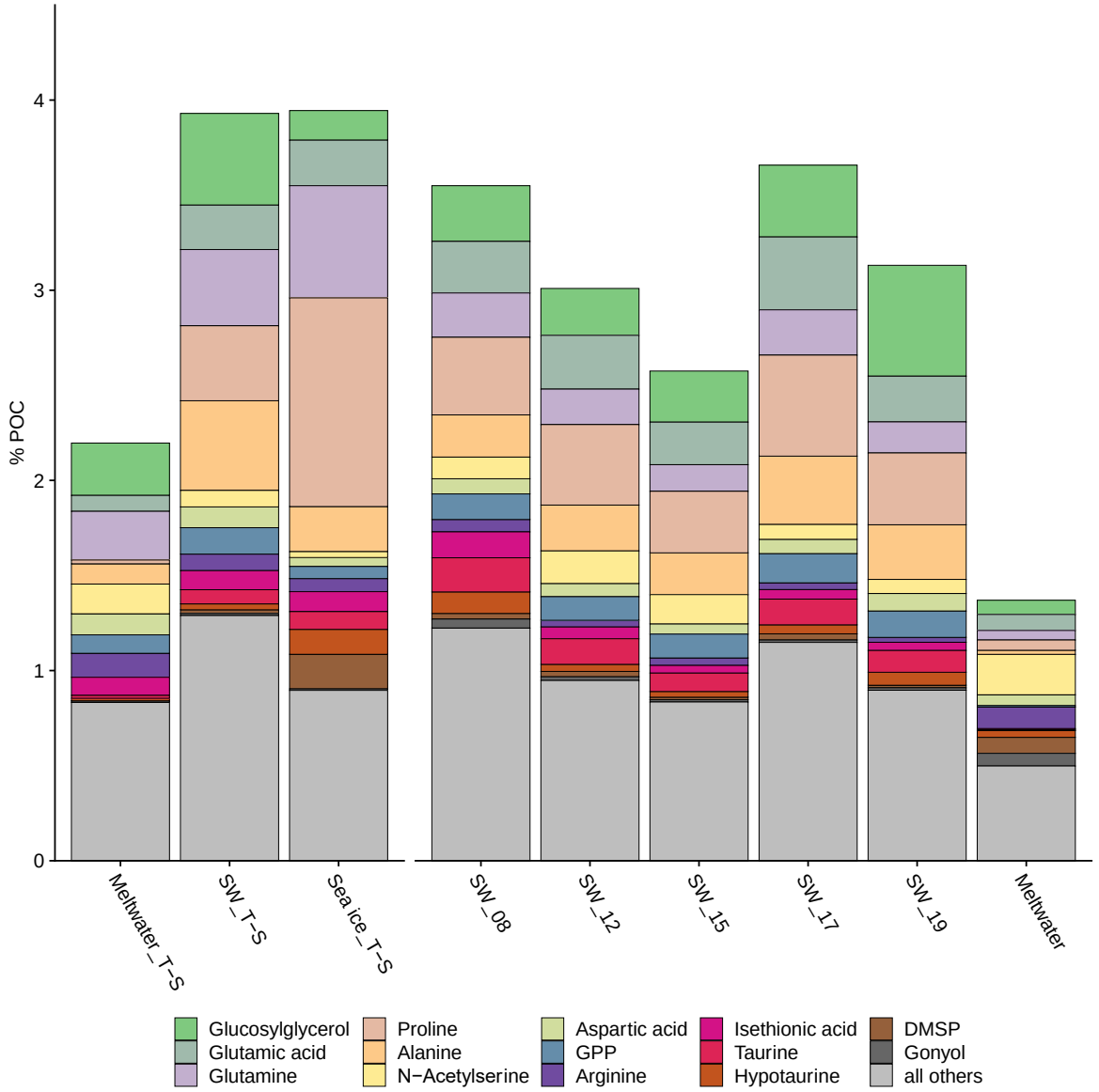

Supplementary Figure 4.8. Total quantified metabolite concentration as the percentage of particulate organic carbon (POC). Average of triplicates is shown. The most abundant 15

molecules for each sample are shown, with “all others” containing the sum of the rest of the metabolites quantified (119). Note that we do not have POC or PN to pair with the sea-ice samples. The x-axis break separates incubation treatment samples on the left and field samples on the right. Full data available in Supplementary Table 4.14.

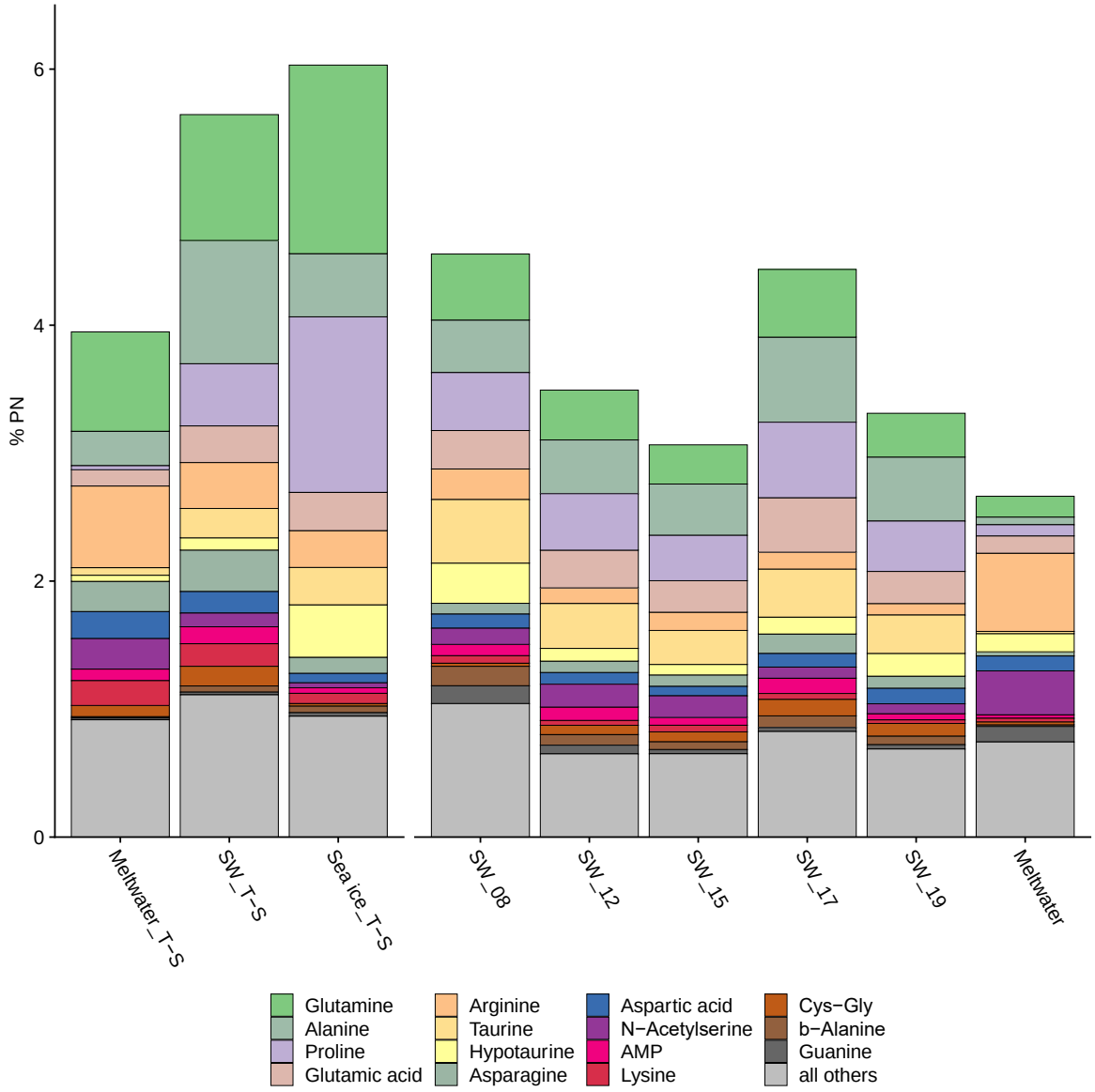

Supplementary Figure 4.9. Total quantified metabolite concentration as the percentage of particulate organic nitrogen (PN). Average of triplicates is shown. The most abundant 15 molecules for each sample are shown, with "all others" containing the sum of the rest of the metabolites quantified (119). Note that we do not have particulate carbon or nitrogen paired with the sea-ice samples. The x-axis break separates incubation treatment samples on the left and field samples on the right. Full data available in Supplementary Table 4.14.

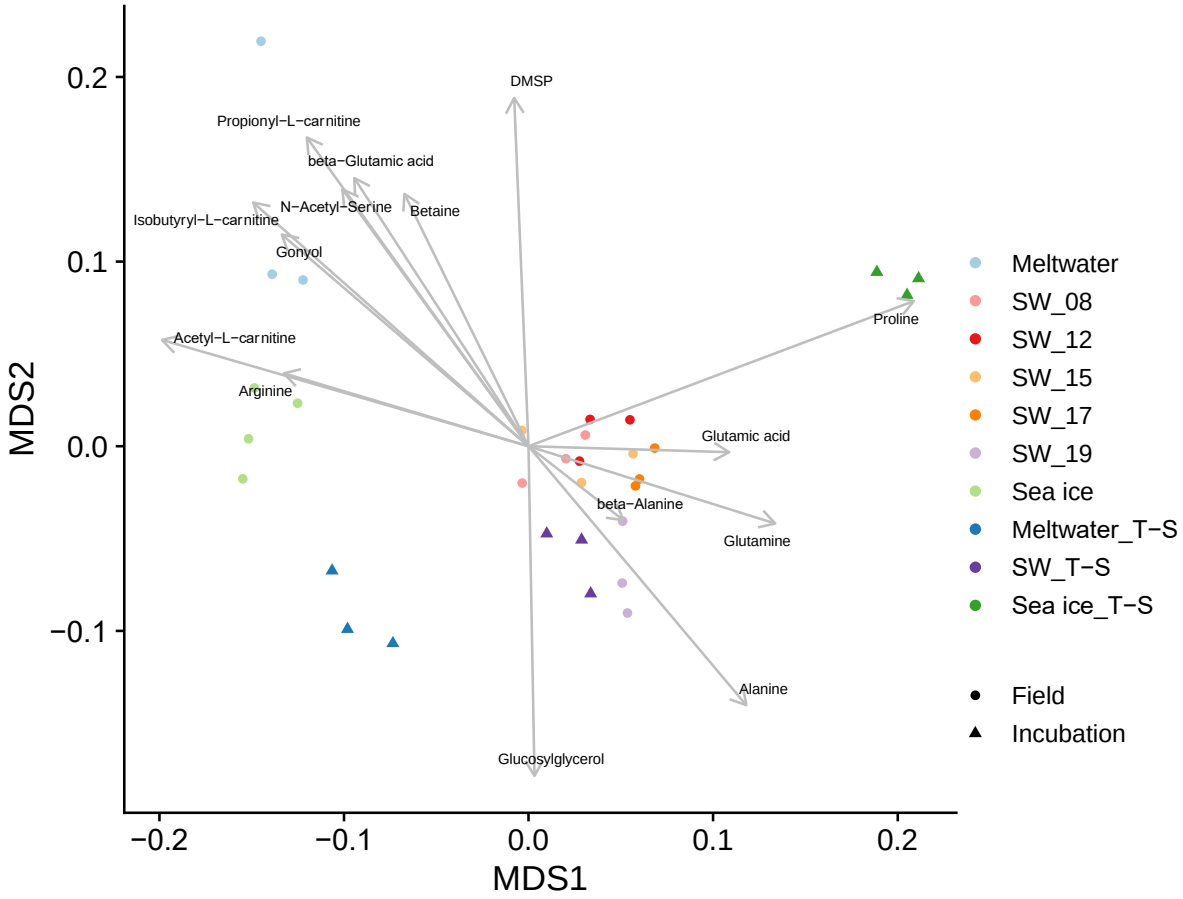

Supplementary Figure 4.10. Metabolite contributions to the sample ordination. NMDS ordination comparing the mole fraction of carbon metabolite composition of each sample (as shown in Figure 4.4d) with overlain vectors showing metabolite "loadings" (i.e., variable weights) on each derived

axis from the NMDS, calculated using the function envfit() from the vegan package. Vector lengths are scaled by their correlation (square root of R2) so that "weak" predictors have shorter arrows than "strong" predictors. Vector directions in ordination space point toward the metabolites that change most rapidly and to which metabolite they have maximal correlations with the ordination configuration (i.e., as you travel along each vector, the samples generally increase with respect to the proportional abundance of that metabolite). Significance determined using a permutation test, with *p*-values corrected for false discovery rate (*q*-value). For ease of visualization, metabolite vectors are only shown for those with statistically significant loadings on the first two NMDS axes ($q < 0.05$) that are highlighted in the main text. Full significance and correlation results for all metabolites are detailed in Supplementary Table 4.15.

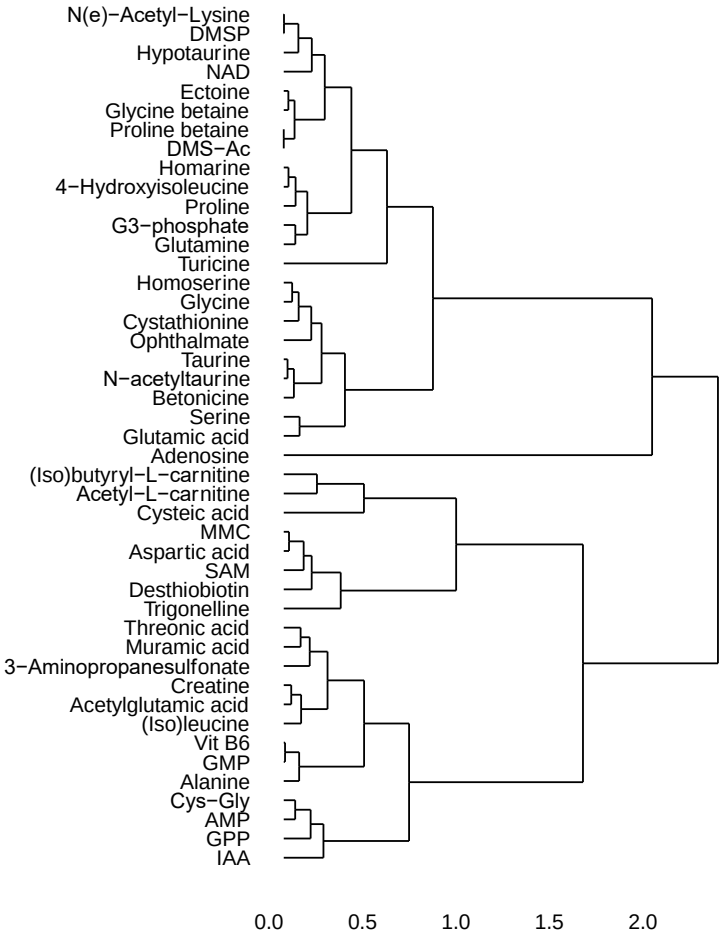

Supplementary Figure 4.11. Patterns of metabolite response to temperature and salinity change in incubation experiments. Dendrogram of metabolites that were significantly different ($p < 0.05$) with treatment, as determined by false discovery rate-corrected *p*-values from one-way ANOVAs (detailed in Supplementary Table 4.13). Metabolites are clustered using average linkage clustering on a Euclidean distance matrix.

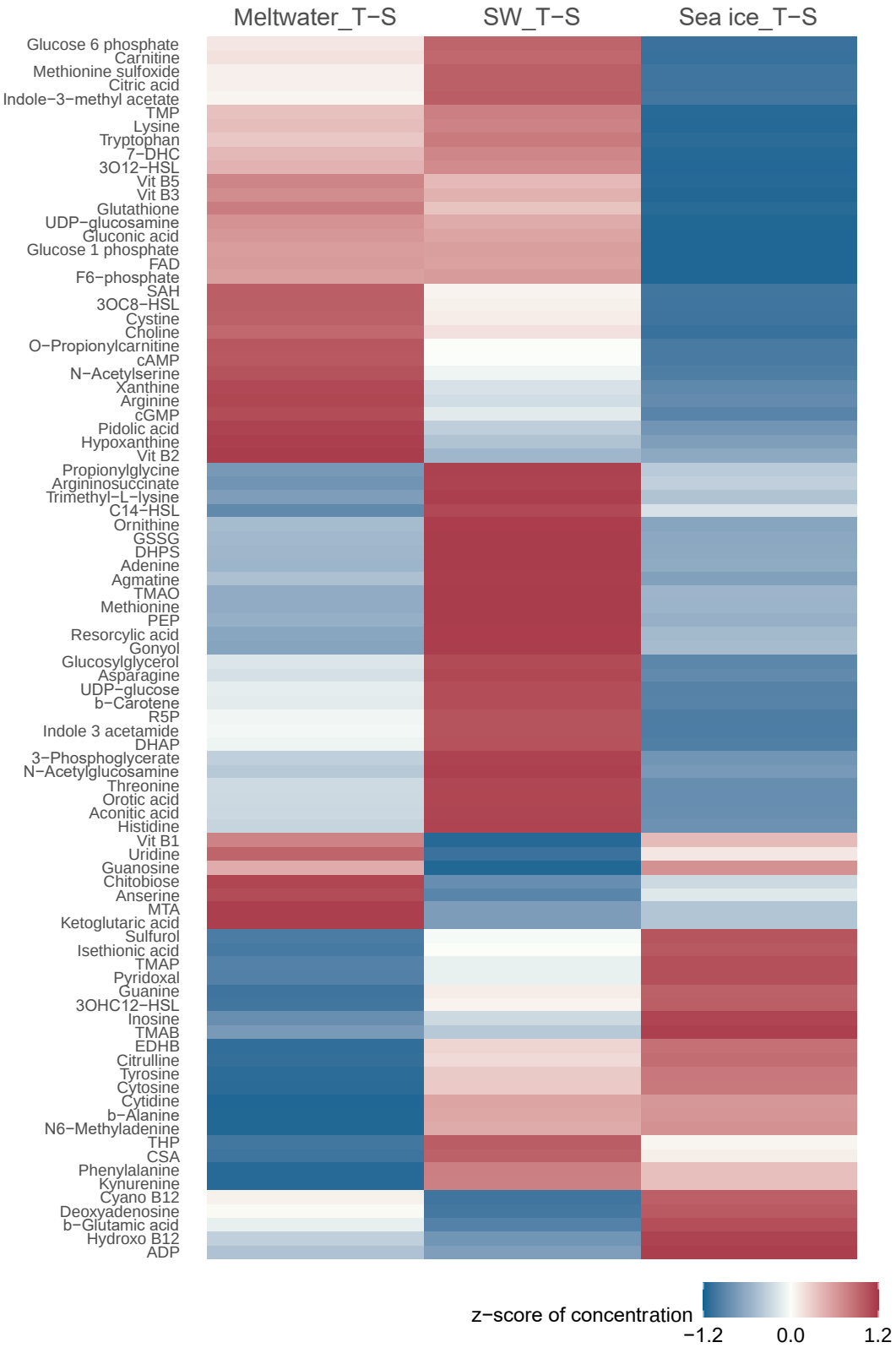
Meltwater_T−S
SW_T−S
Sea ice_T−S
Glucose 6 phosphate
Carnitine
Methionine sulfoxide
Citric acid
Indole−3−methyl acetate
TMP
Lysine
Tryptophan
7−DHC
3O12−HSL
Vit B5
Vit B3
Glutathione
UDP−glucosamine
Gluconic acid
Glucose 1 phosphate
FAD
F6−phosphate
SAH
3OC8−HSL
Cystine
Choline
O−Propionylcarnitine
cAMP
N−Acetylserine
Xanthine
Arginine
cGMP
Pidolic acid
Hypoxanthine
Vit B2
Propionylglycine
Argininosuccinate
Trimethyl−L−lysine
C14−HSL
Ornithine
GSSG
DHPS
Adenine
Agmatine
TMAO
Methionine
PEP
Resorcylic acid
Gonyol
Glucosylglycerol
Asparagine
UDP−glucose
b−Carotene
R5P
Indole 3 acetamide
DHAP
3−Phosphoglycerate
N−Acetylglucosamine
Threonine
Orotic acid
Aconitic acid
Histidine
Vit B1
Uridine
Guanosine
Chitobiose
Anserine
MTA
Ketoglutaric acid
Sulfurol
Isethionic acid
TMAP
Pyridoxal
Guanine
3OHC12−HSL
Inosine
TMAB
EDHB
Citrulline
Tyrosine
Cytosine
Cytidine
b−Alanine
N6−Methyladenine
THP
CSA
Phenylalanine
Kynurenine
Cyano B12
Deoxyadenosine
b−Glutamic acid
Hydroxo B12
ADP
z−score of concentration
−1.2
0.0
1.2

Supplementary Figure 4.12. Particulate metabolite responses to temperature and salinity change during the incubation experiments. Heat map showing color-scaled z-score standardized concentrations of metabolites (nmol metabolite C μmol C^{-1}), arranged by average linkage hierarchical clustering of Euclidean distance. Compounds shown here were not significantly different ($p > 0.05$) with treatment, as determined by false discovery rate-corrected *p*-values from one-way ANOVAs (as detailed in Supplementary Table 4.16).

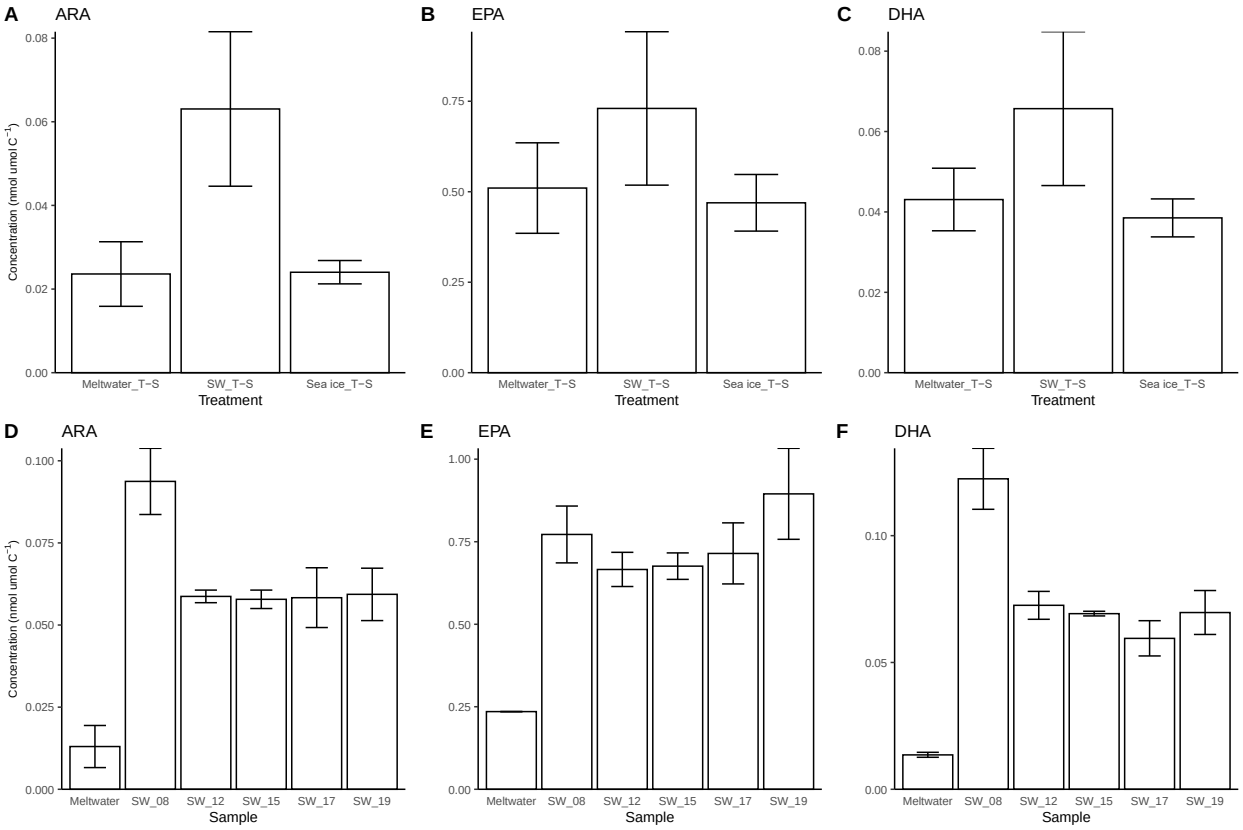

Supplementary Figure 4.13. Select fatty acid concentrations in field and incubation samples. Particulate concentration (nmol metabolite μmol C^{-1}) of free fatty acids in the incubations grouped by treatment (top row) and field (bottom row) for A) and D) arachidonic acid (ARA), B) and E) Eicosapentaenoic acid (EPA), and C) and F) Docosahexaenoic acid (DHA). Error bars represent

standard deviation of the mean (n = 2 for Meltwater_T-S, Meltwater, and SW_15, n = 3 for rest). Full data available in Supplementary Table 4.18.

VITA

Hannah Dawson
University of Washington, School of Oceanography, Astrobiology Program
hmdawson@uw.edu

Education

2022 PhD, Oceanography and Astrobiology
University of Washington, Seattle, WA
Dissertation: Microbial metabolomics in polar oceans: responses to temperature and salinity changes associated with sea ice.
Advised by Asst. Prof. Jodi N. Young

2019 MS, Oceanography
University of Washington, Seattle, WA
Thesis: Effects of temperature and salinity on the physiology of sea-ice algae.
Advised by Asst. Prof. Jodi N. Young

2013 BS, Biology
University of Virginia, Charlottesville, VA
Minor in Astronomy

Professional Experience and Research

2016-2022 Graduate Research Assistant, UW School of Oceanography, Seattle, WA
Supervisor: Dr. Jodi N. Young

2013-2016 Laboratory Specialist, Virginia Tech Marion DuPont Scott Equine Medical Center, Leesburg, VA
Supervisor: Dr. Jennifer Barrett

2012-2013 Undergraduate Independent Researcher, School of Medicine, University of Virginia, Charlottesville, VA
Supervisor: Dr. Benjamin Purow

Publications

Published

Dawson, HM, Heal, KR, Boysen, AK, Carlson, LT, Ingalls, AE and Young, JN. 2020. Potential of temperature and salinity-driven shifts in diatom compatible solute concentrations to impact biogeochemical cycling within sea ice. *Elem Sci Anth*, 8: 25. DOI: https://doi.org/10.1525/elementa.421

Dawson, HM, Heal, KR, Torstensson, A, Carlson, LT, Ingalls, AE, Young, JN. 2020. Large diversity in nitrogen- and sulfur-containing compatible solute profiles in polar and temperate diatoms. *Integr Comp Biol*. 2020;60(6):1401–13. DOI: https://doi.org/10.1093/icb/icaa133

In preparation

Dawson, HM, Connors, E, Erazo, N, Sacks, JS, Mierzejewski, V, Rundell, S, Carlson, LT, Deming, JW, Ingalls, AE, Bowman, J, Young, JN. (In review) Metabolome responses in microbial communities along the western Antarctic Peninsula to changes in temperature and salinity. *ISME J*.

Rundell, S, Young, JN, Cooper, Z, Dawson, HM, Carpenter, SD, Ryan-Keogh, T, Rowland, E, Bertrand, E, Deming, JW. (In prep.) Light or temperature? What controls the rate of carbon fixation during the spring melt of sea ice in the Western Antarctic Peninsula? *Limnol Oceanogr*.

Presentations

Dawson, HM. Microbial metabolomics in changing polar oceans. Talk, Dissertations Symposium in Chemical Oceanography (DISCO XXVIII), Kailua-Kona, HI, October 2022.

Dawson, HM. Seawater microbial communities along the Western Antarctic Peninsula: strong metabolome responses to short-term temperature and salinity perturbations. Talk, Biological Oceanography Seminar, University of Washington, Seattle, WA, June 2022.

Dawson, HM, Connors, E, Erazo, N, Sacks, JS, Mierzejewski, V, Rundell, S, Carlson, LT, Deming, JW, Ingalls, AE, Bowman, J, Young, JN. Seawater microbial communities along the Western Antarctic Peninsula: strong metabolome responses to short-term temperature and salinity perturbations. Talk, Tvärminne Symposium on Polar Microbes and Viruses, Tvärminne, Finland, May 2022.

Dawson, HM, Thamatrakoln, K, Kranzler, C, Zelzion, U. Expanding the known marine virosphere via viromics: first measures of RNA viruses in sea ice. Talk, Astrobiology Colloquium, University of Washington, Seattle, WA, November 2021.

Dawson, HM. Response of polar surface seawater community to change in temperature and salinity. Talk, Biological Oceanography Seminar, University of Washington, Seattle, WA, May 2021.

Dawson, HM. Ecophysiology of sea-ice algae in changing polar oceans. Talk, Biological Oceanography Seminar, University of Washington, Seattle, WA, November 2020.

Dawson, HM., Boysen, A, Heal, KR, Carlson, LT, Ingalls, AE, Young, JN. Using metabolomics as a method to probe the physiological adaptations of sea-ice algae. Talk, Astrobiology Science Conference, Bellevue, WA, July 2019.

Dawson, HM. Effects of temperature and salinity on the physiology of sea-ice algae. Talk, Biological Oceanography Seminar, University of Washington, Seattle, WA, May 2019.

Dawson, HM., Boysen, A, Heal, KR, Carlson, LT, Ingalls, AE, Young, JN. Metabolic response of sea-ice diatoms to shifting temperature and salinity. Poster, POLAR2018 SCAR Open Science Conference, Davos, Switzerland, June 2018.

Dawson, HM., Boysen, A, Heal, KR, Carlson, LT, Ingalls, AE, Young, JN. Characterization of compatible solute use in a cultured sea-ice alga, *Nitzschia lecointei*, and in the environmental algal community of Utqiaġvik (Barrow), AK using a metabolomics approach. Poster, Ocean Sciences Meeting, American Geophysical Union, Portland, OR, February 2018.

Dawson, HM. Metabolic response of sea-ice algae to changes in temperature and salinity. Talk, Biological Oceanography Seminar, University of Washington, Seattle, WA, January 2018.

Dawson, HM. Metabolic response of sea-ice algae to shifting temperature and salinity. Oceanography Second Year Symposium, University of Washington, Seattle, WA, November 2017.

Field Experience

10/26/2019 – 12/15/2019 Ice Breaker *Nathanial B. Palmer*, Antarctica. Participated in the planning and execution of a 2-month field season with the NSF United States Antarctic Program along the Western Antarctic Peninsula as acting PI. Collected samples of seawater for study of microbial responses to temperature and salinity shifts during seasonal transitions. Included extensive laboratory component in addition to field collection.

10/19/2018 – 12/4/2018 Palmer Station, Antarctica. Participated in the planning and execution of a 2-month field season with the NSF United States Antarctic Program on the Western Antarctic Peninsula as acting PI at Palmer Station. Collected samples of seawater for study of microbial responses to temperature and salinity shifts during seasonal transitions. Included extensive laboratory component in addition to field collection.

05/04/2017 – 05/11/2017 Utqiaġvik (Barrow), Alaska. Collected samples of sea-ice cores for the study of sea-ice algal metabolism. Included extensive laboratory component in addition to field collection.

Teaching

2022 Guest Lecture, Biogeochemical cycling, University of Washington, School of Oceanography. Carbon capture geoengineering challenge.

2022 Teaching Assistant, Biogeochemical cycling, University of Washington, School of Oceanography. Instructed two weekly quiz sections, wrote problem set and exam questions, held weekly office hours, and graded student coursework.

2017 Teaching Assistant, Introduction to Oceanography of the Pacific Northwest, University of Washington, School of Oceanography. Instructed twice-weekly lab sections, held weekly office hours, and graded student coursework.

2013 Teaching Assistant, Organic Chemistry II, University of Virginia. Held office hours, led weekly discussions, and graded student coursework.

2013 Biology Lab Peer Teacher, Organismal and Evolutionary Biology Laboratory, University of Virginia. Served as an assistant to a graduate instructor as a resource for students during the labs and aided in lab coordination and preparation outside lab time.

2012 Teaching Assistant, Organic Chemistry I, University of Virginia. Held office hours, led weekly discussions, and graded student coursework.

2012 Biology Lab Peer Teacher, Cellular Biology and Genetics Laboratory, University of Virginia. Served as an assistant to a graduate instructor as a resource for students during the labs and aided in lab coordination and preparation outside lab time.

2012 Biology Lab Peer Teacher, Organismal and Evolutionary Biology Laboratory, University of Virginia. Served as an assistant to a graduate instructor as a resource for students during the labs and aided in lab coordination and preparation outside lab time.

2011 Biology Lab Peer Teacher, Cellular Biology and Genetics Laboratory, University of Virginia. Served as an assistant to a graduate instructor as a resource for students during the labs and aided in lab coordination and preparation outside lab time.

Workshops

01/24/2022 – 01/28/2022 UW Astrobiology Workshop, Mission to Detect Life (Virtual). Worked with scientists from University of Washington (lead by Dr. Brook Nunn) and Astrobiology graduate students to design a lander and orbiter mission to detect life on a hypothetical icy moon, Kwiya. Included instrument payload design, data interpretation, and debate.

10/15/2019 – 10/20/2019 UW Astrobiology Workshop, Friday Harbor Laboratories. Worked with scientists from University of Washington (lead by Dr. Roger Buick) and Astrobiology graduate students to trawl on the R/V *Rachel Carson* and performing dissections of invertebrate specimens to focus the evolution and success of invertebrate body plans.

09/11/2016 – 09/14/2016 UW Astrobiology Workshop, Mt. Rainier National Park. Worked with scientists from Georgia Tech (lead by Dr. Amanda Stockton) and Astrobiology graduate students to sample snow from the Muir Snowfield as an astrobiological analog environment for Mars.

Awards, Honors, and Funding

2021 Hall Conservation Genetics Award, UW College of the Environment ($7,500)
2019 Congressional Antarctic Service Medal
2018 NSF Travel Award SCAR Open Science Conference ($1,200)
2016–2017 Top Scholar Award, University of Washington, School of Oceanography (full coverage of tuition, benefits, and stipend)
2016 Beatrice Crosby Booth Endowed Fellowship, School of Oceanography ($4000)
2016 Astrobiology Scholar Award, University of Washington, Astrobiology Program ($3000)
2012 Junius Pendleton Wilson Memorial Scholarship, University of Virginia ($3000)
2011 University of Virginia College of Arts and Sciences Intermediate Honors
2009–2013 University of Virginia Dean's List

Mentoring

2022 Mentor to undergraduate CICOES intern Bailee Porter, University of Washington, School of Oceanography.
2022 Mentor to undergraduate researcher Dominic Eastburn, University of Washington, School of Oceanography.
2021 Mentor to undergraduate researcher Ashlee Somol, University of Washington, School of Oceanography.
2020–2021 Mentor to post baccalaureate research consultant Veronica Mierzejewski, University of Washington, School of Oceanography.
2017 Mentor to undergraduate researcher Rebecca Schmidt, University of Washington, School of Oceanography.
2016–2017 Mentor to undergraduate senior thesis student Viviana Castillo, University of Washington, School of Oceanography.

Outreach and Volunteering

2021 Graduate Application Mentorship Program (GAMP) mentor, University of Washington, School of Oceanography. Assisted a prospective graduate student in the application process in order to help demystify the graduate application process and provide tips and guidance for submitting an application.

2017–2020 Polar Science Weekend (annual), Pacific Science Center. Co-led a tabletop hands-on outreach activity that demonstrated how life can evolve in extremely cold environments, like sea ice brines. Included development of new activity and visuals for children.

2018–2019 Sammamish High School Antarctica outreach. During the Young lab 2018 field season on the Western Antarctic Peninsula interacted with high school students at Sammamish High School in Lisa Neshyba's science classes via video chat and email correspondence. Upon returning from field work, visited their classes to present a summary of our Antarctic field work and the applications to Astrobiology.

2017–2019 SeaTalk, University of Washington. Aided in the design and planning of quarterly workshops for anti-harassment training aimed at issues relevant for field-going scientists.

2017 Science Communication Fellow, Pacific Science Center. Participated in a six-week science communication course focused on building skills to effectively engage public audiences in research-oriented conversations. Developed a planetarium show related to my area of work in polar science for public presentation to audiences of all ages.